

Gathering & Collective Movement of Unicycle A(ge)nts with Crude Sensing Capabilities

David Dovrat and Alfred M. Bruckstein

Multi Agent Robotic Systems (MARS) Lab
Technion Autonomous Systems Program (TASP)
Center for Intelligent Systems (CIS)
Department of Computer Science
Technion, Haifa 32000, Israel

March 13, 2017

Abstract

We present a local rule of behavior for extremely simple agents, only able to detect the presence of other agents in a visibility sector directly in front of them. By implementing this simple, local, rule of interaction, the agents coordinate their movement without ever acquiring any information on the exact location of any other agent. The simplicity of the agents allow for a cost effective implementation of the model, since the use of sophisticated equipment is rendered unnecessary. The formation to which the agents converge, be it a rotating regular polygon, a set of rotating polygons, or some other cohesive behavior, depends on a set of simple predefined parameters: the agents' field of view, their common speed and their rotation radii. The work presented here contains a full analysis of a beacon-agent system, as well as convergence theorems for a 2-agent system and equilibrium analysis for a N -agent system. Gathering in the N -agent case and orientation synchronization in the 2-agent case are demonstrated in simulation. Methods of controlling the location of such a swarm are also discussed and were tested both in simulations and in the lab with actual robots.

Contents

Index of Symbols	5
1 Introduction	6
1.1 Criteria for Comparing Robotic Swarms	7
1.2 Literature Survey	8
1.2.1 Gathering & Formation	9
1.2.2 Collective Movement	10
1.3 Research Objectives and Expected Significance	12
2 The Model	14
2.1 The Unicycle Model	15
2.2 Sector Visibility	16
2.3 The Controller	17
3 Theoretical Results	18
3.1 A Single Agent and A Beacon	21
3.2 Two Agents Converge	47
3.3 Balanced States of the Swarm	55
4 Controlling the location of the Swarm	60
4.1 Control by Leader Agents	60
4.2 Control by Predefined or Broadcast Potential Field	60
4.3 Control by Local Sensing	61
5 Simulation Results	63
5.1 A Single Agent and A Beacon	63
5.1.1 Evolution of Distance to Beacon	64
5.1.2 Convergence Time is Linearly Bounded as a function of the Beacon's Initial Distance to Agent's Center of Rotation	64
5.1.3 Convergence Time is Affine over Beacon Initial Distance to Agent's Center of Rotation	65
5.2 Two Agents	67
5.2.1 Evolution of Distance between the Agents	67
5.2.2 Evolution of Orientation	68
5.2.3 Upper Bound on Convergence Time	69
5.2.4 Upper Bound on Distances	71
6 Discussion	73

List of Figures

2.1	The "Turtle Bale" project at the Technion MARS Laboratory.	15
2.2	The Unicycle Model	16
2.3	The System and its Graph Representation	16
3.1	The instantaneous center of rotation for agent i	19
3.2	An Agent and its Horizons	19
3.3	The Bearing Angle	20
3.4	The Blind Circle	22
3.5	The Vigil Circle	23
3.6	The Geometry used to prove Lemma 3.1.2	24
3.7	A beacon located at an arbitrary global frame origin rises over an agent's dawn horizon.	26
3.8	A Distant Agent Moving Toward a Beacon	27
3.9	The Geometry used to prove Lemma 3.1.5	28
3.10	The Geometry used to prove Lemma 3.1.6	30
3.11	The Geometric Setting for Lemma 3.1.8	32
3.12	The Geometry used to prove Lemma 3.1.7	33
3.13	The S_X surfaces where vector field X is discontinuous	36
3.14	A single agent spiraling towards a beacon with $0 < \alpha < \pi$	37
3.15	A single agent spiraling away from a beacon with $\pi < \alpha < 2\pi$	38
3.16	Agent-Beacon State Machine	40
3.17	NetLogo Simulations of a Beacon and an Agent	47
3.18	Possible Switching by θ	48
3.19	The Geometry used to prove Lemmas 3.2.1 and 3.2.2	49
3.20	An Illustration of Theorem 3.2.2	54
3.21	NetLogo Simulations of a 2-Agent System	55
3.22	A NetLogo Simulation Verifying Theorem 3.3.2	57
3.23	6-Agent system Simulations with $S \in \mathbb{R}$	58
3.24	A Simulation Demonstrating Conjecture 3.3.2	58
3.25	6-Agent system Simulations with $S \in \mathbb{N}$	59
4.1	8-Agent System Simulation	61
4.2	Controlling the Swarm by a Potential Field	62
5.1	Beacon-Agent System Simulation Results, Distance vs Time	65
5.2	Beacon-Agent System Simulation Results, Convergence Time	65
5.3	Beacon-Agent System Simulation Results, Convergence Time vs Initial Distance	67
5.4	2-Agent System Simulation Results, Distance vs Time	68
5.5	2-Agent System Simulation Results, Orientation vs Time	69

5.6	2-Agent System Simulation Results, Convergence Time vs Initial Distance	71
5.7	2-Agent System Simulation Results, Theorem 3.2.1 and Conjecture 3.2.1	72

Index of Symbols

- N Number of agents in a given system. $N \in \mathbb{N}$.
- α Central angle of agents' sector of visibility. $0 \leq \alpha \leq 2\pi$, $\alpha \in \mathbb{R}$.
- R_v Radius of agents' sector of visibility.
- \mathcal{G} The graph representation of a given system. $\mathcal{G} = \{\mathcal{V}, \mathcal{E}\}$, where \mathcal{V} is the set of vertices representing agents, and \mathcal{E} is the set of directed edges representing data flow to the perceiving agent from the agents perceived by it.
- v_i Agent i 's vertex in the underlying graph representation.
- $\deg^-(v_i)$ The indegree of v_i , i.e. the number of v_i 's incoming edges in the graph representation, or the number of agents detected by agent i . $\deg^-(v_i) \in \mathbb{Z}$.
- O the origin of an arbitrary global reference frame.
- x_i Agent i 's x coordinate in an arbitrary global reference frame. $x_i \in \mathbb{R}$.
- y_i Agent i 's y coordinate in an arbitrary global reference frame. $y_i \in \mathbb{R}$.
- θ_i The angle between agent i 's body frame and an arbitrary global reference frame. $0 \leq \theta_i < 2\pi$.
- v_i The velocity vector of agent i .
- ω_i Agent i 's turning rate, i.e. $\omega_i = \frac{d}{dt}\theta_i$.
- p_i Agent i 's position, i.e. $p_i = (x_i, y_i)^T$. In case of a single agent, p_i is replaced by p_a in order to emphasize the fact that only one agent exists.
- c_i Agent i 's center of rotation. $c_i \in \mathbb{R}^2$.
- p The vector of all agents' positions, i.e. $p^T = (p_1, p_2, \dots, p_N) = (x_1, y_1, \dots, x_N, y_N)$.
- θ The vector of all agents' orientation, i.e. $\theta = (\theta_1, \theta_2, \dots, \theta_N)$
- v The constant speed of all agents in all systems described in this work. $v \in \mathbb{R}$.
- $\mathcal{R}(\mathcal{G}, i)$ Agent i 's turning radius, as a function of the current state of the underlying graph \mathcal{G} . $\mathcal{R}(\mathcal{G}, i) \in \{R, r\}$; $0 < r < R$; $R, r \in \mathbb{R}$
- S The system's switching number, an agent switches its turning radius when the number of agents it senses in its sector of visibility rises above or falls below this number. $S \in \mathbb{N}$.
- φ_i Agent i 's polar angle in an arbitrary global reference frame, i.e. $\varphi_i = \arctan 2(y_i, x_i)$.
- T A time span, usually denotes a period time for systems with periodic orbits. $T \in \mathbb{R}$.

Chapter 1

Introduction

”Go to the ant, thou sluggard; consider her ways, and be wise:
Which having no guide, overseer, or ruler, Provideth her meat in
the summer, and gathereth her food in the harvest.”

- Proverbs 6:6, King James Bible

Since biblical times, and perhaps since the dawn of mankind, the inquisitive human mind has been fascinated by the emergence of complicated collective behaviors in nature, especially when performed by the simplest of creatures. We as a species are enchanted by the emergence of sophisticated patterns from coordinated behavior, perhaps since we find it so difficult to achieve agreement and harmony amongst ourselves. The ant has continued to be the subject of observations throughout the ages, and her ways are still considered by contemporary biologists and physicists such as the authors of [6], [13] and references therein.

The ant and its colony are interesting from an engineering standpoint as well, where the prospect of achieving decentralized coordination using implicit, indirect communication between autonomous a(ge)nts (or man-made ants, either physical robots or virtual agents) with limited sensing capabilities and limited memory and computational power is most appealing. Mathematical models of the ant colony, with some modifications, have been shown to be capable of solving complicated optimization problems, see for instance [4], [33], and [8].

The field of *Swarm Robotics* has emerged from the desire to harness the power of robust, decentralized, cost-effective ant-like systems, having no single point of failure. Though we consider the ant as the paradigm for swarm robotics, inspiration may be found in other occurrences of collective behavior in nature such as schools of fish [34] [25], flocks of birds, herds of mammals [26] and, of course, swarms of insects [27] [15]. Some researchers draw inspiration for their swarm robotics work from the rules governing objects and particles such as planetary motion, thermodynamics [10] and hydrodynamics [24] as well.

The *rendezvous*, or the more general *gathering* problem, i.e. the ability to converge to a single location or to a confined set of configurations from a dispersed initial configuration, is one of the classic concerns of swarm robotics [14]. The *formation* problem is a natural extension of the gathering problem - when we require the set of configurations the agents converge to to have

some predefined shape. Another important problem is the control of *collective movement* - once a cohesive swarm has formed it would be nice to be able to have it move towards some desired goal [21]. Solutions to these problems proposed so far in the literature differ in the level of sophistication required from the swarming agents in order to perform their tasks. The rest of this chapter is dedicated to comparing a few notable works in the field of swarm robotics, based on the criteria listed below.

1.1 Criteria for Comparing Robotic Swarms

Decentralized Control We consider a model where each agent acts locally based on local, partial information to be decentralized. A decentralized model, as we see it, is such that not only the computation effort may be dispersed among the swarm's agents, but that the information is dispersed as well. A model is considered by us as distributed and not decentralized if data is explicitly shared among agents, even if the work examined implemented the model by dispersing the computation efforts across multiple agents. The differentiating factor is whether the single agent has access to information sensed by other agents rather than the agent relying on its own sensing abilities alone, or if all data used by a single agent's behavior protocol is known to all agents. When the availability of global information or the ability to share information explicitly enables a single agent to solve the entire model's behavior, the model might as well be centralized, and therefore is considered by us as such.

Anonymous Agents Agent's that are interchangeable, have no label nor specific role to fulfill are considered by us to be anonymous. Agents may assume a role, such as leaders or followers, while remaining anonymous as long as their role is not specific to them, i.e. an agent may be a leader as long as the fact that the agent is a leader is unknown to the follower agents, and the leader's identity is unknown to the controlling operator. We treat fixed network topologies as labels, since every agent is connected to a specific other agent, even if the agents themselves are identical and follow the same behavioral rule.

Nonholonomic Unicycles The addition of a nonholonomic constraint to an agent makes it implementable by wheeled robots. This criterion differentiates works focused on the popular single integrator linear model from works focused on the nonlinear unicycle model.

Implementable by Fixed Wing UAVs Fixed wing UAVs have a minimal forward velocity constraint. This criterion refines the differentiation of works using unicycle models. While all unicycle model systems are appropriate for wheeled vehicle implementations, only those with a predetermined minimal forward velocity are suitable for fixed wing UAVs.

Implicit Collective Movement Not all local interaction protocols enable arbitrary control with local sensing of shared data, e.g. a potential field. This criterion does not imply considerations of heterogeneous roles in the swarm (such as leaders and followers) since analyzing whether a swarm is susceptible to leader manipulation is out of the scope of most works considered here. Such an analysis can be found, for instance, in [29].

Limiting Shape or Formation of the Swarm Indicates whether the model converges to a predefined formation, i.e. whether given enough time, the relative locations of the agents are a finite set.

Topological Constraints This criterion indicates whether the model has constraints on its underlying neighborhood topology. An example of a model requiring a specific topology is any model based on cyclic pursuit, requiring the underlying neighborhood graph to have ring topology. A pervasive requirement is that the underlying neighborhood communication graph must be connected. In this categorization, the requirement for a connected neighborhood graph is not considered as a topological constraint.

Limited Sensing Abilities A model is considered to have limited sensing if the agents' ability to sense other agents or obstacles depends on their location and orientation relative to the location of the objects being sensed.

Bearing Only Any control which requires only the bearing information from the controlled agent to other objects is a bearing only control.

Crude Sensing A model with a control that does not require exact information is considered crude. Crude sensing implies low cost equipment and less computation power required for the model. An example of crude sensing is given in a model where the agents can only detect whether another agent is in a sector in front of them or not, opposed a model where exact bearing angles to other agents need to be measured.

Memoryless Agents Agents that can recall past states are considered to have memory, and are therefore less simple than agents that rely only on the current system state.

Global Position Obliviousness Agents are unaware of a global frame.

Global Orientation Obliviousness Agents are unaware of a global direction, i.e. agents that carry no compass are called oblivious to global orientation.

The discussion below, in light of of the criteria set above, is summarized in Tables 1.1, and 1.2, 1.3.

1.2 Literature Survey

In this section a short description of a few examples of notable trends in swarm gathering, formation and collective movement is given. The examples are then compared using the criteria in Section 1.1. For other criteria and categorization of swarm robotics, see surveys by Barel et al. [3] focused on the gathering problem, Oh et al. [23] focused on formation control and Navarro & Matía [22], focused on collective movement. For further reading see the bibliography of the surveys just given as reference, as most of the work cited here is from extra sources.

1.2.1 Gathering & Formation

Bruckstein in [4] solves the gathering problem using cyclic pursuit with first order integrators. Any pure cyclic pursuit solution such as the one introduced by Bruckstein involves labeling the agents, keeping the topology of the underlying interaction graph invariant.

Marshall et al. [19] introduce unicycle agents in cyclic pursuit, showing that their equilibrium formations are regular polygons, not discussing however their convergence to those formations from any initial condition.

Dimarogonas and Kyriakopoulos solve the gathering problem in [7] for a group of nonholonomic unicycles able to measure relative distances and having access to a common compass direction, for both static and dynamic communication topologies.

Zheng et. al. build upon the foundations set in [19] and present a unicycle model which solves the formation problem in [39] for circular formations using cyclic pursuit with agents able to stop and go backwards while sensing relative position of one pursued agent for each vehicle. In [37] Zheng et al. show that the results in [39] can solve the gathering problem for N wheeled unicycle model agents, without the need for the agents to rely on any global measurement, replacing the unidirectional cyclic topology with a more general bidirectional position measurement, as long as the underlying graph is uniformly jointly connected. Their results include proof of convergence for the fixed topology case, and ultimate boundedness analysis around a stationary point depending on initial conditions for systems with dynamic topology. In [42] Zheng et al. present two bearing only controllers, based on prior results in [41], that solve the rendezvous problem for N wheeled unicycle model agents, and two distance only controllers that solve the rendezvous problem for up to 2 wheeled unicycle model agents, while showing through Monte Carlo [18] simulations that the distance only controllers proposed achieve practical convergence as well for the N agent case. Zheng et al. then extend their finds in [38] and [40], achieving circumnavigation of a static target with multiple, customizable, radii by a swarm of unicycle agents using relative, omnidirectional position measurements or bearing only measurements.

Gauci et al. took a different approach to solve the gathering problem in [12], and proposed a controller where agents equipped with very simple binary sensors were considered and a controller was synthesized and refined via an optimization process. The agents considered there were differential wheeled robots, which are equivalent to the unicycle model.

	Reference					
	[4]	[7]	[37]	[41]	[42]	[12]
Decentralized Control	Yes	Yes	Yes	Yes	Yes	Yes
Anonymous Agents	No	Yes	No	No	No	Yes
Nonholonomic Unicycles	No	Yes	Yes	Yes	Yes	Yes
Fit for Fixed Wing UAVs	No	No	No	No	No	No
No Topological Constraints	No	Yes	Yes	Yes	Yes	Yes
Limited Sensing Abilities	No	Yes	No	No	No	Yes
Bearing Only	Yes	No	No	Yes	Yes	Yes
Crude Sensing	No	No	No	No	No	Yes
Memoryless Agents	Yes	Yes	Yes	Yes	Yes	Yes
Global Position Obliviousness	Yes	Yes	Yes	Yes	Yes	Yes
Global Orientation Obliviousness	Yes	No	Yes	Yes	Yes	Yes

Table 1.1: A Comparison of Solutions to the Gathering Problem

1.2.2 Collective Movement

Egerstedt and Hu present a solution to the collective movement problem in [9] where a virtual leader follows a reference trajectory, and actual robots maintain formation relative to the virtual leader. The control scheme presented is platform independent, and is demonstrated on the unicycle model. They use both position and orientation error feedback. The underlying formation constraint function may require all-to-all communication and measurement of relative positions, as well as the position relative to a virtual leader, and the protocol is not anonymous. The actual robots are assigned to virtual robots that maintain the formation.

Elor and Bruckstein consider a "cloud" of random walking agents that perform gradient climbing without converging to a predetermined formation in [11]. In [29], Segall and Bruckstein analyze a broadcast control mechanism, where collective movement is achieved by identical agents that follow the same interaction rule while some of the agents detect and also incorporate a globally broadcast control signal, implicitly making them leaders. This approach requires the agents to share a global reference orientation, e.g. a "global north".

Schoof et al. solve the formation and collective movement problems in [28] for single integrator agents, equipped with compasses, using bearing only measurements. They implement change in scale by sending at least two agents equal magnitude controls along the vector between them yet in opposite directions, and translation by sending all agents the same control input signals. Any other combination of control input transmission results in changes both in scale and the location of the centroid. Rotation is achieved by broadcasting a constant rotation control input to all agents. Shiell and Vardy introduce in [32] modifications to the model presented in [28], while using Schoof's model as a benchmark, by using a Dynamic Neighbor Selection (DNS) algorithm in order to form the swarm's underlying communication graph. The use of DNS improves the model's scalability, flexibility, robustness and performance

	Reference			
	[19]	[39]	[38]	[40]
Decentralized Control	Yes	Yes	Yes	Yes
Anonymous Agents	No	No	No	Yes
Nonholonomic Unicycles	Yes	Yes	Yes	Yes
Fit for Fixed Wing UAVs	Yes	No	No	No
Implicit Collective Movement	Yes	Yes	Yes	Yes
No Topological Constraints	No	No	No	Yes
Limited Sensing Abilities	No	No	No	Yes
Bearing Only	No	No	No	Yes
Crude Sensing	No	No	No	No
Memoryless Agents	Yes	Yes	Yes	Yes
Global Position Obliviousness	Yes	Yes	Yes	Yes
Global Orientation Obliviousness	Yes	Yes	Yes	Yes

Table 1.2: A Comparison of Solutions to the Formation Problem

as defined in [32], at the cost of a reduced set of possible formations and loss of rigidity. The convergence to a formation for the model in [32], based on DNS, has no analytical proof.

Zhao and Zelazo achieve formation and collective movement for single integrator agents in [36] without the need for broadcasting control inputs to all agents and without requiring any information about the global frame, yet they require relative position measurements. Proof that scale and translation of the formation can be controlled if at least two leader agents are introduced to the swarm is presented. Zhao and Zelazo use infinitesimal bearing rigidity considerations in order to prove convergence to the desired formation.

Yu and Liu present and analyze a method for anonymous unicycle agents to form a circular formation around a moving target in [35], yet their method requires relative position measurements and measuring the tracked target's second derivative in order to do so.

Pimenta et al. in [24] use Smoothed Particle Hydrodynamics (SPH), utilizing a global potential function, to let the agents flow down the gradient while avoiding collisions and obstacles. The unicycle agents only need to measure the location of nearby agents in order to calculate the "forces" that their neighbors apply on them.

Sepulchre et al. use relative heading and position in [30] to induce their agents to circle a common center of rotation, to form a balanced splay state formation where the agents' orientation phases are uniformly spaced around the circle, or to move together in parallel. In [31] Sepulchre et al. do the same with a general communication framework. Jain and Ghose extend the Sepulchre model to a system of heterogeneous agents, by reaching the splay state in [17], and reaching velocity synchronization in [16], for two and three agent systems and with simulations for the N-agent system case. Arranz et al [2] extended [31] to deal with a moving center of rotation, requiring all agents to measure the second derivative of the center of rotation. Moore and de Wit [20] adjusted [2] for gradient climbing by letting the agents communicate

their potential readings to one another and calculating the center of rotation's movement accordingly.

	Reference					
	[9]	[11]	[29]	[28]	[32]	[36]
Decentralized Control	No	Yes	Yes	Yes	Yes	Yes
Anonymous Agents	No	Yes	No	No	Yes	No
Nonholonomic Unicycles	Yes	No	No	No	No	No
Fit for Fixed Wing UAVs	No	No	No	No	No	No
Implicit Collective Movement	No	Yes	No	Yes	No	No
Formation	Yes	No	No	Yes	Yes	Yes
No Topological Constraints	No	No	Yes	No	Yes	No
Limited Sensing Abilities	No	No	No	No	No	No
Bearing Only Sensing	No	No	No	Yes	Yes	No
Crude Sensing	No	No	No	No	No	No
Memoryless Agents	Yes	Yes	Yes	Yes	Yes	No
Global Position Obliviousness	No	Yes	Yes	Yes	Yes	Yes
Global Orientation Obliviousness	Yes	Yes	No	No	No	Yes

	Reference					Our Model
	[35]	[24]	[30]	[31],[17],[16],[2],[20]		
Decentralized Control	Yes	Yes	Yes	Yes	Yes	
Anonymous Agents	Yes	Yes	Yes	Yes	Yes	
Nonholonomic Unicycles	Yes	Yes	Yes	Yes	Yes	
Fit for Fixed Wing UAVs	No	No	Yes	Yes	Yes	
Implicit Collective Movement	No	Yes	Yes	Yes	Yes	
Formation	Yes	No	Yes	Yes	Yes	
No Topological Constraints	Yes	Yes	No	Yes	Yes	
Limited Sensing Abilities	Yes	Yes	No	No	Yes	
Bearing Only Sensing	No	No	No	No	Yes	
Crude Sensing	No	No	No	No	Yes	
Memoryless Agents	Yes	Yes	Yes	Yes	Yes	
Global Position Obliviousness	Yes	No	Yes	Yes	Yes	
Global Orientation Obliviousness	Yes	Yes	Yes	Yes	Yes	

Table 1.3: A Comparison of Solutions to the Collective Movement Problem

1.3 Research Objectives and Expected Significance

In this work a decentralized, scalable, self organizing swarm of anonymous unicycle type agents with a constant forward velocity is presented. The swarm solves the formation problem by forming either a moving regular polygon, or

a moving formation comprised of several regular polygons, or simply by maintaining cohesiveness. The end result is a consequence of very few parameters that can be programmed into the agents' local behavior protocol. The agents forming the swarm are limited in their sensing abilities. We assume they can only make a crude judgment on how many other agents are in a sector ahead of them. The agents are also memoryless and oblivious in the sense that they do not share a global frame of reference in space. The swarm is capable of collective movement and we impose no topology constraints. Collective movement is achieved by manipulating the swarm's formation, by interfering with one, some, or all of the member agents' behavior. The motivation for our work stems from a desire to bridge the gap from previous theoretical results, such as in [11], to practical micro-robotic systems based on agents that live in a world imposing severe physical constraints on agent motion rules and sensing capabilities. We here built upon the foundations set by [37] and [42] on unicycle-agent based swarms, and propose a way to keep the the agents' velocity input free for use in controlling the swarm's location. This leads to novel challenges in both theory and practice. Additional constraints on the model are also imposed to make the robotic agents as simple as possible. The agents' sensing capabilities are further reduced by not requiring to measure relative orientations and not requiring omni-directional sensing. These reductions may indeed imply less sophisticated and expensive equipment upon implementation. Our aims in considering simplified sensing are similar to those recently proposed in [12]. Finally, several methods for controlling the swarm's location are presented, while ensuring cohesive, dynamic and flexible, shaped formations.

Chapter 2

The Model

Simplicity is key when designing swarming agents and is the main ingredient in the model proposed here. One of the greatest promises of swarm robotics is functionality invariant to scale, and scale invariance must stem from the simplicity of the agents in order to allow cost efficient swarms. The proposed model is based on the popular *Unicycle Model*, allowing implementation using a variety of platforms, including wheeled vehicles subject to nonholonomic constraints. The proposed model also dictates a forward motion greater than some defined positive parameter, allowing implementation on platforms that have a minimal velocity constraint, such as some fixed wing drone-like flying robots. *Sector Visibility*, when compared to omni-directional sensing, is quite straightforward. Omni-directional sensing is not trivial to achieve using on-board sensing. A robot agent would have to have at least one expensive wide angle lens, and then would have to do some computing in order to translate from camera coordinates to real world bearing, or have an array of sensors, then stitch the sensors' outputs into a coherent snapshot of the current situation, requiring computational power, which is neither lightweight, low on power consumption, nor is it cheap. None of these problems arise in a robot with sector visibility, simply because any camera will do the job and minimal computational power is required to translate the sensor output into the necessary input for local behavior control algorithms. Figure 2.1 shows an implementation of the presented model using TurtleBot2 platforms¹. Though equipped with a Kinect and a netbook running ROS, the implementation uses only the RGB camera on the Kinect and could do with far less computational power than the netbook provides.

¹<http://www.turtlebot.com/>



(a) Having gathered from their initial locations, the agents congregate in a circular formation.



(b) An operator controlled "shepherd" agent is introduced to the swarm.



(c) The swarming agents, true to their protocol, follow the shepherd agent.



(d) Once removed, the shepherd agent no longer influences the swarming agents and they return to their circular formation in their new location.

Figure 2.1: The "Turtle Bale" project at the Technion MARS Laboratory.

2.1 The Unicycle Model

Agent i 's motion in the plane is governed by the equation

$$\begin{bmatrix} \dot{x}_i \\ \dot{y}_i \\ \dot{\theta}_i \end{bmatrix} = \begin{bmatrix} v_i \cos(\theta_i) \\ v_i \sin(\theta_i) \\ \omega_i \end{bmatrix} \quad (2.1)$$

where $(x_i, y_i, \theta_i)^T$ are the agent's state, comprising agent i 's location, $p_i = (x_i, y_i)^T$, and orientation θ_i in an arbitrary global frame of reference (see Figure 2.2). Here, v_i and ω_i are agent i 's control inputs, determining its speed and rotation rate respectively.

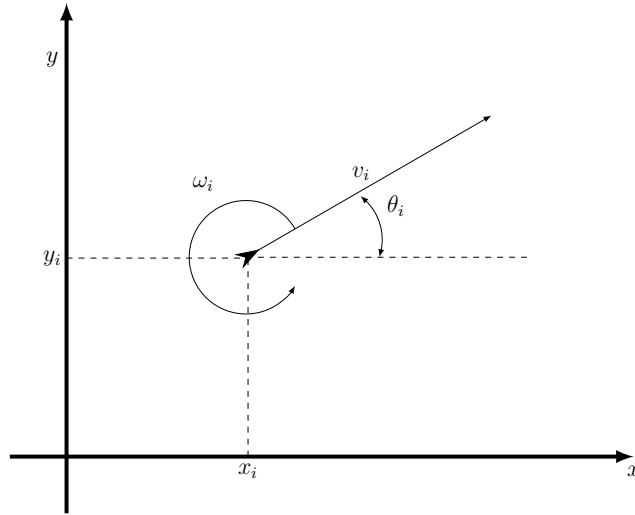


Figure 2.2: The Unicycle Model

2.2 Sector Visibility

Consider a system of N agents, each equipped with a sensor able to count only the number of other agents it perceives in a sector with visibility radius R_v and a central angle α in the direction the agent is facing. A graph representation of such a system, $\mathcal{G} = \{\mathcal{V}, \mathcal{E}\}$, can be constructed such that every agent in the system is represented by a vertex in the graph, and all agents within agent i 's sector of visibility have edges directed from them to agent i . Figure 2.3 shows an example of such a system and its underlying graph. The sensor output given to agent i is the count of agents seen, i.e. the number of edges directed at agent i 's vertex in the underlying graph, or v_i 's indegree $\text{deg}^-(v_i)$.

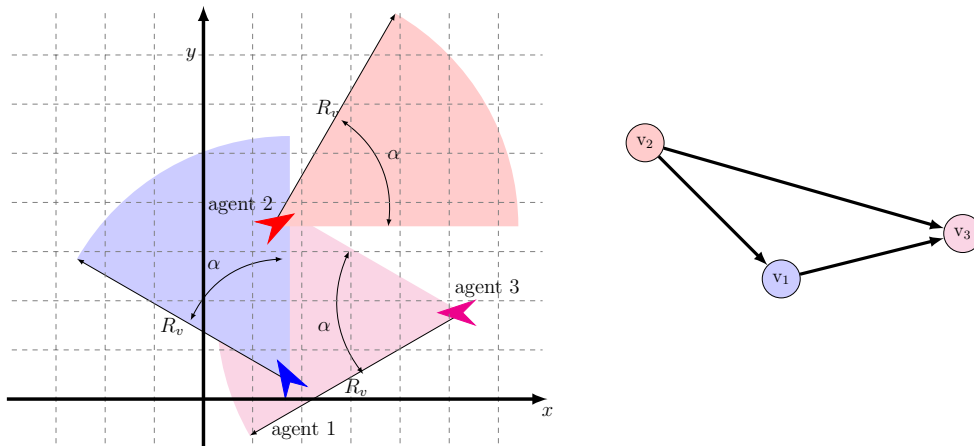


Figure 2.3: On the left, three agents in an arbitrary global frame for which the agent's coordinates (x, y, θ) are defined. To the right, the system's underlying graph representation.

2.3 The Controller

The unicycle agent described in Section 2.1 is controlled by

$$\begin{bmatrix} v_i \\ \omega_i \end{bmatrix} = \begin{bmatrix} v \\ \frac{v}{\mathcal{R}(\mathcal{G}, i)} \end{bmatrix} \quad (2.2)$$

where v is a positive constant and $\mathcal{R}(\mathcal{G}, i)$ is a scalar function defined over the graph $\mathcal{G} = \{\mathcal{V}, \mathcal{E}\}$ such that

$$\mathcal{R}(\mathcal{G}, i) = \begin{cases} r & \text{if } \deg^-(v_i) < S \\ R & \text{if } \deg^-(v_i) \geq S. \end{cases} \quad (2.3)$$

Here $\deg^-(v_i)$ is the number of neighbors perceived by agent i , i.e. the indegree of agent i 's vertex in the system's graph representation, $0 < r < R$, and $S \in \mathbb{N}$ is defined as the system's *Switching Number*, a threshold of detected agents given as a system design parameter known to all agents.

The controller presented here is decentralized in the sense that every agent's behavior relies solely on the single agent's indegree, information that is not shared with other agents. Scalability is a byproduct of this decentralization. Furthermore, in the controller's perspective, all agents are anonymous, and the controller isn't affected by which edge, and therefore which agent, contributes to the indegree of any specific agent. The fact that only the indegree matters renders exact measurement of bearing angles and relative positions unnecessary, allowing the agents to be fitted with crude sensors, such as a single camera with limited field of view and no depth perception. Additional sensors such as GPS or compasses are also unnecessary due to the fact that the controller does not have a global reference point, or even a global direction reference, making the agents content in their obliviousness. Finally, the controller is stateless as only the current system state is used to resolve the value of $\mathcal{R}(\mathcal{G}, i)$, making all agents memoryless.

Chapter 3

Theoretical Results

Simple as the model presented in Chapter 2 may be, its theoretical analysis is surprisingly highly non-trivial. In this chapter three interesting instances of such systems are analyzed. One consists of a single agent interacting with a static beacon perceived by it as an agent. Then proof is given that 2-agent systems always converge to a configuration where the agents closely orbit each other. Finally some periodic orbits for N agent systems are discovered and discussed. In order to facilitate the discussion, a few definitions are introduced:

Definition 1. *When an agent changes its angular velocity it is said to have switched its turning radius.*

Definition 2. *A system is said to be periodic when all its agents repeat some pattern of movement, i.e. the system state has a periodic orbit. Hence there exists some minimal time interval T in which a repetitive movement pattern is completed, i.e.,*

$$\begin{bmatrix} p(t) \\ \theta(t) \end{bmatrix} = \begin{bmatrix} p(t+T) \\ \theta(t+T) \end{bmatrix} \quad (3.1)$$

where $p(t) \in \mathbb{R}^{(2N \times 1)}$ and $\theta(t) \in \mathbb{R}^{(N \times 1)}$ are the agents' position and orientation vectors.

Definition 3. *The instantaneous center of rotation for agent i is denoted by c_i hence:*

$$c_i(t) = p_i(t) + \mathcal{R}(\mathcal{G}, i) \begin{bmatrix} -\sin(\theta_i(t)) \\ \cos(\theta_i(t)) \end{bmatrix} .$$

See illustration in Figure 3.1.

Definition 4. *A system is said to converge to a periodic orbit if there exists some T_c such that for $\forall t > T_c$, the system is periodic.*

Definition 5. *The ray starting at an agent's location and going off in an angle of $\frac{\alpha}{2}$ relative to the agent's body frame is called the agent's dawn horizon, as it is on the outermost edge of the agent's visibility sector in the direction of the agent's rotation. See illustration in Figure 3.2.*

Definition 6. *The ray starting at an agent's location and going off in an angle of $-\frac{\alpha}{2}$ relative to the agent's body frame is called the agent's dusk horizon, as it is on the outermost edge of the agent's visibility sector in the direction opposite of the agent's rotation. See illustration in Figure 3.2.*

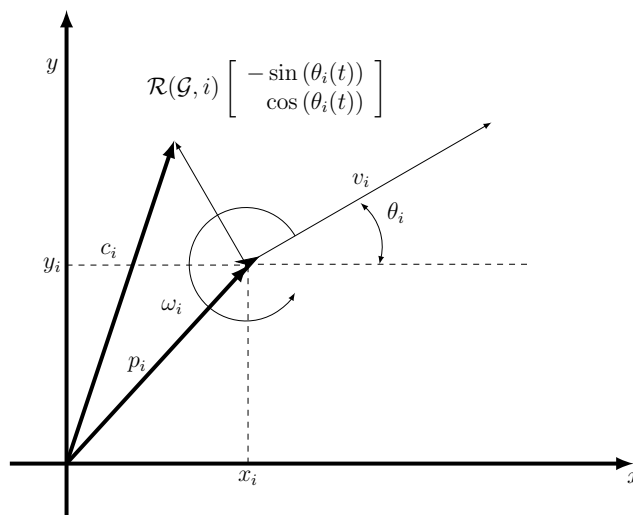


Figure 3.1: The instantaneous center of rotation for agent i

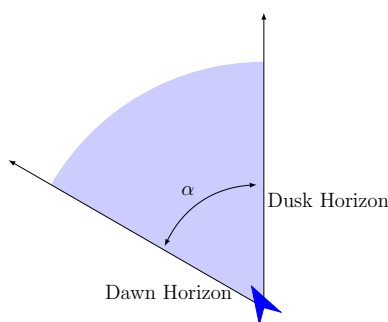


Figure 3.2: The agent seen here has a visibility sector with central angle α , defining its dawn and dusk horizons.

Definition 7. When an agent crosses another agent's horizon it is said to either rise or set. An agent rises over some other agent's horizon if it enters the other agent's field of view. An agent sets over some other agent's horizon if it leaves the other agent's field of view.

Definition 8. If an agent rotates around point c with radius r and field of view angle $0 < \alpha < \pi$, then the circle centered at c with radius $r \cos(\frac{\alpha}{2})$ is called the agent's blind circle, since anything inside this circle is never perceived by it. See illustration in Figure 3.4.

Definition 9. If an agent rotates around point c with radius R and field of view angle $\pi < \alpha < 2\pi$, then the circle centered at c with radius $r \cos(\frac{\alpha}{2})$ is called the agent's vigil circle, since anything inside this circle is perpetually perceived by it. See illustration in Figure 3.5.

Definition 10. A beacon is an agent which is stationary. A beacon is perceived by other agents as another agent.

Definition 11. A multi agent system is said to converge to a moving formation if all agents eventually reach a configuration where their relative positions and velocities are constant.

Definition 12. A multi agent system is said to converge to a behavioral cohesive formation if all agents eventually reach a configuration in which the agents' relative positions are bounded, i.e. there exists an upper bound to the distance between any two agents.

Definition 13. The bearing angle β_{ji} is defined as the argument of agent j 's position vector in agent i 's local frame. In the global frame perspective,

$$\beta_{ji} = \angle(p_j - p_i) - \theta_i.$$

Figure 3.3 shows an illustration of this definition.

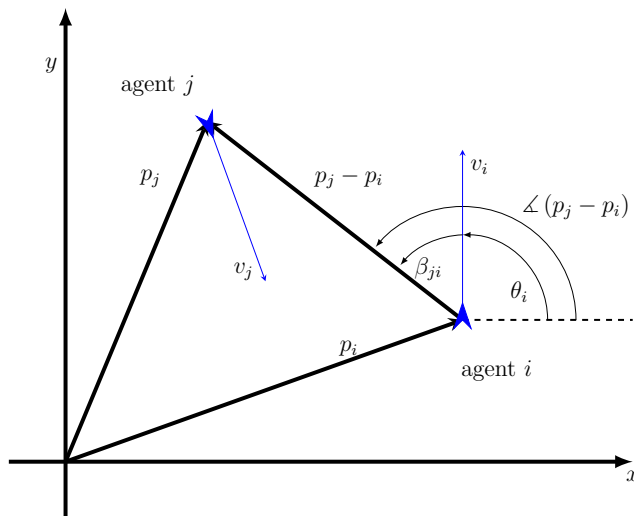


Figure 3.3: The bearing angle β_{ji} .

3.1 A Single Agent and A Beacon

Consider a system comprised of one agent and one static beacon, located without loss of generality at $(0,0)$ in the global frame. Other than being static the beacon is an agent for all purposes, and is detected by the single agent as another agent. In this section $S = 1$, since any other value would cause the agent to never switch turning radii. With $S = 1$, the agent rotates with radius r when not observing the beacon, and R otherwise.

The goal of this section is to show that the system described here converges in linear time to a configuration which is defined and predetermined by the system's parameters (Theorem 3.1.1), where the agent either rotates in a circle with radius r around a fixed point c such that $\|c\| \leq r \cos \frac{\alpha}{2}$ (Lemma 3.1.9), rotates in a circle with radius R around a fixed point c such that $\|c\| \leq R \cos \frac{\alpha}{2}$ (Corollary 3.1.5), or rotates in a circle with radius $r_a \in [r, R]$ around the origin (Corollary 3.1.6). This goal is achieved by showing that a distant agent always gets closer to the beacon (Lemmas 3.1.5, 3.1.6, 3.1.8 and Corollaries 3.1.3, 3.1.4), an agent too close to the beacon gets pushed back (Lemma 3.1.7) and an agent whose center of rotation is located just right stops switching, making the system periodic as described here (Lemma 3.1.1 and Corollary 3.1.1). Lemmas 3.1.2 and 3.1.3 serve to show that Theorem 3.1.1 holds for any initial condition as long as the visibility radius is bigger than the maximal distance between the beacon and the agent along the agent's trajectory.

We shall begin our analysis with Lemma 3.1.1 and Corollary 3.1.1, identifying the conditions under which the system is periodic, i.e. the agent's motion around the beacon is a periodic orbit.

Lemma 3.1.1. *Given a single agent with $0 < \alpha < \pi$ controlled by (2.2) and a beacon located at the origin and perceived as an agent by the single agent's sensors, if at time t_0 , $\|c_a(t_0)\| < r \cos(\frac{\alpha}{2})$, then the system is periodic with*

$$\dot{\theta}_a(t) = \frac{v}{r}.$$

Proof. Figure 3.4 shows the geometry of this proof. Once the beacon enters the inner circle it remains outside of the agent's field of view. Since the beacon is forever outside the agent's field of view, no switching occurs, and the agent remains on the r radius circle with $\dot{\theta}(t) = \frac{v}{r}$, and the system is periodic. \square

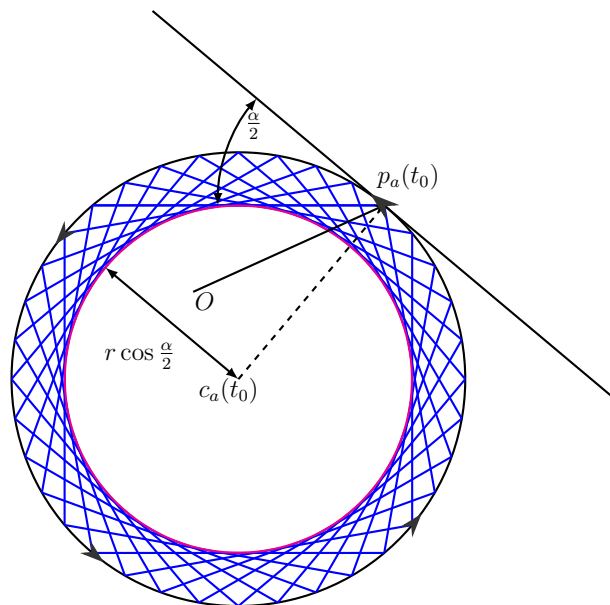


Figure 3.4: An agent traveling upon the r radius circle with α field of view never perceives the beacon (located at O) if it is inside a concentric circle with radius $r \cos\left(\frac{\alpha}{2}\right)$.

Corollary 3.1.1. *Given a single agent with $\pi \leq \alpha < 2\pi$ and $R_v > R(1 - \cos(\frac{\alpha}{2}))$ controlled by (2.2) and a beacon located at the origin and perceived as an agent by the single agent's sensors, if at time t_0 , $\|c_a(t_0)\| \leq -R \cos(\frac{\alpha}{2})$, then the system is periodic with*

$$\dot{\theta}_a(t) = \frac{v}{R}.$$

Proof. Figure 3.5 shows the geometry of this proof. Once the beacon enters the inner circle it remains inside the agent's field of view. Since the beacon is forever inside the agent's field of view, no switching occurs, and the agent remains on the R radius circle with $\dot{\theta}(t) = \frac{v}{R}$, and the system is periodic. \square

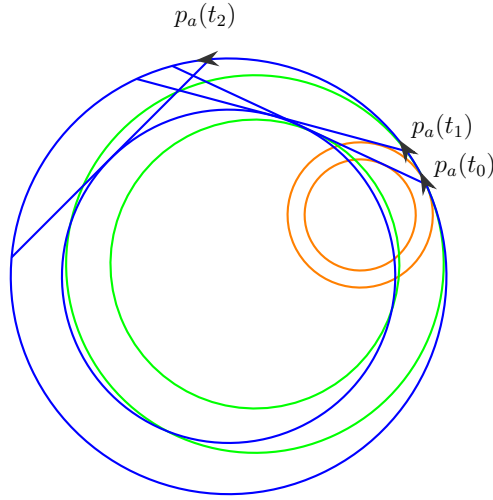


Figure 3.6: The three circles in the diagram that touch at $p_a(t_0)$ have radii R, r_2, r_1 in descending order of magnitude such that $2r_1 < R < 2r_2$. For each circle with radius r , an inner circle with radius $r \cos \frac{\alpha}{2}$ is drawn, and for each agent location $p_a(t)$ presented, a line depicting the agent's field of view limit is drawn as well.

furthest point possible. More accurately put,

$$\begin{cases} \|p_a(t_0^-)\| &= r^- \sin \frac{\alpha}{2} \\ \theta_a(t_0^-) &= \varphi(t_0^-) + \pi - \frac{\alpha}{2}, \end{cases}$$

where t_0^- is an instant just before t_0 and r^- is just a bit smaller than r . In this case, the agent will have to come just under full circle before seeing the beacon again, therefore the configuration depicted by the lemma must be reached in less than $\frac{2\pi r}{v}$ time. \square

Lemma 3.1.3. *Given a single agent with $0 < \alpha < \pi$ and $R_v > \|p_a(t_0)\| + 2r$ controlled by (2.2) and a beacon located at the origin and perceived as an agent by the single agent's sensors, if at time t_0 , $r \leq \|c_a(t_0)\|$, then the system will reach a configuration where $\theta(t) = \varphi(t) + \pi - \frac{\alpha}{2}$, where the agent's position is $p_a(t) = (x_a(t), y_a(t))^T$ and $\varphi(t) = \arctan 2(y_a(t), x_a(t))$ in less than $\frac{2\pi r + (R-r)\alpha}{v}$ time.*

Proof. Similarly to the proof given for Lemma 3.1.2, if the beacon is in the agent's field of view at t_0 , the intersection between all possible locations of the beacon and the agent's field of view reduces to null by the time required for the agent to complete an α arc on the R circle. The fact that $0 < \alpha < \pi$ and $R_v > \|p_a(t_0)\| + 2r$ means that once detected, the beacon leaves the agent's sector of visibility only when setting over its dusk horizon and not by becoming too distant. If the beacon has just left the agent's field of view, then it will take the agent less than $\frac{(2\pi-\alpha)r}{v}$ time to have the beacon enter its field of view again. By assuming $R_v > \|p_a(t_0)\| + 2r$ we can guarantee that when the beacon rises over the agent's dawn horizon, the agent will still be able to detect it. \square

Corollary 3.1.2. *Given a single agent with $\pi \leq \alpha < 2\pi$ and $R_v > \|p_a(t_0)\| + 2R$ controlled by (2.2) and a beacon located at the origin and perceived as an agent by the single agent's sensors, if at time t_0 , $-R \cos\left(\frac{\alpha}{2}\right) \leq \|c_a(t_0)\|$, then the system will reach a configuration where $\theta(t) = \varphi(t) + \pi - \frac{\alpha}{2}$, where the agent's position is $p_a(t) = (x_a(t), y_a(t))^T$ and $\varphi(t) = \arctan 2(y_a(t), x_a(t))$ in less than $\frac{2\pi R}{v}$ time.*

Proof. Since the beacon is out of the vigil circle yet at a distance where the agent is able to detect it even if moving the farthest it can away from the beacon under control (2.2), the beacon is bound to set over the agent's dusk horizon if it is detected at t_0 by $t_0 + \frac{\alpha R}{v}$, only to rise again over the agent's dawn horizon by $t_0 + \frac{\alpha R + (2\pi - \alpha)r}{v}$, or to rise over the agent's dawn horizon if the beacon was out of the agent's field of view at t_0 by $t_0 + \frac{(2\pi - \alpha)r}{v}$. In any case, the beacon rises over the agent's dawn horizon in less than $\frac{2\pi R}{v}$ time. \square

To sum up all previous results, the following lemma is given to formally claim that the beacon-agent system is either periodic from initial conditions, or reaches a point in time where the beacon is rising over the agent's dawn horizon in less than $\frac{2\pi R}{v}$ time.

Lemma 3.1.4. *Given a single agent with $0 < \alpha < 2\pi$ and $R_v > \|p_a(t_0)\| + 2R$ controlled by (2.2) and a beacon located at the origin and perceived as an agent by the single agent's sensors, the system is either periodic or reaches a configuration where $\theta_a(t) = \varphi(t) + \pi - \frac{\alpha}{2}$, where the agent's position is $p_a(t) = (x_a(t), y_a(t))^T$ and $\varphi(t) = \arctan 2(y_a(t), x_a(t))$ in less than $\frac{2\pi R}{v}$ time.*

Proof. Given $0 < \alpha < \pi$, the beacon-agent system is periodic if $\|c_a(t_0)\| < r \cos\left(\frac{\alpha}{2}\right)$ by Lemma 3.1.1. An agent with $0 < \alpha < \pi$ starting at $r \cos\left(\frac{\alpha}{2}\right) \leq \|c_a(t_0)\|$ will detect the beacon within $\max\left(\frac{\alpha R}{v}, \frac{2\pi r}{v}, \frac{2\pi r + (R-r)\alpha}{v}\right) < \frac{2\pi R}{v}$ time by Lemmas 3.1.2 and 3.1.3. Similarly, given $\pi \leq \alpha < 2\pi$, the beacon-agent system is periodic if $\|c_a(t_0)\| \leq -R \cos\left(\frac{\alpha}{2}\right)$ by Corollary 3.1.1, and the agent detects the beacon in less than $\frac{2\pi R}{v}$ time by Corollary 3.1.2 otherwise. \square

The following Lemmas, 3.1.5, 3.1.6, 3.1.8, 3.1.7 and Corollaries, 3.1.3 and 3.1.4 serve to set up a state machine used in Lemma 3.1.9's proof. The state machine has states defined by the agent's distance from the beacon at the moment, denoted t_0 , in which the beacon rises over the agent's dawn horizon for the first time under the conditions defined, i.e. $\theta_a(t_0) = \varphi(t_0) + \pi - \frac{\alpha}{2}$, as shown in Figure 3.7. For the remainder of the discussion, the visibility radius is taken such that it is always greater than the distance between the agent and the beacon, i.e. $R_v > \|p_a(t_0)\| + 2R$.

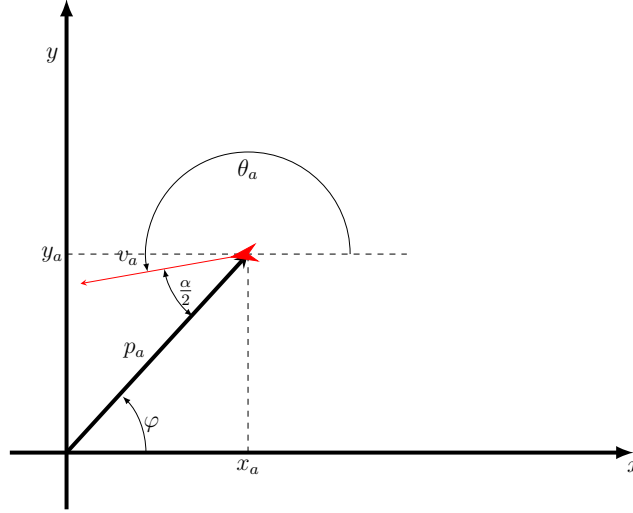


Figure 3.7: A beacon located at an arbitrary global frame origin rises over an agent's dawn horizon.

Lemma 3.1.5. *Given a single agent controlled by (2.2) with $0 < \alpha < 2\pi$ and a beacon located at the origin, for T defined as $T = \frac{2\pi r + \alpha(R - r)}{v}$, and for every $t_0 \leq t \leq t_0 + kT$ and $k \in \mathbb{N}$ such that $\|p_a(t_0 + (k - 1)T)\| \geq 2R \sin(\frac{\alpha}{2})$, where t_0 is the moment when the agent first detected the beacon, the agent approaches the beacon in a periodic manner, described by the following equations:*

$$\left\{ \begin{array}{l} \varphi(t_0 + kT) = \varphi(t_0) \\ \theta_a(t) = \begin{cases} \varphi(t_0) + \pi - \frac{\alpha}{2} + \frac{v}{R}t, & (t_0 + kT) \leq t \leq (t_0 + \frac{\alpha R}{v} + kT) \\ \varphi(t_0) + \pi + \frac{\alpha}{2} + \frac{v}{r}t, & (t_0 + \frac{\alpha R}{v} + kT) < t \leq (t_0 + (k + 1)T) \end{cases} \\ p_a(t) = \begin{cases} p_a(t_0) + R \begin{bmatrix} \sin(\theta_a(t)) - \sin(\theta_a(t_0)) \\ \cos(\theta_a(t_0)) - \cos(\theta_a(t)) \end{bmatrix}, & (t_0 + kT) \leq t \leq (t_0 + \frac{\alpha R}{v} + kT) \\ p_a(t_0) - 2R \sin(\frac{\alpha}{2}) \begin{bmatrix} \cos(\varphi(t_0)) \\ \sin(\varphi(t_0)) \end{bmatrix} + r \begin{bmatrix} \sin(\theta_a(t)) - \sin(\theta_a(t_0 + \frac{\alpha R}{v})) \\ \cos(\theta_a(t_0 + \frac{\alpha R}{v})) - \cos(\theta_a(t)) \end{bmatrix}, & o.w. \end{cases} \\ p_a(t + kT) = p_a(t) + 2k(r - R) \sin(\frac{\alpha}{2}) \begin{bmatrix} \cos(\varphi(t_0)) \\ \sin(\varphi(t_0)) \end{bmatrix}. \end{array} \right. \quad (3.2)$$

Proof. The significance of t_0 is that it is the exact moment when the beacon enters the agent's field of view, causing a transition in the underlying graph from $\deg^-(v_a) = 0$ to $\deg^-(v_a) = 1$, where v_a is the vertex corresponding with the agent in the underlying graph. Figure 3.8 shows a trajectory of an agent returning twice to $\theta_a(t) = \theta_a(t_0)$. Let T be the time it takes an agent

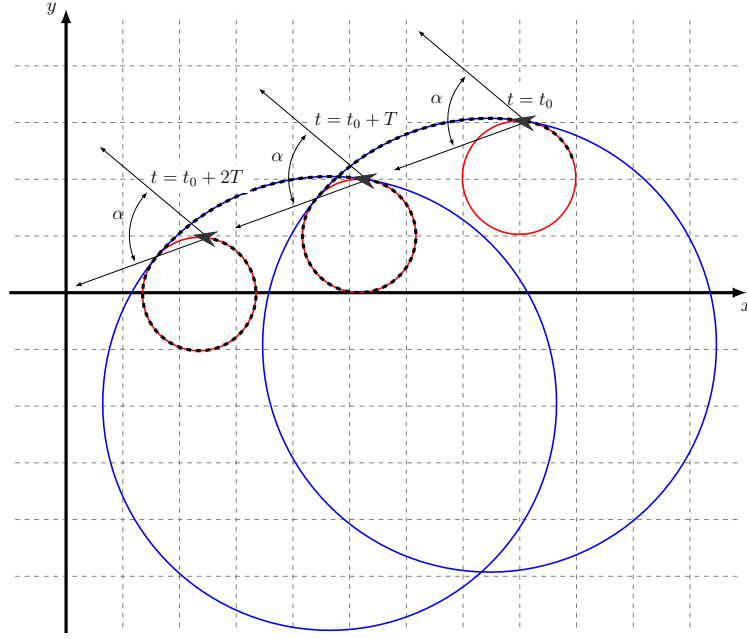


Figure 3.8: An agent moving toward a beacon. Beginning its journey slightly before t_0 , three instances of the agent are shown at $t = t_0$, $t = t_0 + T$ and $t = t_0 + 2T$ for $\alpha = \frac{\pi}{3}$ and $R = 4r$.

to complete a full rotation, i.e., if $\theta_a(t_0) = \theta_0$, then T is the shortest amount of time between t_0 and whenever $\theta_a(t) = \theta_0$ again:

$$\begin{aligned}
 \frac{d\theta_a}{dt} &= \omega_a(t) \\
 &\Downarrow \\
 T &= \int_{t_0}^{t_0+T} dt = \int_{\theta_0}^{\theta_0+2\pi} \frac{d\theta_a}{\omega_a(\theta_a(t))} = \int_{\theta_0}^{\theta_0+\alpha} \frac{d\theta_a}{\omega_a(\theta_a)} + \int_{\theta_0+\alpha}^{\theta_0+2\pi} \frac{d\theta_a}{\omega_a(\theta_a)} \\
 &= \int_{\theta_0}^{\theta_0+\alpha} \frac{R}{v} d\theta_a + \int_{\theta_0+\alpha}^{\theta_0+2\pi} \frac{r}{v} d\theta_a = \frac{R\alpha}{v} + \frac{r(2\pi - \alpha)}{v} \\
 &\Downarrow \\
 T &= \frac{2\pi r + \alpha(R - r)}{v}. \tag{3.3}
 \end{aligned}$$

Figure 3.9 shows a diagram depicting the geometry of this proof. At t_0 , the agent is located at B , with its forward direction tangent to the circles centered at E and A , aligning with \overline{BK} . The segment \overline{BC} is a segment of the line connecting the agent and the beacon. Since $\angle CBK = \frac{\alpha}{2}$, the beacon enters the agent's field of view and the agent switches from traveling upon the circle centered at E with radius r to the circle centered at A with radius R . The agent traverses on the circle centered at A until the beacon leaves the

segment of \overline{BC} , making $\varphi(t_0 + T) = \varphi(t_0)$. Also notice that once reaching H , the beacon enters the agent's field of view once more, and the cycle repeats.

Since \overline{AD} is the altitude of the isosceles triangle $\triangle BAC$, it is also the angle bisector of $\angle BAC = \alpha$ and the perpendicular bisector of \overline{BC} , therefore

$$|BD| = |CD| = R \sin \frac{\alpha}{2} \Rightarrow |BC| = 2R \sin \frac{\alpha}{2}.$$

Using the fact that $\triangle ABC$ is similar to $\triangle GHC$ we get

$$\frac{|CH|}{|BC|} = \frac{r}{R} \Rightarrow |CH| = \frac{2rR \sin \frac{\alpha}{2}}{R} = 2r \sin \frac{\alpha}{2}$$

↓

$$|BH| = 2(R - r) \sin \frac{\alpha}{2}.$$

Since $\varphi(t_0 + T) = \varphi(t_0)$ and the beacon is located at the origin,

$$\|p(t_0)\| - \|p(t_0 + T)\| = |BH| = 2(R - r) \sin \frac{\alpha}{2}.$$

As the only difference in the agent's state after T time is that the agent's location p_a is closer to the beacon, the agent repeats the exact cycle again, as seen in Figure 3.8 for as long as the beacon is outside the circle with radius R when $\theta_a = \theta_0$, i.e., for every $k \in \mathbb{N}$ such that

$$\|p(t_0 + (k - 1)T)\| \geq |BC| = 2R \sin \left(\frac{\alpha}{2}\right).$$

Since the entire cycle is exactly the same as the cycle before, except for a translation transformation $A(p(t), k)$ such that

$$A(p(t), k) = p(t) + 2k(r - R) \sin \left(\frac{\alpha}{2}\right) \begin{bmatrix} \cos(\varphi(t_0)) \\ \sin(\varphi(t_0)) \end{bmatrix}$$

and

$$p_a(t + kT) = A(p_a(t), k) = p_a(t) + 2k(r - R) \sin \left(\frac{\alpha}{2}\right) \begin{bmatrix} \cos(\varphi(t_0)) \\ \sin(\varphi(t_0)) \end{bmatrix},$$

reaching the statement in (3.2). □

Lemma 3.1.6. *Given a single agent controlled by (2.2) with $0 < \alpha < 2\pi$, if $d = \|p_a(t_0)\|$, where t_0 is the moment when the beacon is on the agent's dawn*

horizon such that $1 < \frac{d}{R \sin(\frac{\alpha}{2})} \leq 2$ and $\gamma = 2 \arcsin \left(\frac{d \cos(\frac{\alpha}{2})}{\sqrt{R^2 + d^2 - 2dR \sin(\frac{\alpha}{2})}} \right) - \alpha$,

then

$$\begin{cases} \left\| p_a \left(t_0 + \frac{\gamma R}{v} \right) \right\| &= 2R \sin \left(\frac{\alpha}{2} \right) - d < R \sin \left(\frac{\alpha}{2} \right) \\ \varphi \left(t_0 + \frac{\gamma R}{v} \right) &= \varphi(t_0) + \gamma \\ \theta_a \left(t_0 + \frac{\gamma R}{v} \right) &= \varphi \left(t_0 + \frac{\gamma R}{v} \right) + \pi - \frac{\alpha}{2}. \end{cases} \quad (3.4)$$

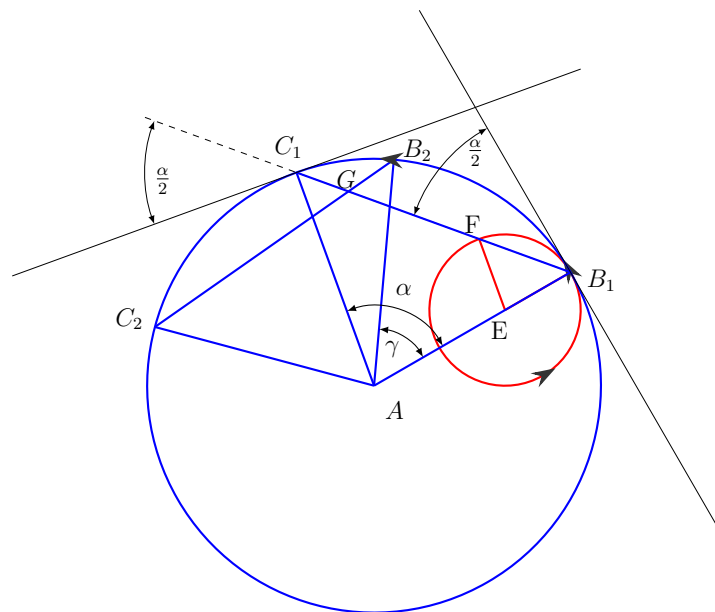


Figure 3.10: An agent traveling upon the circle centered at E reaches point B_1 at t_0 , at which time the beacon located at point G rises over the agent's dawn horizon and the agent consequently switches radius from r to R . When arriving at point B_2 , the beacon sets over the agent's dawn horizon.

Proof. Figure 3.10 shows the geometry used in this proof. Consider a beacon at point G and an agent traveling counter clockwise upon the circle centered at point E , somewhere between points F and B_1 . When the agent reaches B_1 , the beacon enters the agent's field of view and the agent switches from traveling the circle centered at E to the circle centered at A . We denote this moment as t_0 and $d = \|p_a(t_0)\| = |\overline{B_1G}|$. If $d > R \sin(\frac{\alpha}{2})$ then the beacon will stay in the agent's field of view until leaving it at point B_2 .

Notice that $\triangle AB_2C_2$ is $\triangle AB_1C_1$ rotated by γ around A , making the two triangles congruent. These triangles are also isosceles, making

$$\angle AB_1G = \angle AB_2G = \angle AC_1G = \frac{\pi - \alpha}{2}.$$

Furthermore, $\triangle AB_2C_1$ is an isosceles triangle, therefore

$$\angle AB_2C_1 = \angle AC_1B_2.$$

Since:

$$\angle GB_2C_1 = \angle AB_2C_1 - \angle AB_2G$$

and

$$\angle GC_1B_2 = \angle AC_1B_2 - \angle AC_1G,$$

the triangle $\triangle GC_1B_2$ is also isosceles.

Using the law of cosines on the triangle $\triangle AGB_1$,

$$|AG|^2 = R^2 + d^2 - 2dR \cos\left(\frac{\pi - \alpha}{2}\right) = R^2 + d^2 - 2dR \sin\left(\frac{\alpha}{2}\right).$$

Using the law of sines on the triangle $\triangle AGB_1$,

$$\begin{aligned}
\frac{|AG|}{\sin\left(\frac{\pi-\alpha}{2}\right)} &= \frac{d}{\sin\left(\gamma + \frac{\alpha-\gamma}{2}\right)} \\
&\Downarrow \\
\sin\left(\frac{2\gamma + \alpha - \gamma}{2}\right) &= \frac{d}{|AG|} \sin\left(\frac{\pi - \alpha}{2}\right) \\
&\Downarrow \\
\sin\left(\frac{\alpha + \gamma}{2}\right) &= \frac{d}{|AG|} \cos\left(\frac{\alpha}{2}\right) \\
&\Downarrow \\
\frac{\alpha + \gamma}{2} &= \arcsin\left(\frac{d}{|AG|} \cos\left(\frac{\alpha}{2}\right)\right) \\
&\Downarrow \\
\gamma &= 2 \arcsin\left(\frac{d}{|AG|} \cos\left(\frac{\alpha}{2}\right)\right) - \alpha \\
&\Downarrow \\
\gamma &= 2 \arcsin\left(\frac{d \cos\left(\frac{\alpha}{2}\right)}{\sqrt{R^2 + d^2 - 2dR \sin\left(\frac{\alpha}{2}\right)}}\right) - \alpha.
\end{aligned}$$

Since the agent travels at v speed, it will take it T time to reach B_2 from B_1 where

$$T = \frac{\gamma R}{v}.$$

Once reaching B_2 , using the fact that $\triangle GC_1B_2$ is isosceles and $|\overline{B_1C_1}| = 2R \sin\left(\frac{\alpha}{2}\right)$, we get

$$\left\|p\left(t_0 + \frac{\gamma R}{v}\right)\right\| = 2R \sin\left(\frac{\alpha}{2}\right) - d.$$

Also,

$$\begin{aligned}
\angle AB_1G &= \angle GB_2A \\
&\Downarrow \\
\angle B_1AB_2 &= \angle B_2GB_1 = \gamma \\
&\Downarrow \\
\varphi\left(t_0 + \frac{\gamma R}{v}\right) &= \varphi(t_0) + \gamma.
\end{aligned}$$

Finally, since the beacon leaves the agent's field of view at B_2 :

$$\theta_a\left(t_0 + \frac{\gamma R}{v}\right) = \varphi\left(t_0 + \frac{\gamma R}{v}\right) + \pi - \frac{\alpha}{2}.$$

□

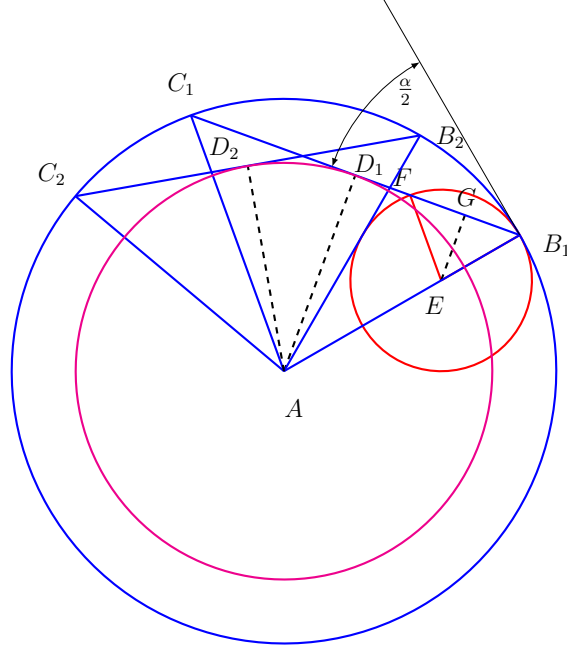


Figure 3.11: The outer circle centered at A has a R radius, the inner circle centered at A has a $R \cos\left(\frac{\alpha}{2}\right)$ radius.

Lemma 3.1.7. *Given a single agent controlled by (2.2) with $0 < \alpha < 2\pi$ such that $d = \|p_a(t_0)\|$, where t_0 is the moment when the beacon is on the agent's dawn horizon and $0 \leq d < r \sin\left(\frac{\alpha}{2}\right)$, then*

$$\begin{cases} \|p_a(t_0 + T)\| &= 2r \sin\left(\frac{\alpha}{2}\right) - d > r \sin\left(\frac{\alpha}{2}\right) \\ \varphi(t_0 + T) &= \varphi(t_0) + \gamma \\ \theta_a(t_0 + T) &= \varphi(t_0 + T) + \pi - \frac{\alpha}{2} \end{cases} \quad (3.5)$$

where $T = \frac{r\gamma}{v}$ and $\gamma = 2\pi + 2 \arcsin\left(\frac{d \cos\left(\frac{\alpha}{2}\right)}{\sqrt{d^2 + r^2 - 2dr \sin\left(\frac{\alpha}{2}\right)}}\right) - \alpha$.

Proof. Figure 3.12 shows the geometry of this proof. Consider a beacon at point G and an agent at point B_1 traveling upon the circle with radius r centered at point A . Even though the agent perceives the beacon, any infinitesimal movement in the agent's direction θ perpendicular to $\overline{AB_1}$ would result in the beacon leaving the agent's field of view and the agent continuing on the circle with radius r centered at A . The next time the agent perceives the beacon would be after it has traversed an arc length of $r\gamma$ and has arrived at point B_2 . Traversing an arc of $r\gamma$ length at constant speed v takes $T = \frac{r\gamma}{v}$ time. Using the cosine law on $\triangle AGB_1$ we get

$$\begin{aligned} |\overline{AG}|^2 &= |\overline{GB_1}|^2 + |\overline{AB_1}|^2 - 2|\overline{GB_1}||\overline{AB_1}|\cos(\angle AB_1G) \\ &= d^2 + r^2 - 2dr \cos\left(\frac{\pi - \alpha}{2}\right) = d^2 + r^2 - 2dr \sin\left(\frac{\alpha}{2}\right). \end{aligned}$$

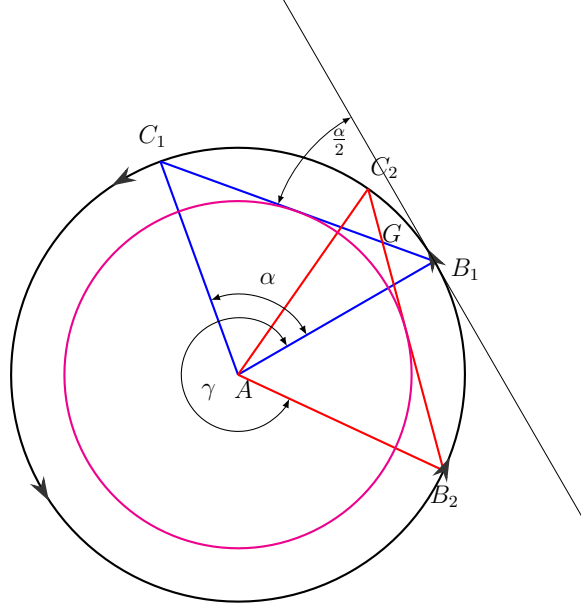


Figure 3.12: An agent traveling from point B_1 away from a beacon located at point G .

Using the sine law on $\triangle AGB_1$ we get

$$\begin{aligned}
 \frac{|\overline{AG}|}{\sin\left(\frac{\pi-\alpha}{2}\right)} &= \frac{|\overline{B_1G}|}{\sin(\angle GAB_1)} = \frac{d}{\sin\left(\frac{\alpha+\gamma}{2} - \pi\right)} \\
 &\Downarrow \\
 \frac{\sqrt{d^2 + r^2 - 2dr \sin\left(\frac{\alpha}{2}\right)}}{\cos\left(\frac{\alpha}{2}\right)} &= \frac{d}{\sin\left(\frac{\alpha+\gamma}{2} - \pi\right)} \\
 &\Downarrow \\
 \sin\left(\frac{\alpha+\gamma}{2} - \pi\right) &= \frac{d \cos\left(\frac{\alpha}{2}\right)}{\sqrt{d^2 + r^2 - 2dr \sin\left(\frac{\alpha}{2}\right)}} \\
 &\Downarrow \\
 \gamma &= 2\pi + 2 \arcsin\left(\frac{d \cos\left(\frac{\alpha}{2}\right)}{\sqrt{d^2 + r^2 - 2dr \sin\left(\frac{\alpha}{2}\right)}}\right) - \alpha.
 \end{aligned}$$

Since triangles $\triangle AB_1C_1$ $\triangle AB_2C_2$ are congruent and $\triangle AB_1C_2$ is an isosceles triangle,

$$\angle AB_1C_2 = \angle AC_2B_1$$

along with the congruent angles

$$\angle AB_1G = \angle AC_2G$$

identifying $\triangle GB_1C_2$ as an isosceles triangle by $\angle GB_1C_2 = \angle GC_2B_1$ with $d = |B_1G| = |C_2G|$. Therefore

$$\|p(t_0 + T)\| = |\overline{B_2G}| = |\overline{B_2C_2}| - |\overline{GC_2}| = 2r \sin\left(\frac{\alpha}{2}\right) - d.$$

□

The agent's behavior as described in Lemmas 3.1.5, 3.1.6 and 3.1.7 can be viewed as a transition from one system state to another state, beacon rise to beacon rise over the agent's dawn horizon. The next lemma and its corollaries correspond to a *sink state*, i.e. there is no transition out of the system state described therein, and this final state is such that brings the agent-beacon system to its final periodic orbit.

Lemma 3.1.8. *Given a single agent controlled by (2.2) with $0 < \alpha < \pi$ such that $d = \|p_a(t_0)\|$, where t_0 is the moment when the beacon is on the agent's dawn horizon and $r \sin(\frac{\alpha}{2}) \leq d \leq R \sin(\frac{\alpha}{2})$, then*

$$\begin{cases} \|p_a(t_0 + T)\| &= r \sin(\frac{\alpha}{2}) \\ \varphi(t_0 + T) &= \varphi(t_0) + \tan(\frac{\alpha}{2})(\ln(d) - \ln(r \sin(\frac{\alpha}{2}))) \\ \theta_a(t_0 + T) &= \varphi(t_0 + T) + \pi - \frac{\alpha}{2} \end{cases} \quad (3.6)$$

$$\text{where } T = \frac{d - r \sin(\frac{\alpha}{2})}{v \cos(\frac{\alpha}{2})}.$$

Proof. Consider the diagram presented in Figure 3.14. As long as the beacon is on the segment \overline{GD} , any movement the agent makes with $\omega_a = \frac{v}{R}$ will cause the beacon to slip out of the agent's field of view, while any movement the agent makes with $\omega_a = \frac{v}{r}$ pushes the beacon deeper into the agent's field of view. Yet, when the beacon is within the agent's field of view the agent has $\omega_a = \frac{v}{R}$ and when not the agent moves with $\omega_a = \frac{v}{r}$. This type of control is called *Sliding Mode Control*, and it serves this case by maintaining the beacon exactly at $\frac{\alpha}{2}$ in the agent's body frame for as long as $r \sin \frac{\alpha}{2} \leq \|p_a(t)\| \leq R \sin \frac{\alpha}{2}$ as will be shown presently.

Let β_{ba} be the beacon's bearing angle from the agent's perspective, and let β_r be the angle at which the beacon rises over the agent's dawn horizon, i.e. $\beta_r(y_a, x_a) = \arctan 2(y_a, x_a) + \pi - \frac{\alpha}{2}$. Similarly, let β_s be the angle at which the beacon sets over the agent's dusk horizon, i.e. $\beta_s(y_a, x_a) = \arctan 2(y_a, x_a) + \pi + \frac{\alpha}{2}$.

Let $X : \mathbb{R}^3 \mapsto \mathbb{R}^3$ be the vector field describing the agent's control input given the agent's state such that:

$$X(x_a, y_a, \theta_a) = \begin{cases} (v \cos \theta_a, v \sin \theta_a, \frac{v}{R}) & \left| \beta_r(y_a, x_a) + 2\pi k \leq \theta_a \leq \beta_r(y_a, x_a) + 2\pi(k+1) \right. \\ (v \cos \theta_a, v \sin \theta_a, \frac{v}{r}) & \left| \beta_s(y_a, x_a) + 2\pi k < \theta_a < \beta_s(y_a, x_a) + 2\pi(k+1) \right. \end{cases}$$

The vector field X is *piecewise continuous* in the sense that for every $k \in \mathbb{Z}$ and $2\pi k < \theta_a \leq 2\pi(k+1)$, the $\mathcal{D}_k \in \mathbb{R}^3$ space where

$$\mathcal{D}_k = \{(-\infty, \infty) \times (-\infty, \infty) \times (2\pi k, 2\pi(k+1))\} \setminus (0, 0, \theta)$$

can be divided into 2 disjoint, open, and connected sets $\mathcal{D}_{r,k}, \mathcal{D}_{R,k}$ as seen in Figure 3.13, in which X has a constant, hence continuous, value and $\mathbb{R}^3 = \bigcup_k \mathcal{D}_k$, where $\overline{\mathcal{D}_k} = \overline{\mathcal{D}_{r,k}} \cup \overline{\mathcal{D}_{R,k}}$ and $\overline{\mathcal{D}_{i,k}}$ is the closure of $\mathcal{D}_{i,k}$. Let $S_X = \{\theta_a = \beta_r + 2\pi k\}$ be the set of points at which X is discontinuous such that the agent has the beacon on its dawn horizon and $r \sin(\frac{\alpha}{2}) \leq \|p_a(t)\| \leq R \sin(\frac{\alpha}{2})$,

and let $X_{\mathcal{D}^+} = (v \cos \theta_a, v \sin \theta_a, \frac{v}{R})$ be the continuous extension of X to S_X "above" the S_X spiral and $X_{\mathcal{D}^-} = (v \cos \theta_a, v \sin \theta_a, \frac{v}{r})$ "under" the S_X spiral. Notice that $X_{\mathcal{D}^+}$, $X_{\mathcal{D}^-}$ and $(X_{\mathcal{D}^-} - X_{\mathcal{D}^+}) = (0, 0, \frac{(R-r)v}{Rr})$ are all constant and therefore continuously differential on S_X . The Filippov set-value map in the vicinity of S_X is therefore given as:

$$F[X](x, y, \theta) = F[X](u) = \overline{\text{co}} \left\{ \lim_{i \rightarrow \infty} X(u_i) : u_i \rightarrow u, u_i \notin S_X \right\}$$

$$= \begin{cases} \begin{pmatrix} v \cos \theta, v \sin \theta, \frac{v}{R} \end{pmatrix} & \left| \begin{array}{l} \beta_r + 2\pi k < \theta < \beta_s + 2\pi k \\ \theta = \beta_r + 2\pi k \end{array} \right. \\ \begin{pmatrix} v \cos \theta, v \sin \theta, [\frac{v}{R}, \frac{v}{r}] \end{pmatrix} & \\ \begin{pmatrix} v \cos \theta, v \sin \theta, \frac{v}{r} \end{pmatrix} & \left| \begin{array}{l} \beta_s + 2\pi k < \theta < \beta_r + 2\pi(k+1) \end{array} \right. \end{cases}$$

where $\overline{\text{co}}$ stands for convex closure. Notice that for an agent with configuration $u \in \{S_X \setminus (0, 0, \theta)\}$:

$$\begin{aligned} \dot{\theta}_a &= \frac{d}{dt} (\beta_r(x_a, y_a) + 2\pi k) = \frac{d}{dt} \left(\arctan 2(y_a, x_a) - \frac{\alpha}{2} + 2\pi k \right) \\ &= \frac{d}{dt} \arctan \left(\frac{y_a}{x_a} \right) = \frac{1}{1 + \left(\frac{y_a}{x_a} \right)^2} \frac{d}{dt} \left(\frac{y_a}{x_a} \right) \\ &= \frac{x_a^2 y_a \dot{x}_a - y_a x_a \dot{y}_a}{x_a^2 + y_a^2} = \frac{x_a v \sin \theta_a - y_a v \cos \theta_a}{\|p_a\|^2} \\ &= \frac{\|p_a\| v (\cos(\theta_a + \frac{\alpha}{2} - \pi) \sin \theta_a - \sin(\theta_a + \frac{\alpha}{2} - \pi) \cos \theta_a)}{\|p_a\|^2} \\ &= \frac{v}{\|p_a\|} \sin \left(\pi - \frac{\alpha}{2} \right) = \frac{v}{\|p_a\|} \sin \left(\frac{\alpha}{2} \right) \end{aligned}$$

For each agent configuration $u \in S_X$, i.e. $(x_a, y_a, \theta_a) \in S_X$, the vector $X_{\mathcal{D}^+}(u) = (v \cos \theta_a, v \sin \theta_a, \frac{v}{R})$ either points into \mathcal{D}^- ,

$$\|p_a\| < R \sin \left(\frac{\alpha}{2} \right) \Rightarrow \frac{v}{R} < \frac{v}{\|p_a\|} \sin \left(\frac{\alpha}{2} \right),$$

or points into S_X ,

$$\|p_a\| = R \sin \left(\frac{\alpha}{2} \right) \Rightarrow \frac{v}{R} = \frac{v}{\|p_a\|} \sin \left(\frac{\alpha}{2} \right).$$

Similarly, for each $u = (x_a, y_a, \theta_a) \in S_X$, the vector $X_{\mathcal{D}^-}(u) = (v \cos \theta_a, v \sin \theta_a, \frac{v}{r})$ either points into \mathcal{D}^+ ,

$$\|p_a\| > r \sin \left(\frac{\alpha}{2} \right) \Rightarrow \frac{v}{r} > \frac{v}{\|p_a\|} \sin \left(\frac{\alpha}{2} \right),$$

or points into S_X ,

$$\|p_a\| = r \sin \left(\frac{\alpha}{2} \right) \Rightarrow \frac{v}{r} = \frac{v}{\|p_a\|} \sin \left(\frac{\alpha}{2} \right).$$

Hence, by proposition 5 in [5], there exists a unique Filippov solution for (2.1) with control inputs (2.2) for every initial condition $r \sin(\frac{\alpha}{2}) < \|p_a(t_0)\| < R \sin(\frac{\alpha}{2})$, and in particular for $u \in S_X$, the agent's dynamics become

$$\begin{pmatrix} \dot{x}_a \\ \dot{y}_a \\ \dot{\theta}_a \end{pmatrix} = \begin{pmatrix} v \cos \theta_a \\ v \sin \theta_a \\ \frac{v}{\|p_a\|} \sin \left(\frac{\alpha}{2} \right) \end{pmatrix} \quad (3.7)$$

resulting in a solution for $\dot{u} = X(u)$ which slides along S_X and maintains the beacon on the agent's dawn horizon while sliding.

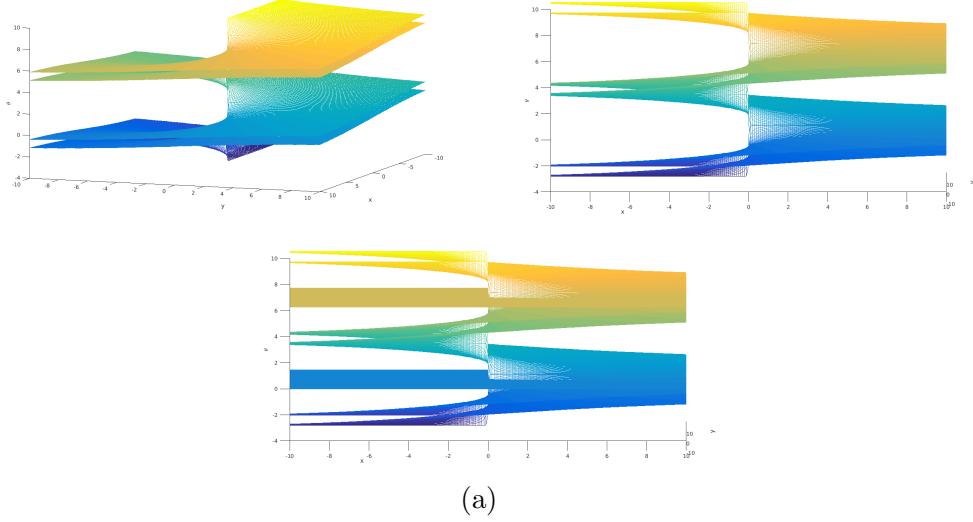


Figure 3.13: The surfaces $\theta = \beta_r + 2\pi k$ (lower) and $\theta = \beta_s + 2\pi k$ (upper), with $k \in \{0, 1\}$ and $\alpha = \frac{\pi}{4}$. In 3.13a, $\mathcal{D}_0 = \{(-\infty, \infty) \times (-\infty, \infty) \times (0, 2\pi] \setminus (0, 0, \theta)\}$ is shown to be divided into 2 disjoint, open, and connected sets.

Since the beacon is maintained at $\frac{\alpha}{2}$ in the agent's body frame, the agent spirals into the beacon with a radial velocity of $v \cos\left(\frac{\alpha}{2}\right)$ towards the beacon, and tangent velocity $v \sin\left(\frac{\alpha}{2}\right)$, as seen in Figure 3.14, and the distance between the agent and the beacon becomes $r \sin\left(\frac{\alpha}{2}\right)$ after T time,

$$v \cos\left(\frac{\alpha}{2}\right) T = d - r \sin\left(\frac{\alpha}{2}\right).$$

Solving for T results in

$$T = \frac{d - r \sin\left(\frac{\alpha}{2}\right)}{v \cos\left(\frac{\alpha}{2}\right)}.$$

Since the agent spirals towards the beacon with angular velocity $\omega_b(t) = \frac{v \sin\left(\frac{\alpha}{2}\right)}{\|p_a(t)\|}$, we can calculate the location of the agent in the global coordinates at the moment when $\|p_a(t)\| = \|p_a(t_0 + T)\| = r \sin\left(\frac{\alpha}{2}\right)$,

$$\begin{aligned} \varphi(t_0 + T) &= \varphi(t_0) + \int_{t_0}^{t_0+T} \omega_b(t) dt \\ &= \varphi(t_0) + \int_{t_0}^{t_0+T} \frac{v \sin\left(\frac{\alpha}{2}\right)}{\|p_a(t)\|} dt = \varphi(t_0) + \int_{t_0}^{t_0+T} \frac{v \sin\left(\frac{\alpha}{2}\right)}{\|p_a(t_0)\| - v \cos\left(\frac{\alpha}{2}\right) (t - t_0)} dt \\ &= \varphi(t_0) - \tan \frac{\alpha}{2} \int_{t_0}^{t_0+T} \frac{-v \cos\left(\frac{\alpha}{2}\right)}{d - v \cos\left(\frac{\alpha}{2}\right) t + v \cos\left(\frac{\alpha}{2}\right) t_0} dt \end{aligned}$$

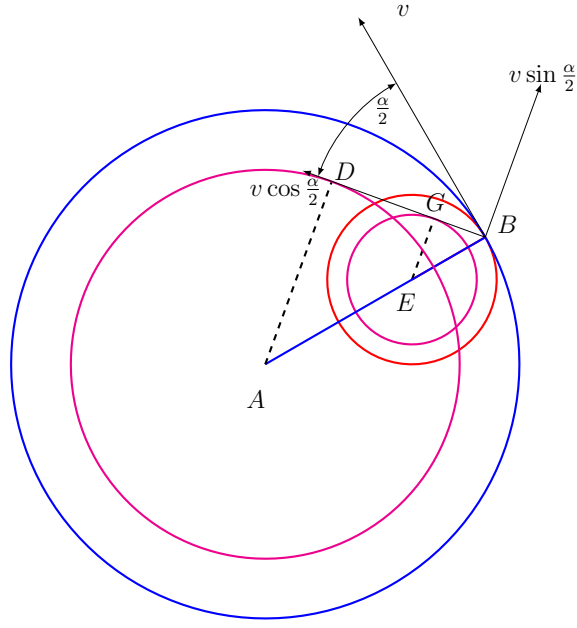


Figure 3.14: A single agent spiraling towards a beacon with $0 < \alpha < \pi$. If the beacon is anywhere on the segment between points G and D , then the agent, detecting the beacon, travels on the circle centered at A , causing the beacon to set over the agent's dawn horizon, which in turn brings the agent to switch and travel upon the circle centered at E , bringing the beacon to rise over the agent's dawn horizon, making the agent travel upon the circle centered at A and so forth.

$$\begin{aligned}
 &= \varphi(t_0) - \tan\left(\frac{\alpha}{2}\right) \left[\ln\left(d + v \cos\left(\frac{\alpha}{2}\right) t_0 - v \cos\left(\frac{\alpha}{2}\right) t\right) \right]_{t_0}^{t_0+T} \\
 &= \varphi(t_0) + \tan\left(\frac{\alpha}{2}\right) \left(\ln(d) - \ln\left(d - v \cos\left(\frac{\alpha}{2}\right) T\right) \right) \\
 &= \varphi(t_0) + \tan\left(\frac{\alpha}{2}\right) \left(\ln(d) - \ln\left(r \sin\left(\frac{\alpha}{2}\right)\right) \right).
 \end{aligned}$$

Notice that at $t = t_0 + T$, $\omega_b = \frac{v}{r}$. □

Corollary 3.1.3. *Given a single agent controlled by (2.2) with $\alpha = \pi$ such that $d = \|p_a(t_0)\|$, where t_0 is the moment when the beacon is on the agent's dawn horizon and $r \leq d \leq R$, then the system is periodic with period $T = \frac{2\pi d}{v}$.*

Proof. Similar to the proof given for Lemma 3.1.8, the same considerations lead the agent with $\alpha = \pi$ to maintain the beacon at $\frac{\pi}{2}$ in the agent's body frame, essentially orbiting the beacon with the dynamics described in equation 3.7,

$$\begin{pmatrix} \dot{x}_a \\ \dot{y}_a \\ \dot{\theta}_a \end{pmatrix} = \begin{pmatrix} v \cos \theta_a \\ v \sin \theta_a \\ \frac{v}{\|p_a\|} \sin\left(\frac{\pi}{2}\right) \end{pmatrix} = \begin{pmatrix} v \cos \theta_a \\ v \sin \theta_a \\ \frac{v}{d} \end{pmatrix}.$$

□

Corollary 3.1.4. *Given a single agent controlled by (2.2) with $\pi < \alpha < 2\pi$ such that $d = \|p_a(t_0)\|$, where t_0 is the moment when the beacon is on the agent's dawn horizon and $r \sin(\frac{\alpha}{2}) \leq d \leq R \sin(\frac{\alpha}{2})$, then*

$$\begin{cases} \|p_a(t_0 + T)\| &= R \sin(\frac{\alpha}{2}) \\ \varphi(t_0 + T) &= \varphi(t_0) + \tan(\frac{\alpha}{2})(\ln(d) - \ln(2d - R \sin(\frac{\alpha}{2}))) \\ \theta_a(t_0 + T) &= \varphi(t_0 + T) + \pi - \frac{\alpha}{2} \end{cases} \quad (3.8)$$

where $T = \frac{R \sin(\frac{\alpha}{2}) - d}{v \cos(\frac{\alpha}{2})}$.

Proof. Similar to the proof given for Lemma 3.1.8, the same considerations lead the agent with $\pi < \alpha < 2\pi$ to maintain the beacon at $\frac{\alpha}{2}$ in the agent's body frame. The agent therefore spirals away from the beacon with a radial velocity of $v \cos \frac{\alpha}{2}$, and tangent velocity $v \sin \frac{\alpha}{2}$, as seen in Figure 3.15. The distance between the agent and the beacon becomes $R \sin(\frac{\alpha}{2})$ after T time,

$$v \cos\left(\frac{\alpha}{2}\right) T = R \sin\left(\frac{\alpha}{2}\right) - d$$

↓

$$T = \frac{R \sin\left(\frac{\alpha}{2}\right) - d}{v \cos\left(\frac{\alpha}{2}\right)}.$$

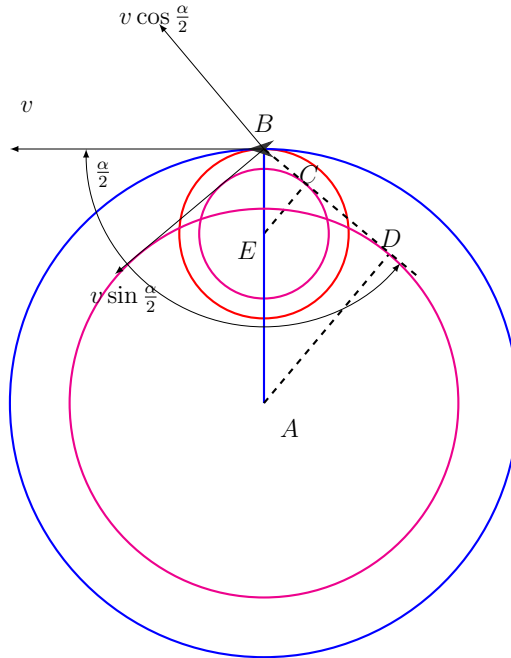


Figure 3.15: A single agent spiraling away from a beacon with $\pi < \alpha < 2\pi$.

Since the agent spirals away from the beacon with angular velocity $\omega_b(t) = \frac{v \sin(\frac{\alpha}{2})}{\|p_a(t)\|}$, we can calculate the location of the agent in the global coordinates

at the moment when $\|p_a(t)\| = \|p_a(t_0 + T)\| = R \sin\left(\frac{\alpha}{2}\right)$:

$$\begin{aligned}
\varphi(t_0 + T) &= \varphi(t_0) + \int_{t_0}^{t_0+T} \omega_b(t) dt \\
&= \varphi(t_0) + \int_{t_0}^{t_0+T} \frac{v \sin\left(\frac{\alpha}{2}\right)}{\|p_a(t)\|} dt = \varphi(t_0) + \int_{t_0}^{t_0+T} \frac{v \sin\left(\frac{\alpha}{2}\right)}{\|p_a(t_0)\| - v \cos\left(\frac{\alpha}{2}\right) (t - t_0)} dt \\
&= \varphi(t_0) - \tan \frac{\alpha}{2} \int_{t_0}^{t_0+T} \frac{-v \cos\left(\frac{\alpha}{2}\right)}{d - v \cos\left(\frac{\alpha}{2}\right) t + v \cos\left(\frac{\alpha}{2}\right) t_0} dt \\
&= \varphi(t_0) - \tan\left(\frac{\alpha}{2}\right) \left[\ln\left(d + v \cos\left(\frac{\alpha}{2}\right) t_0 - v \cos\left(\frac{\alpha}{2}\right) t\right) \right]_{t_0}^{t_0+T} \\
&= \varphi(t_0) + \tan\left(\frac{\alpha}{2}\right) \left(\ln(d) - \ln\left(d - v \cos\left(\frac{\alpha}{2}\right) T\right) \right) \\
&= \varphi(t_0) + \tan\left(\frac{\alpha}{2}\right) \left(\ln(d) - \ln\left(2d - R \sin\left(\frac{\alpha}{2}\right)\right) \right).
\end{aligned}$$

Notice that at $t = t_0 + T$, $\omega_b = \frac{v}{R}$. \square

Lemma 3.1.9 and its Corollaries, 3.1.5 and 3.1.6, use the results obtained so far to set the stage for Theorem 3.1.1.

Lemma 3.1.9. *A system consisting of a single agent controlled by (2.2) with $0 < \alpha < \pi$ and a beacon located at the origin and perceived as an agent by the single agent's sensors converges to a trajectory having an invariant center of rotation $\|c_a(t)\| \leq r \cos\left(\frac{\alpha}{2}\right)$ for $t \geq t_{\text{initial}} + T_{\text{total}}(\|c_a(t_{\text{initial}})\|)$ where*

$$\begin{aligned}
T_{\text{total}}(x) &= \frac{2\pi r + \alpha(R - r)}{2v(R - r) \sin\left(\frac{\alpha}{2}\right)} x + \frac{R - r}{v} \tan\left(\frac{\alpha}{2}\right) \\
&+ \frac{3\alpha R + (6\pi + \alpha)r}{v} + \frac{(2\pi + \alpha)r^2}{v(R - r)} + \frac{\alpha R + 2\pi r}{2v \sin\left(\frac{\alpha}{2}\right)} + \frac{\pi r^2}{v(R - r) \sin\left(\frac{\alpha}{2}\right)}.
\end{aligned}$$

Proof. If the initial conditions are such that $\|c_a(t = 0)\| < r \cos\left(\frac{\alpha}{2}\right)$, then by Lemma 3.1.1, the system is periodic. By Lemmas 3.1.2 and 3.1.3, for every $\|c_a(t = 0)\| \geq r \cos\left(\frac{\alpha}{2}\right)$, the beacon enters the agent's field of view in less than $T_S = \frac{2\pi r + \alpha R}{v}$ time, putting the system at the starting configuration required for each of the Lemmas 3.1.5, 3.1.6, 3.1.8, 3.1.7. Following the dynamics described in this section, each of the lemmas 3.1.5, 3.1.6, 3.1.8, 3.1.7 corresponds with a transition in a state machine, where the states are ranges of $\|p_a(t)\|$ at the point in time where $\theta_a(t) = \varphi(t) + \pi - \frac{\alpha}{2}$, and the transitions between states reflect where the agent will be the next time $\theta_a(t) = \varphi(t) + \pi - \frac{\alpha}{2}$.

Figure 3.16 shows two state machines corresponding with $R < 2r$ and $R \geq 2r$ configurations. In both configurations shown, state E is the state representing all cases where $\|p_a(t_0)\| \geq 2R \sin\left(\frac{\alpha}{2}\right)$ and $\theta_a(t_0) = \varphi(t_0) + \pi - \frac{\alpha}{2}$. By Lemma

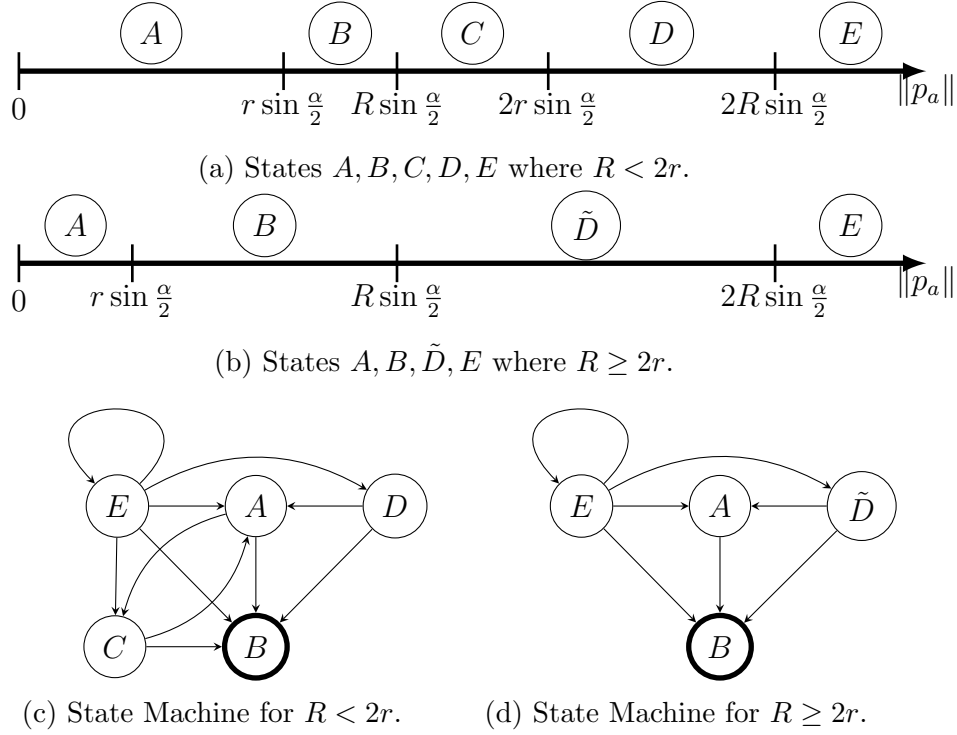


Figure 3.16

3.1.5, $\theta_a \left(t_0 + k \left(\frac{2\pi r + \alpha(R-r)}{v} \right) \right) = \theta_a(t_0)$, $\varphi \left(t_0 + k \left(\frac{2\pi r + \alpha(R-r)}{v} \right) \right) = \varphi(t_0)$ and

$$\left\| p_a \left(t_0 + (k-1) \left(\frac{2\pi r + \alpha(R-r)}{v} \right) \right) \right\| \geq 2R \sin \left(\frac{\alpha}{2} \right)$$

remaining in state E for as long as $t \leq t_0 + (k-1) \left(\frac{2\pi r + \alpha(R-r)}{v} \right)$, at which point $\|p_a(t)\| < 2R \sin \left(\frac{\alpha}{2} \right)$ and the state machine transitions into one of the other states. Given a distance d_0 at which the agent entered state E for the first time and is at most $\|c_a(t_{initial})\| + R$, the total time an agent spends in state E is $T_E = \left\lfloor \frac{d_0}{2(R-r) \sin \left(\frac{\alpha}{2} \right)} \right\rfloor \frac{2\pi r + \alpha(R-r)}{v}$.

Similarly, state A is the state representing all cases where $\|p_a(t_0)\| < r \sin \frac{\alpha}{2}$ and $\theta_a(t_0) = \varphi(t_0) + \pi - \frac{\alpha}{2}$. By Lemma 3.1.7,

$$\begin{aligned} & \theta_a \left(t_0 + \frac{r \left(2\pi + 2 \arcsin \left(\frac{\|p_a(t_0)\| \cos \left(\frac{\alpha}{2} \right)}{\sqrt{\|p_a(t_0)\|^2 + r^2 - 2\|p(t_0)\| r \sin \left(\frac{\alpha}{2} \right)}} \right) - \alpha \right)}{v} \right) \\ &= \varphi \left(t_0 + \frac{r \left(2\pi + 2 \arcsin \left(\frac{\|p_a(t_0)\| \cos \left(\frac{\alpha}{2} \right)}{\sqrt{\|p_a(t_0)\|^2 + r^2 - 2\|p(t_0)\| r \sin \left(\frac{\alpha}{2} \right)}} \right) - \alpha \right)}{v} \right) + \pi - \frac{\alpha}{2} \end{aligned}$$

and

$$r \sin\left(\frac{\alpha}{2}\right) < \left\| p_a \left(t_0 + \frac{r \left(2\pi + 2 \arcsin \left(\frac{\|p_a(t_0)\| \cos\left(\frac{\alpha}{2}\right)}{\sqrt{\|p_a(t_0)\|^2 + r^2 - 2\|p_a(t_0)\| r \sin\left(\frac{\alpha}{2}\right)}} \right) - \alpha \right)}{v} \right) \right\| \leq 2r \sin\left(\frac{\alpha}{2}\right),$$

transitioning from A to B if $R \geq 2r$ or to either B or C if $R < 2r$. In the worst case, where $\|p_a(t_0)\| = r \sin\left(\frac{\alpha}{2}\right) - \varepsilon$ for a positive yet arbitrarily small ε , the state machine will transition out of state A in $T_A = \frac{2\pi r}{v}$ time.

State B represents all cases in which $r \sin\frac{\alpha}{2} \leq \|p_a(t_0)\| \leq R \sin\frac{\alpha}{2}$ and $\theta_a(t_0) = \varphi(t_0) + \pi - \frac{\alpha}{2}$. By Lemma 3.1.8, state B is a sink state which brings the system to $\|p_a(t_0)\| = r \sin\left(\frac{\alpha}{2}\right)$, $\|c(t)\| = r \cos\left(\frac{\alpha}{2}\right)$ and $\theta_a(t) = \theta_a(t_0) + \frac{v}{r}(t - t_0)$, at which point the system is periodic. In the worst case, where $\|p_a(t_0)\| = R \sin\left(\frac{\alpha}{2}\right)$, the system becomes periodic once entering state B in $T_B = \frac{R-r}{v} \tan\left(\frac{\alpha}{2}\right)$ time.

State C represents all cases in which $R \sin\frac{\alpha}{2} < \|p_a(t_0)\| \leq 2r \sin\frac{\alpha}{2}$ and $\theta_a(t_0) = \varphi(t_0) + \pi - \frac{\alpha}{2}$ with $R < 2r$. State D represents all cases in which $2r \sin\frac{\alpha}{2} < \|p_a(t_0)\| < 2R \sin\frac{\alpha}{2}$ and $\theta_a(t_0) = \varphi(t_0) + \pi - \frac{\alpha}{2}$ with $R < 2r$. State \tilde{D} represents all cases in which $R \sin\frac{\alpha}{2} < \|p_a(t_0)\| < 2R \sin\frac{\alpha}{2}$ and $\theta_a(t_0) = \varphi(t_0) + \pi - \frac{\alpha}{2}$ with $R > 2r$. Lemma 3.1.6 shows that states C , D and \tilde{D} transition to either states A or B in a time span less than or equal to $T_D = \frac{\alpha R}{v}$. The state machine corresponding with $R \geq 2r$ seen in Figure 3.16d has no transition loops, except for state E which was discussed earlier, and eventually transitions to other states. On the other hand, the state machine corresponding with $R < 2r$ seen in Figure 3.16c has a loop between states A and C , yet as will be shown presently, the loop resolves in an eventual transition to state B .

Suppose that $\|p_a(t = t_0)\|$ is such that corresponds with the system being at state C , i.e. $R \sin\frac{\alpha}{2} < \|p_a(t = t_0)\| \leq 2r \sin\frac{\alpha}{2}$. According to Lemma 3.1.6, the system transitions either to state A or B , whichever state

$$\begin{aligned} \|p_a(t = t_1)\| &= \left\| p_a(t = t_0) + \frac{R}{v} \left(2 \arcsin \left(\frac{\|p_a(t_0)\| \cos\left(\frac{\alpha}{2}\right)}{\sqrt{R^2 + \|p_a(t_0)\|^2 - 2\|p_a(t_0)\| R \sin\left(\frac{\alpha}{2}\right)}} \right) - \alpha \right) \right\| \\ &= 2R \sin\left(\frac{\alpha}{2}\right) - \|p_a(t_0)\| \end{aligned}$$

falls into. Let us assume that $2R \sin\left(\frac{\alpha}{2}\right) - \|p_a(t_0)\|$ lies in state A , then according to Lemma 3.1.7 the system transitions either to state B or state C , whichever state

$$\begin{aligned} \|p_a(t = t_2)\| &= \left\| p_a \left(t_1 + \frac{r}{v} \left(2\pi + 2 \arcsin \left(\frac{\|p_a(t_1)\| \cos\left(\frac{\alpha}{2}\right)}{\sqrt{\|p_a(t_1)\|^2 + r^2 - 2\|p_a(t_1)\| r \sin\left(\frac{\alpha}{2}\right)}} \right) - \alpha \right) \right) \right\| \\ &= 2r \sin\left(\frac{\alpha}{2}\right) - \|p_a(t_1)\| \\ &= \|p_a(t_0)\| - 2(R - r) \sin\left(\frac{\alpha}{2}\right) \end{aligned}$$

lies in. Since $0 < 2(R - r) \sin\left(\frac{\alpha}{2}\right)$ for all $0 < \alpha < 2\pi$, then $\|p_a(t_2)\| < \|p_a(t_0)\|$ for any $\|p_a(t_0)\|$ in state C , causing the system to take a constant sized step towards never returning to state C every time the state leaves state C .

Similarly, suppose that $\|p_a(t = t_0)\|$ is such that corresponds with the system being at state A , i.e. $0 \leq \|p_a(t = t_0)\| < r \sin\left(\frac{\alpha}{2}\right)$. According to Lemma 3.1.7, the system transitions either to state B or C , whichever state

$$\begin{aligned} \|p_a(t = t_1)\| &= \left\| p_a(t = t_0) + \frac{r}{v} \left(2\pi + 2 \arcsin \left(\frac{\|p_a(t_0)\| \cos\left(\frac{\alpha}{2}\right)}{\sqrt{r^2 + \|p_a(t_0)\|^2 - 2\|p_a(t_0)\| r \sin\left(\frac{\alpha}{2}\right)}} \right) - \alpha \right) \right\| \\ &= 2r \sin\left(\frac{\alpha}{2}\right) - \|p_a(t_0)\| \end{aligned}$$

falls into. Let us assume that $2r \sin\left(\frac{\alpha}{2}\right) - \|p_a(t_0)\|$ lies in state C , then according to Lemma 3.1.6 the system transitions either to state B or back to state A , whichever state

$$\begin{aligned} \|p_a(t = t_2)\| &= \left\| p_a \left(t_1 + \frac{R}{v} \left(2 \arcsin \left(\frac{\|p_a(t_1)\| \cos\left(\frac{\alpha}{2}\right)}{\sqrt{\|p_a(t_1)\|^2 + R^2 - 2\|p_a(t_1)\| R \sin\left(\frac{\alpha}{2}\right)}} \right) - \alpha \right) \right) \right\| \\ &= 2R \sin\left(\frac{\alpha}{2}\right) - \|p_a(t_1)\| \\ &= \|p_a(t_0)\| + 2(R - r) \sin\left(\frac{\alpha}{2}\right) \end{aligned}$$

lies in. Since $0 < 2(R - r) \sin\left(\frac{\alpha}{2}\right)$ for all $0 < \alpha < 2\pi$, then $\|p_a(t_2)\| > \|p_a(t_0)\|$ for any $\|p_a(t_0)\|$ in state A , causing the system to take a constant sized step towards never returning to state A every time the state leaves state A . Combining these two results concludes this proof since any cycle between states A and C must end eventually in a transition to state B in a time span equal to or less than

$$\begin{aligned} T_C &= \max \left((T_A + T_D) \left\lfloor \frac{r \sin\left(\frac{\alpha}{2}\right)}{2(R - r) \sin\left(\frac{\alpha}{2}\right)} \right\rfloor + T_A, (T_A + T_D) \left\lfloor \frac{2r \sin\left(\frac{\alpha}{2}\right)}{2(R - r) \sin\left(\frac{\alpha}{2}\right)} \right\rfloor + T_D \right) \\ &\leq \frac{2\pi r + \alpha R}{v} \frac{r}{R - r} + \max \left(\frac{2\pi r}{v}, \frac{\alpha R}{v} \right). \end{aligned}$$

The overall time for the agent to converge to the beacon is therefore assured to be at most

$$\begin{aligned} T_{total} &= T_S + T_A + T_B + T_C + T_D + T_E \\ &\leq \frac{2\pi r + \alpha R}{v} + \frac{2\pi r}{v} + \frac{R - r}{v} \tan\left(\frac{\alpha}{2}\right) + \left(\frac{2\pi r + \alpha R}{v} \frac{r}{R - r} + \max \left(\frac{2\pi r}{v}, \frac{\alpha R}{v} \right) \right) \\ &\quad + \frac{\alpha R}{v} + \left\lfloor \frac{\|c_a(t_{initial})\| + R}{2(R - r) \sin\left(\frac{\alpha}{2}\right)} \right\rfloor \frac{2\pi r + \alpha(R - r)}{v} \\ &= 2 \frac{2\pi r + \alpha R}{v} + \frac{R - r}{v} \tan\left(\frac{\alpha}{2}\right) + \left(\frac{2\pi r + \alpha R}{v} \frac{r}{R - r} + \max \left(\frac{2\pi r}{v}, \frac{\alpha R}{v} \right) \right) \\ &\quad + \left\lfloor \frac{\|c_a(t_{initial})\| + R}{2(R - r) \sin\left(\frac{\alpha}{2}\right)} \right\rfloor \frac{2\pi r + \alpha(R - r)}{v} \end{aligned}$$

$$\begin{aligned}
&\leq \frac{2\pi r + \alpha R}{v} \left(3 + \frac{r}{R-r} + \left\lfloor \frac{\|c_a(t_{initial})\| + R}{2(R-r)\sin(\frac{\alpha}{2})} \right\rfloor \right) + \frac{R-r}{v} \tan\left(\frac{\alpha}{2}\right) \\
&\quad - \frac{\alpha r}{v} \left\lfloor \frac{\|c_a(t_{initial})\| + R}{2(R-r)\sin(\frac{\alpha}{2})} \right\rfloor \\
&\leq \frac{2\pi r + \alpha R}{v} \left(3 + \frac{r}{R-r} + \left(\frac{\|c_a(t_{initial})\| + R}{2(R-r)\sin(\frac{\alpha}{2})} \right) \right) + \frac{R-r}{v} \tan\left(\frac{\alpha}{2}\right) \\
&\quad - \frac{\alpha r}{v} \left(\frac{\|c_a(t_{initial})\| + R}{2(R-r)\sin(\frac{\alpha}{2})} \right) \\
&= \frac{2\pi r + \alpha R}{v} \left(\frac{6R\sin(\frac{\alpha}{2}) - 4r\sin(\frac{\alpha}{2}) + \|c_a(t_{initial})\| + R}{2(R-r)\sin(\frac{\alpha}{2})} \right) + \frac{R-r}{v} \tan\left(\frac{\alpha}{2}\right) \\
&\quad - \frac{\alpha r}{v} \left(\frac{\|c_a(t_{initial})\| + R}{2(R-r)\sin(\frac{\alpha}{2})} \right) \\
&= \frac{2\pi r + \alpha(R-r)}{2v(R-r)\sin(\frac{\alpha}{2})} \|c_a(t_{initial})\| + \frac{R-r}{v} \tan\left(\frac{\alpha}{2}\right) \\
&\quad + \frac{(2\pi r + \alpha R)(6R\sin(\frac{\alpha}{2}) - 4r\sin(\frac{\alpha}{2}) + R) - \alpha Rr}{2v(R-r)\sin(\frac{\alpha}{2})} \\
&= \frac{2\pi r + \alpha(R-r)}{2v(R-r)\sin(\frac{\alpha}{2})} \|c_a(t_{initial})\| + \frac{R-r}{v} \tan\left(\frac{\alpha}{2}\right) \\
&\quad + \frac{12\pi Rr\sin(\frac{\alpha}{2}) - 8\pi r^2\sin(\frac{\alpha}{2}) + 2\pi Rr + 6\alpha R^2\sin(\frac{\alpha}{2}) - 4\alpha Rr\sin(\frac{\alpha}{2}) + \alpha R^2 - \alpha Rr}{2v(R-r)\sin(\frac{\alpha}{2})} \\
&= \frac{2\pi r + \alpha(R-r)}{2v(R-r)\sin(\frac{\alpha}{2})} \|c_a(t_{initial})\| + \frac{R-r}{v} \tan\left(\frac{\alpha}{2}\right) \\
&\quad + \frac{2(3\alpha R^2 + (6\pi - 2\alpha)Rr - 4\pi r^2)\sin(\frac{\alpha}{2}) + 2\pi Rr + \alpha R^2 - \alpha Rr}{2v(R-r)\sin(\frac{\alpha}{2})} \\
&= \frac{2\pi r + \alpha(R-r)}{2v(R-r)\sin(\frac{\alpha}{2})} \|c_a(t_{initial})\| + \frac{R-r}{v} \tan\left(\frac{\alpha}{2}\right) \\
&\quad + \frac{3\alpha R^2 + (6\pi - 2\alpha)Rr - 4\pi r^2}{v(R-r)} + \frac{\alpha R^2 + (2\pi - \alpha)Rr}{2v(R-r)\sin(\frac{\alpha}{2})} \\
&= \frac{2\pi r + \alpha(R-r)}{2v(R-r)\sin(\frac{\alpha}{2})} \|c_a(t_{initial})\| + \frac{R-r}{v} \tan\left(\frac{\alpha}{2}\right) \\
&\quad + \frac{3\alpha R + (6\pi + \alpha)r}{v} + \frac{(2\pi + \alpha)r^2}{v(R-r)} + \frac{\alpha R + 2\pi r}{2v\sin(\frac{\alpha}{2})} + \frac{\pi r^2}{v(R-r)\sin(\frac{\alpha}{2})}.
\end{aligned}$$

□

Corollary 3.1.5. *A system consisting of a single agent controlled by (2.2) with $\pi < \alpha < 2\pi$ and a beacon located at the origin and perceived as an agent by the single agent's sensors converges to a trajectory having an invariant center of rotation $\|c_a(t)\| \leq -R \cos \frac{\alpha}{2}$ for $t \geq t_{initial} + T_{total}(\|c_a(t_{initial})\|)$ where*

$$T_{total}(x) = \frac{2\pi r + \alpha(R-r)}{2v(R-r)\sin\left(\frac{\alpha}{2}\right)}x + \frac{R-r}{v}\tan\left(\frac{\alpha}{2}\right) + \frac{(2\pi + \alpha)R + 4\pi r}{v} + \frac{2\pi r^2}{v(R-r)} + \frac{\alpha R + 2\pi r}{2v\sin\left(\frac{\alpha}{2}\right)} + \frac{\pi r^2}{v(R-r)\sin\left(\frac{\alpha}{2}\right)}.$$

Proof. This proof differs the proof given for Lemma 3.1.9 only by referring to Corollary 3.1.2 instead of Lemmas 3.1.2 and 3.1.3 for the time it takes to enter any one of the states of the state machine in Figure 3.16 for the first time, and by referring to Corollary 3.1.4 instead of Lemma 3.1.8 when entering state B in the state machine.

$$\begin{aligned} T_{total} &= T_S + T_A + T_B + T_C + T_D + T_E \\ &\leq \frac{2\pi R}{v} + \frac{2\pi r}{v} + \frac{R-r}{v}\tan\left(\frac{\alpha}{2}\right) + \left(\frac{2\pi r + \alpha R}{v}\frac{r}{R-r} + \max\left(\frac{2\pi r}{v}, \frac{\alpha R}{v}\right)\right) \\ &\quad + \frac{\alpha R}{v} + \left\lfloor \frac{\|c_a(t_{initial})\| + R}{2(R-r)\sin\left(\frac{\alpha}{2}\right)} \right\rfloor \frac{2\pi r + \alpha(R-r)}{v} \\ &= \frac{2\pi R}{v} + \frac{2\pi r + \alpha R}{v} + \frac{R-r}{v}\tan\left(\frac{\alpha}{2}\right) + \left(\frac{2\pi r + \alpha R}{v}\frac{r}{R-r} + \max\left(\frac{2\pi r}{v}, \frac{\alpha R}{v}\right)\right) \\ &\quad + \left\lfloor \frac{\|c_a(t_{initial})\| + R}{2(R-r)\sin\left(\frac{\alpha}{2}\right)} \right\rfloor \frac{2\pi r + \alpha(R-r)}{v} \\ &\leq \frac{2\pi r + \alpha R}{v} \left(2 + \frac{r}{R-r} + \left\lfloor \frac{\|c_a(t_{initial})\| + R}{2(R-r)\sin\left(\frac{\alpha}{2}\right)} \right\rfloor\right) + \frac{R-r}{v}\tan\left(\frac{\alpha}{2}\right) + \frac{2\pi R}{v} \\ &\quad - \frac{\alpha r}{v} \left(\left\lfloor \frac{\|c_a(t_{initial})\| + R}{2(R-r)\sin\left(\frac{\alpha}{2}\right)} \right\rfloor\right) \\ &\leq \frac{2\pi r + \alpha R}{v} \left(2 + \frac{r}{R-r} + \left(\frac{\|c_a(t_{initial})\| + R}{2(R-r)\sin\left(\frac{\alpha}{2}\right)}\right)\right) + \frac{R-r}{v}\tan\left(\frac{\alpha}{2}\right) + \frac{2\pi R}{v} \\ &\quad - \frac{\alpha r}{v} \left(\frac{\|c_a(t_{initial})\| + R}{2(R-r)\sin\left(\frac{\alpha}{2}\right)}\right) \\ &= \frac{2\pi r + \alpha R}{v} \left(\frac{4R\sin\left(\frac{\alpha}{2}\right) - 2r\sin\left(\frac{\alpha}{2}\right) + \|c_a(t_{initial})\| + R}{2(R-r)\sin\left(\frac{\alpha}{2}\right)}\right) + \frac{R-r}{v}\tan\left(\frac{\alpha}{2}\right) + \frac{2\pi R}{v} \\ &\quad - \frac{\alpha r}{2v(R-r)\sin\left(\frac{\alpha}{2}\right)}\|c_a(t_{initial})\| - \frac{\alpha R r}{2v(R-r)\sin\left(\frac{\alpha}{2}\right)} \\ &= \frac{2\pi r + \alpha(R-r)}{2v(R-r)\sin\left(\frac{\alpha}{2}\right)}\|c_a(t_{initial})\| + \frac{R-r}{v}\tan\left(\frac{\alpha}{2}\right) \\ &\quad + \frac{(2\pi r + \alpha R)(4R\sin\left(\frac{\alpha}{2}\right) - 2r\sin\left(\frac{\alpha}{2}\right) + R) - \alpha R r + 4\pi R(R-r)\sin\frac{\alpha}{2}}{2v(R-r)\sin\left(\frac{\alpha}{2}\right)} \end{aligned}$$

$$\begin{aligned}
 &= \frac{2\pi r + \alpha(R-r)}{2v(R-r)\sin\left(\frac{\alpha}{2}\right)} \|c_a(t_{initial})\| + \frac{R-r}{v} \tan\left(\frac{\alpha}{2}\right) \\
 &+ \frac{8\pi Rr \sin\left(\frac{\alpha}{2}\right) - 4\pi r^2 \sin\left(\frac{\alpha}{2}\right) + 2\pi Rr + 4\alpha R^2 \sin\left(\frac{\alpha}{2}\right) - 2\alpha Rr \sin\left(\frac{\alpha}{2}\right)}{2v(R-r)\sin\left(\frac{\alpha}{2}\right)} \\
 &+ \frac{\alpha R^2 - \alpha Rr + 4\pi R^2 \sin\left(\frac{\alpha}{2}\right) - 4\pi Rr \sin\left(\frac{\alpha}{2}\right)}{2v(R-r)\sin\left(\frac{\alpha}{2}\right)} \\
 &= \frac{2\pi r + \alpha(R-r)}{2v(R-r)\sin\left(\frac{\alpha}{2}\right)} \|c_a(t_{initial})\| + \frac{R-r}{v} \tan\left(\frac{\alpha}{2}\right) \\
 &+ \frac{2(4\pi Rr - 2\pi r^2 + 2\alpha R^2 - \alpha Rr + 2\pi R^2 - 2\pi Rr) \sin\left(\frac{\alpha}{2}\right)}{2v(R-r)\sin\left(\frac{\alpha}{2}\right)} \\
 &+ \frac{2\pi Rr + \alpha R^2 - \alpha Rr}{2v(R-r)\sin\left(\frac{\alpha}{2}\right)} \\
 &= \frac{2\pi r + \alpha(R-r)}{2v(R-r)\sin\left(\frac{\alpha}{2}\right)} \|c_a(t_{initial})\| + \frac{R-r}{v} \tan\left(\frac{\alpha}{2}\right) \\
 &+ \frac{2(2(\pi + \alpha)R^2 + (2\pi - \alpha)Rr - 2\pi r^2) \sin\left(\frac{\alpha}{2}\right) + \alpha R^2 + (2\pi - \alpha)Rr}{2v(R-r)\sin\left(\frac{\alpha}{2}\right)} \\
 &= \frac{2\pi r + \alpha(R-r)}{2v(R-r)\sin\left(\frac{\alpha}{2}\right)} \|c_a(t_{initial})\| + \frac{R-r}{v} \tan\left(\frac{\alpha}{2}\right) \\
 &+ \frac{(2\pi + \alpha)R + 4\pi r}{v} + \frac{2\pi r^2}{v(R-r)} + \frac{\alpha R + 2\pi r}{2v \sin\left(\frac{\alpha}{2}\right)} + \frac{\pi r^2}{v(R-r)\sin\left(\frac{\alpha}{2}\right)}
 \end{aligned}$$

□

Corollary 3.1.6. *A system consisting of a single agent controlled by (2.2) with $\alpha = \pi$ and a beacon located at the origin and perceived as an agent by the single agent's sensors converges to a trajectory having constant angular velocity and the agent's distance from the beacon is invariant such that*

$$r \leq \|p_a(t)\| \leq R$$

for $t \geq t_{initial} + T_{total}(\|c_a(t_{initial})\|)$ where:

$$T_{total}(x) = \frac{\pi(R+r)}{2v(R-r)}x + \frac{4\pi r^2}{v(R-r)} + \frac{13R+12r}{2v}\pi.$$

Proof. This proof differs the proof given for Corollary 3.1.6 only by referring to Corollary 3.1.3 instead of Lemma 3.1.8 when entering state B in the state machine. Upon entering state B at time t_0 , the agent instantaneously enters the steady state with radius $\|p_a(t_0)\|$. The upper bound on convergence time therefore becomes

$$T_{total} = T_S + T_A + T_C + T_D + T_E.$$

Using the proof of Corollary 3.1.5 we get

$$= \frac{2\pi r + \alpha(R-r)}{2v(R-r)\sin\left(\frac{\alpha}{2}\right)} \|c_a(t_{initial})\| + \frac{(2\pi + \alpha)R + 4\pi r}{v}$$

$$+ \frac{2\pi r^2}{v(R-r)} + \frac{\alpha R + 2\pi r}{2v \sin\left(\frac{\alpha}{2}\right)} + \frac{\pi r^2}{v(R-r) \sin\left(\frac{\alpha}{2}\right)}.$$

Substituting α with π we get:

$$= \frac{\pi(R+r)}{2v(R-r)} \|c_a(t_{initial})\| + \frac{3\pi r^2}{v(R-r)} + \frac{7\pi R + 10\pi r}{2v}.$$

□

Theorem 3.1.1. *A system consisting of a beacon located at the origin and a single agent controlled by (2.2) with visibility range $R_v \geq \|c_a(t_{initial})\| + R$ converges to a periodic orbit having a stationary center of rotation c_a and constant angular velocity $\dot{\theta}_a$ such that*

$$\|c_a\| \begin{cases} \leq r \cos\left(\frac{\alpha}{2}\right) & \text{for } 0 < \alpha < \pi \\ = 0 & \text{for } \alpha = \pi \\ \leq -R \cos\left(\frac{\alpha}{2}\right) & \text{for } \pi < \alpha < 2\pi \end{cases} \quad \text{and} \quad \dot{\theta}_a \begin{cases} = \frac{v}{r} & \text{for } 0 < \alpha < \pi \\ \in \left[\frac{v}{R}, \frac{v}{r}\right] & \text{for } \alpha = \pi \\ = \frac{v}{R} & \text{for } \pi < \alpha < 2\pi \end{cases}$$

in finite time, where $(t_{final} - t_{initial}) \leq T(\|c_a(t_{initial})\|)$ and $T(x)$ is given by

$$T(x) = \begin{cases} \frac{2\pi r + \alpha(R-r)}{2v(R-r) \sin\left(\frac{\alpha}{2}\right)} x + \frac{R-r}{v} \tan\left(\frac{\alpha}{2}\right) + \frac{3\alpha R + (6\pi + \alpha)r}{v} + \frac{(2\pi + \alpha)r^2}{v(R-r)} + \frac{\alpha R + 2\pi r}{2v \sin\left(\frac{\alpha}{2}\right)} + \frac{\pi r^2}{v(R-r) \sin\left(\frac{\alpha}{2}\right)}, & 0 < \alpha < \pi \\ \left(\frac{(R+r)}{2v(R-r)} x + \frac{4r^2}{v(R-r)} + \frac{13R+12r}{2v}\right) \pi, & \alpha = \pi \\ \frac{2\pi r + \alpha(R-r)}{2v(R-r) \sin\left(\frac{\alpha}{2}\right)} x + \frac{R-r}{v} \tan\left(\frac{\alpha}{2}\right) + \frac{(2\pi + \alpha)R + 4\pi r}{v} + \frac{2\pi r^2}{v(R-r)} + \frac{\alpha R + 2\pi r}{2v \sin\left(\frac{\alpha}{2}\right)} + \frac{\pi r^2}{v(R-r) \sin\left(\frac{\alpha}{2}\right)}, & \pi < \alpha < 2\pi \end{cases}$$

Proof. By combination of Lemma 3.1.9, Corollary 3.1.5 and Corollary 3.1.6. □

Figure 3.17 shows two NetLogo¹ simulations of a single agent and a beacon scenario. The difference between the two simulations, other than the difference in initial conditions, is that the agent in Figure 3.17e has a central angle $\frac{\pi}{3}$ while the agent in Figure 3.17j has a central angle π . The initial conditions can be seen in Figures 3.17a and 3.17f. The agent travels towards the beacon in Figures 3.17b and 3.17g, this stage corresponds with state E in Lemma 3.1.9. The transition through other states of Lemma 3.1.9 can be seen in Figures 3.17c and 3.17h. In Figure 3.17h the signature spiral of state B is clearly visible. The periodic orbit state can be seen in Figure 3.17d and 3.17i, where the agent repeats the same circle over and over again.

¹<https://ccl.northwestern.edu/netlogo/>

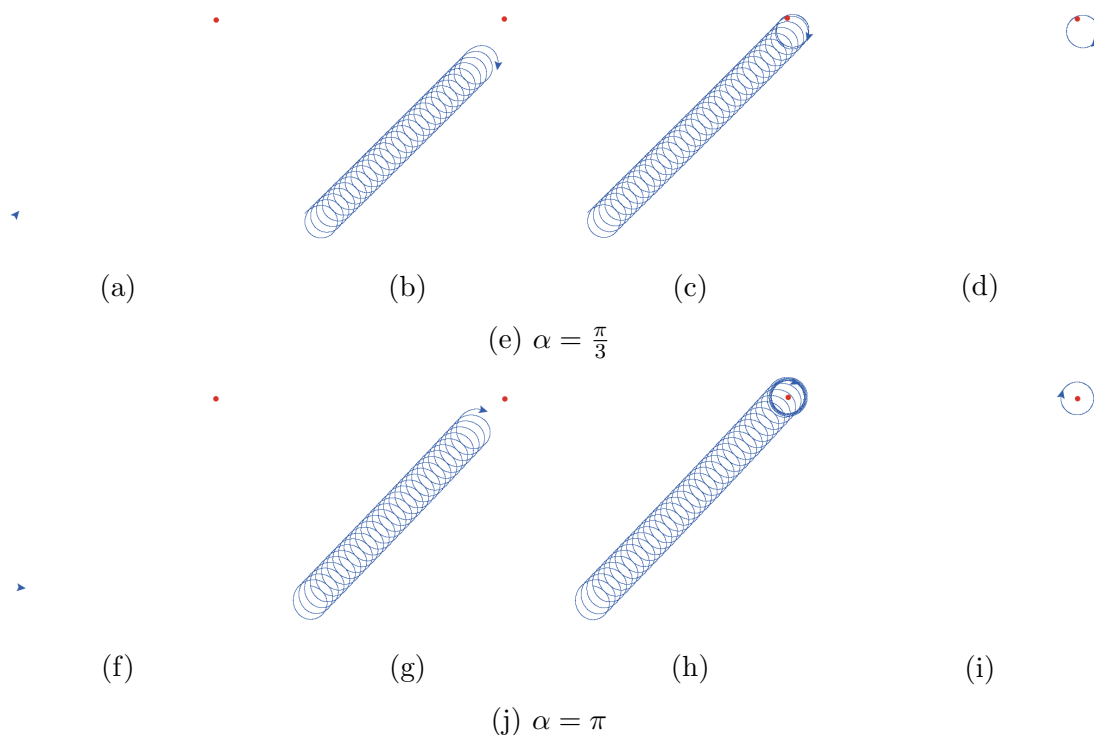


Figure 3.17: Two NetLogo simulations of a beacon and an agent with $R = 6$ and $r = 4$. The red dot represents the beacon, the blue arrowhead represents the agent.

3.2 Two Agents Converge

Consider a system consisting of two agents. In this section we take $S = 1$ in order to allow each agent to rotate with radius r when not observing the other agent, and R otherwise. The goal of this section is to show that the system described here reaches a configuration where the distance between the agents is bounded by a constant defined by the system parameters in finite time (Theorem 3.2.1). Another result given here shows that the 2-agent system converges in linear time to a predetermined configuration defined by the system's parameters when initial conditions are set such that one agent's orientation is opposite the other agent's orientation (Theorem 3.2.2). The first goal is achieved by identifying the potential switching agent's orientation which brings the agents' centers of rotation farthest apart (Lemma 3.2.1), and then by showing that even the worst possible switch in terms of bringing the centers of rotation towards each other still brings the agents' centers of rotation closer than they were before switching, as long as the distance between centers of rotation before switching was greater than some constant defined by system parameters (Lemma 3.2.2). The second goal is achieved by recognizing the similarities between the 2-agent system and the agent-beacon system discussed previously.

The following lemma describes the worst case scenario with regards to bringing the two agents together, by identifying θ_* , the worst possible orientation of the agent performing a radius switch.

Lemma 3.2.1. *For $0 < \alpha < 2\pi$ and every p_1, p_2 configuration, let $d =$*

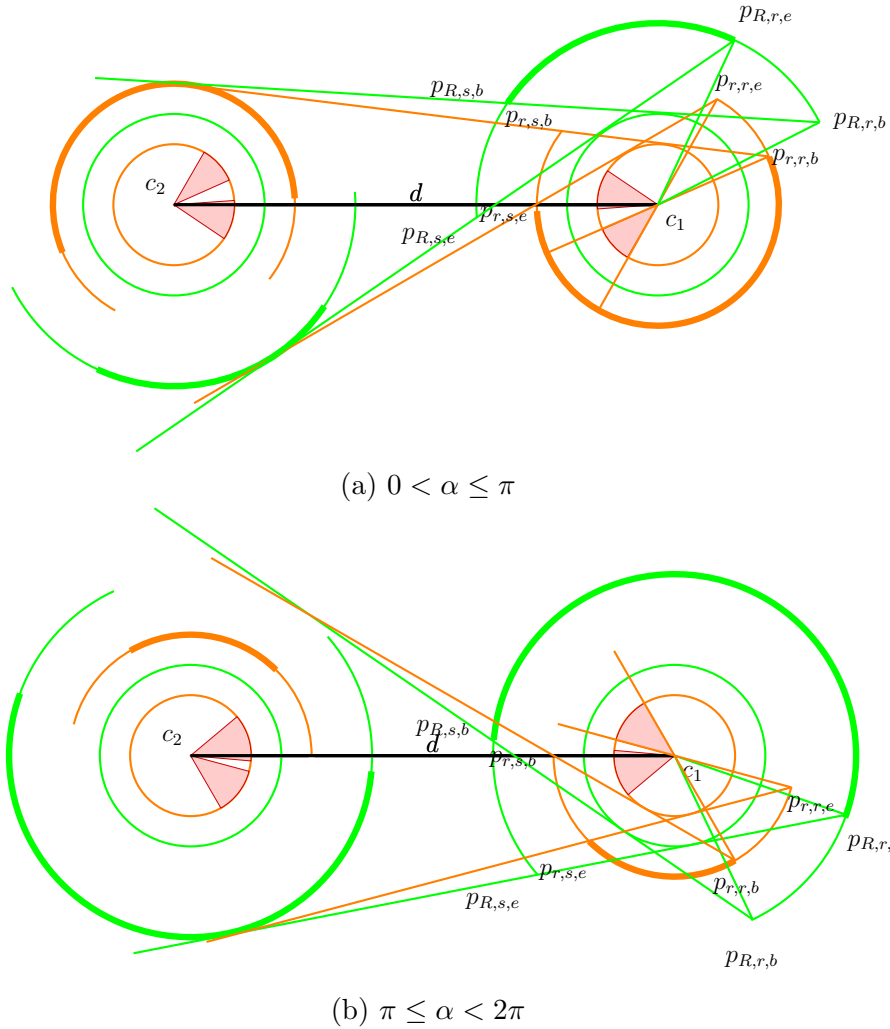


Figure 3.18: A general configuration for two agents with centers of rotation c_1, c_2 at distance d from one another. Arcs in bold represent all θ_i values for which $\mathcal{R}(\mathcal{G}, i)$ can be determined solely by d and θ_i , regardless of θ_j . The arcs of the filled sectors represent possible locations of c_i after switching. $p_{a,b,c}$ represents the location of an agent with center of rotation c_i where a is the agent's radius at the time (either r or R), b can be either r or s depending on whether the other agent is rising or setting, and c can be either b or e , representing the beginning and the end of an arc in which switching is possible.

$\|c_1 - c_2\|$ and let θ_* be agent i 's orientation corresponding with the radius switch that brings c_i closer to c_j the least, then

$$\theta_* = \arcsin\left(\frac{R + r \cos \frac{\alpha}{2}}{d}\right) + \pi - \frac{\alpha}{2}.$$

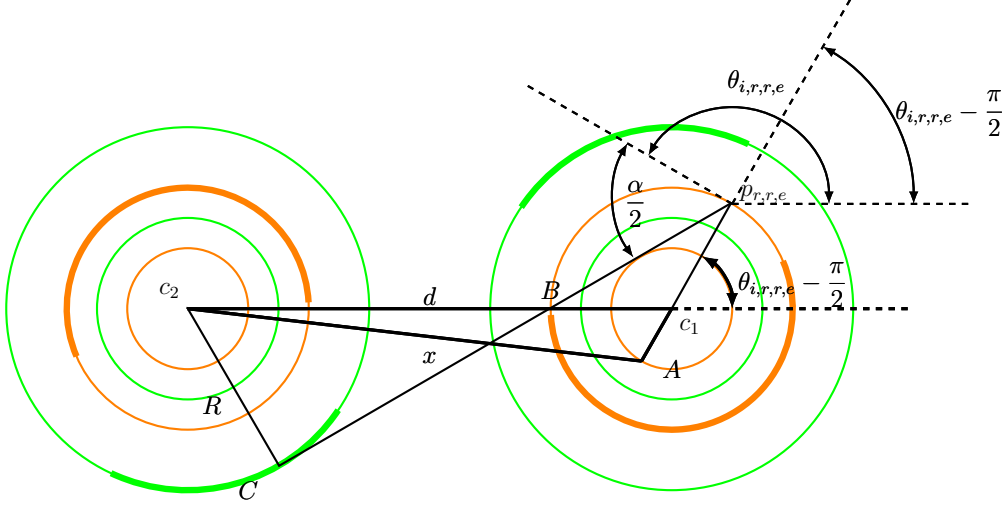


Figure 3.19: The geometry used to prove Lemmas 3.2.1 and 3.2.2.

Proof. For $0 < \alpha \leq \pi$, let $p_{i,r,r,e}$ be agent i 's position as its dawn horizon becomes tangent to the R radius circle around c_j at the point where agent i 's rotation takes agent i 's dawn horizon away from agent j 's R circle, as shown in Figure 3.18a. If agent i has not switched radius from r to R until reaching $p_{i,r,r,e}$, agent i must switch at that point since by that point all the possible locations of agent j have risen over agent i 's dawn horizon. The orientation of agent i at $p_{i,r,r,e}$ relative to the vector $c_i - c_j$, $\theta_{i,r,r,e}$, is therefore the greatest possible angle where switching from r to R is possible for any c_i, c_j configuration when at distance d from one another. Using Figure 3.19, and the law of sines we get

$$\frac{|Bc_1|}{\sin \frac{\pi - \alpha}{2}} = \frac{r}{\sin\left(\pi - \left(\frac{\pi - \alpha}{2}\right) - \left(\pi - \left(\theta_{i,r,r,e} - \frac{\pi}{2}\right)\right)\right)} = \frac{r}{\sin\left(\theta_{i,r,r,e} + \frac{\alpha}{2} - \pi\right)}$$

↓

$$|Bc_1| = \frac{r \cos \frac{\alpha}{2}}{\sin\left(\theta_{i,r,r,e} + \frac{\alpha}{2} - \pi\right)}$$

and

$$|Bc_2| = \frac{R}{\sin\left(\theta_{i,r,r,e} + \frac{\alpha}{2} - \pi\right)}.$$

Similarly, for $\pi \leq \alpha < 2\pi$, $\theta_{i,r,r,b}$ corresponds with the earliest opportunity for agent j to rise over agent i 's dawn horizon, making it the worst case

for bringing c_i closer to c_j , as can be seen in Figure 3.18b. By geometric consideration similar to those presented in Figure 3.19, we get

$$\begin{aligned} \frac{|Bc_1|}{\sin \frac{\alpha-\pi}{2}} &= \frac{r}{\sin \left(3\pi - \left(\theta_{i,r,r,b} + \frac{\alpha}{2} \right) \right)} = \frac{r}{\sin \left(2\pi - \left(\theta_{i,r,r,b} + \frac{\alpha}{2} - \pi \right) \right)} \\ &\Downarrow \\ |Bc_1| &= \frac{r \cos \frac{\alpha}{2}}{\sin \left(\theta_{i,r,r,b} + \frac{\alpha}{2} - \pi \right)} \end{aligned}$$

and

$$|Bc_2| = \frac{R}{\sin \left(\theta_{i,r,r,b} + \frac{\alpha}{2} - \pi \right)}.$$

Noticing that $\theta_{i,r,r,e}$ for $0 < \alpha \leq \pi$ and $\theta_{i,r,r,b}$ for $\pi \leq \alpha < 2\pi$ are interchangeable, we denote

$$\theta_* = \begin{cases} \theta_{i,r,r,e} & | \ 0 < \alpha \leq \pi \\ \theta_{i,r,r,b} & | \ \pi < \alpha < 2\pi \end{cases}$$

therefore,

$$\begin{aligned} d = |Bc_1| + |Bc_2| &= \frac{R + r \cos \frac{\alpha}{2}}{\sin \left(\theta_* + \frac{\alpha}{2} - \pi \right)} \\ &\Downarrow \\ \sin \left(\theta_* + \frac{\alpha}{2} - \pi \right) &= \frac{R + r \cos \frac{\alpha}{2}}{d} \\ &\Downarrow \\ \theta_* + \frac{\alpha}{2} - \pi &= \arcsin \left(\frac{R + r \cos \frac{\alpha}{2}}{d} \right) \\ &\Downarrow \\ \theta_* &= \arcsin \left(\frac{R + r \cos \frac{\alpha}{2}}{d} \right) + \pi - \frac{\alpha}{2}. \end{aligned}$$

□

Lemma 3.2.2. *Given two agents with $0 < \alpha < 2\pi$ and $R_v > d + 2R$ controlled by (2.2), where d is the distance between the agents' centers of rotation before switching, the agents' centers of rotation get closer together upon every switch as long as*

$$d > \sqrt{\left(\frac{R \left(1 + 2 \cos \left(\frac{\alpha}{2} \right) \right) - r \left(1 - 2 \cos^2 \frac{\alpha}{2} \right)}{2 \sin \left(\frac{\alpha}{2} \right)} \right)^2 + \left(R + r \cos \frac{\alpha}{2} \right)^2}.$$

Proof. Figure 3.19 shows a general configuration of c_i and c_j , where d is the current distance between centers of rotation, and x is the longest distance possible between centers of rotation post switch. Using the law of cosines,

$$x^2 = \begin{cases} d^2 + (R-r)^2 - 2d(R-r) \cos\left(\theta_* - \frac{\pi}{2}\right) & 0 < \alpha \leq \pi \\ d^2 + (R-r)^2 - 2d(R-r) \cos\left(2\pi - \left(\theta_* - \frac{\pi}{2}\right)\right) & \pi < \alpha < 2\pi \end{cases}$$

where θ_* is the same as in Lemma 3.2.1. Notice that

$$\cos\left(2\pi - \left(\theta_* - \frac{\pi}{2}\right)\right) = \cos\left(\theta_* - \frac{\pi}{2}\right) = \sin(\theta_*)$$

therefore,

$$x^2 = d^2 + (R-r)^2 - 2d(R-r) \sin(\theta_*).$$

If the centers of rotation are to get closer by the switch, x must be smaller than d :

$$x < d \Rightarrow x^2 < d^2$$

↓

$$d^2 + (R-r)^2 - 2d(R-r) \sin(\theta_*) < d^2$$

↓

$$(R-r) < 2d \sin(\theta_*).$$

Using Lemma 3.2.1 we get

$$(R-r) < 2d \sin\left(\arcsin\left(\frac{R+r \cos \frac{\alpha}{2}}{d}\right) + \pi - \frac{\alpha}{2}\right)$$

↓

$$(R-r) < 2d \left(\cos\left(\arcsin\left(\frac{R+r \cos \frac{\alpha}{2}}{d}\right)\right) \sin\left(\pi - \frac{\alpha}{2}\right) + \frac{R+r \cos \frac{\alpha}{2}}{d} \cos\left(\pi - \frac{\alpha}{2}\right) \right)$$

↓

$$(R-r) < 2d \cos\left(\arcsin\left(\frac{R+r \cos \frac{\alpha}{2}}{d}\right)\right) \sin\left(\frac{\alpha}{2}\right) - 2\left(R+r \cos \frac{\alpha}{2}\right) \cos\left(\frac{\alpha}{2}\right)$$

↓

$$R\left(1 + 2 \cos\left(\frac{\alpha}{2}\right)\right) - r\left(1 - 2 \cos^2 \frac{\alpha}{2}\right) < 2d \sin\left(\frac{\alpha}{2}\right) \sqrt{1 - \left(\frac{R+r \cos \frac{\alpha}{2}}{d}\right)^2}$$

↓

$$R\left(1 + 2 \cos\left(\frac{\alpha}{2}\right)\right) - r\left(1 - 2 \cos^2 \frac{\alpha}{2}\right) < 2d \sin\left(\frac{\alpha}{2}\right) \frac{\sqrt{d^2 - \left(R+r \cos \frac{\alpha}{2}\right)^2}}{d}$$

↓

$$\begin{aligned}
 R \left(1 + 2 \cos \left(\frac{\alpha}{2}\right)\right) - r \left(1 - 2 \cos^2 \frac{\alpha}{2}\right) &< 2 \sin \left(\frac{\alpha}{2}\right) \sqrt{d^2 - \left(R + r \cos \frac{\alpha}{2}\right)^2} \\
 &\Downarrow \\
 \frac{R \left(1 + 2 \cos \left(\frac{\alpha}{2}\right)\right) - r \left(1 - 2 \cos^2 \frac{\alpha}{2}\right)}{2 \sin \left(\frac{\alpha}{2}\right)} &< \sqrt{d^2 - \left(R + r \cos \frac{\alpha}{2}\right)^2} \\
 &\Downarrow \\
 \left(\frac{R \left(1 + 2 \cos \left(\frac{\alpha}{2}\right)\right) - r \left(1 - 2 \cos^2 \frac{\alpha}{2}\right)}{2 \sin \left(\frac{\alpha}{2}\right)}\right)^2 + \left(R + r \cos \frac{\alpha}{2}\right)^2 &< d^2 \\
 &\Downarrow \\
 d &> \sqrt{\left(\frac{R \left(1 + 2 \cos \left(\frac{\alpha}{2}\right)\right) - r \left(1 - 2 \cos^2 \frac{\alpha}{2}\right)}{2 \sin \left(\frac{\alpha}{2}\right)}\right)^2 + \left(R + r \cos \frac{\alpha}{2}\right)^2}.
 \end{aligned}$$

□

Throughout the rest of this section, R_v is taken such that the agents leave each-other's field of view only by setting over each-other's dawn of dusk horizons.

Theorem 3.2.1. *The distance between two agents controlled by (2.2) with $0 < \alpha < 2\pi$ becomes bounded in finite time such that:*

$$\|p_j(t) - p_i(t)\| \leq \sqrt{\left(\frac{R \left(1 + 2 \cos \left(\frac{\alpha}{2}\right)\right) - r \left(1 - 2 \cos^2 \frac{\alpha}{2}\right)}{2 \sin \left(\frac{\alpha}{2}\right)}\right)^2 + \left(R + r \cos \frac{\alpha}{2}\right)^2} + (R-r) + 2R.$$

Proof. As seen in Lemma 3.2.2, two agents controlled by (2.2) get closer by each switch as long as

$$\|c_j - c_i\| > \sqrt{\left(\frac{R \left(1 + 2 \cos \left(\frac{\alpha}{2}\right)\right) - r \left(1 - 2 \cos^2 \frac{\alpha}{2}\right)}{2 \sin \left(\frac{\alpha}{2}\right)}\right)^2 + \left(R + r \cos \frac{\alpha}{2}\right)^2} = d_{critical}.$$

Once closer than $d_{critical}$, the next switch could at most add a distance of $R - r$ to the centers of rotation, as $R - r$ is the step size for any center of rotation upon each switch. Given the centers of rotation, the actual position of each agent is at most R from its center, leaving us with

$$\|p_j - p_i\| \leq \sqrt{\left(\frac{R \left(1 - 2 \cos \left(\frac{\alpha}{2}\right)\right) - r \left(1 + 2 \cos^2 \frac{\alpha}{2}\right)}{2 \sin \left(\frac{\alpha}{2}\right)}\right)^2 + \left(R + r \cos \frac{\alpha}{2}\right)^2} + (R-r) + 2R.$$

□

The upper bound in the previous result can be considerably shrunk given the agents have opposite orientation at some point in time. Lemma 3.2.3 shows that once two agents have opposite orientations, they remain that way. Theorem 3.2.2 uses this fact, as well as the result of Theorem 3.1.1, in order to present a tighter bound on the distances between agents in a 2-agent system.

Lemma 3.2.3. *In a system consisting of two agents controlled by (2.2) with $0 < \alpha < 2\pi$, if at some time t_0 , $\cos(\theta_1(t_0) - \theta_2(t_0)) = -1$, then $\cos(\theta_1(t) - \theta_2(t)) = -1 \forall t > t_0$.*

Proof. If $\cos(\theta_1(t_0) - \theta_2(t_0)) = -1$, then the agents get into and out of each others sector of visibility at the same time, causing $\forall t > t_0$,

$$\begin{aligned} \dot{\theta}_1(t) &= \dot{\theta}_2(t) \\ \Downarrow \\ \frac{d}{dt}(\theta_1(t_0) - \theta_2(t_0)) &= \dot{\theta}_1(t) - \dot{\theta}_2(t) = 0 \\ \Downarrow \\ \theta_1(t) - \theta_2(t) &= \text{const} \\ \Downarrow \\ \cos(\theta_1(t) - \theta_2(t)) &\equiv -1. \end{aligned}$$

□

Theorem 3.2.2. *In a system consisting of two agents controlled by (2.2) with $0 < \alpha < 2\pi$, if at time t_0 , $\cos(\theta_1(t_0) - \theta_2(t_0)) = -1$ then for $t \geq t_0 + T_{total}(\|c_2(t_0) - c_1(t_0)\|)$ where $T_{total}(x)$ is affine in x , the system converges to a configuration where both agents' centers of rotation are invariant and*

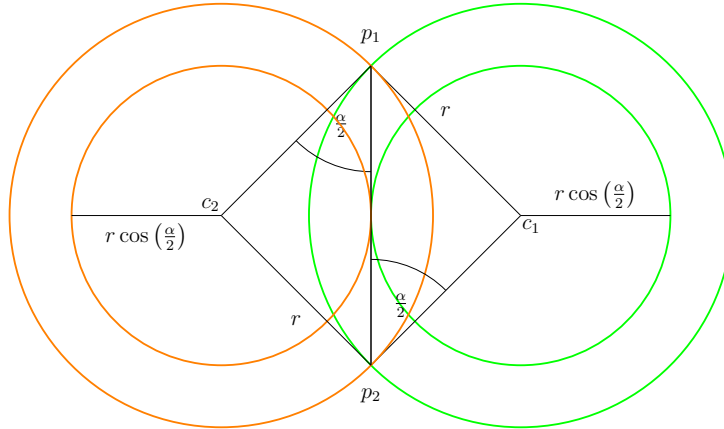
$$\|c_1(t) - c_2(t)\| \leq \begin{cases} 2r \cos\left(\frac{\alpha}{2}\right) & 0 < \alpha < \pi \\ -2R \cos\left(\frac{\alpha}{2}\right) & \pi \leq \alpha < 2\pi. \end{cases}$$

In addition, the agents' angular velocity remains constant and common to both agents, $\dot{\theta}_1(t) = \dot{\theta}_2(t) = \dot{\theta}_a$,

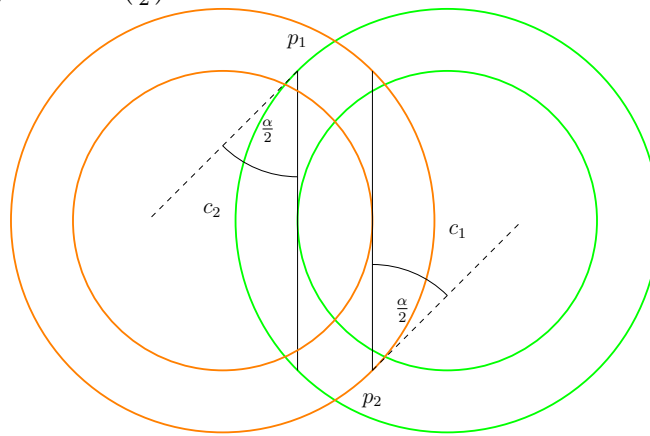
$$\dot{\theta}_a \begin{cases} = \frac{v}{r} & 0 < \alpha < \pi \\ \in \left[\frac{v}{R}, \frac{v}{r}\right] & \alpha = \pi \\ = \frac{v}{R} & \pi < \alpha < 2\pi. \end{cases}$$

Proof. If $\cos(\theta_1(t_0) - \theta_2(t_0)) = -1$, then the agents get into and out of each others sector of visibility at the same time, creating point symmetry at $b = \frac{p_2 - p_1}{2}$ with regards to the agent's trajectories. Point b is therefore stationary, and since the agents have bearing only sensing, sensing point b is equivalent to sensing the other agent. Invoking Theorem 3.1.1 for each of the agents with point b as the beacon concludes this proof. □

Figure 3.20 presents a visualization of the steady state reached by Theorem 3.2.2.



(a) With $\|c_1 - c_2\| = 2r \cos\left(\frac{\alpha}{2}\right)$, point b is located where both agents' blind circles touch.



(b) When $\|c_1 - c_2\| < 2r \cos\left(\frac{\alpha}{2}\right)$, point b is in both agents' blind circles.

Figure 3.20: Two configurations with $\alpha = \frac{\pi}{2}$ and $\cos(\theta_1 - \theta_2) = -1$. Agent 1 rotates on the green circle on the right, agent 2 rotates on the orange circle on the left. The blind circle of each agent, with radius $r \cos\left(\frac{\alpha}{2}\right)$ is shown as well.

Conjecture 3.2.1. *A 2-agent system controlled by (2.2), with $0 < \alpha < 2\pi$ converges in finite time to a periodic orbit such that both agents rotate in a circular pattern with a common, invariant radius around stationary centers of rotation, such that*

$$\|c_1(t) - c_2(t)\| \leq \begin{cases} 2r \cos\left(\frac{\alpha}{2}\right) & 0 < \alpha < \pi \\ -2R \cos\left(\frac{\alpha}{2}\right) & \pi \leq \alpha < 2\pi \end{cases} \quad \text{and} \quad r \begin{cases} = r & 0 < \alpha < \pi \\ \in [r, R] & \alpha = \pi \\ = R & \pi < \alpha < 2\pi. \end{cases}$$

Figure 3.21 shows two NetLogo simulations of a 2-agent system. The difference between the two simulations, other than the difference in initial conditions, is that the agent in Figure 3.21e has a central angle $\frac{\pi}{3}$ while the agent in Figure 3.21j has a central angle π . The initial conditions can be seen in Figures 3.21a and 3.21f. The agents travel towards each other in Figures 3.21b and 3.21g, notice that the agents' orientation becomes increasingly synchronized during this stage. The agents negotiate a final configuration in Figures 3.21c and 3.21h, reaching a configuration that enables the steady periodic orbit states in Figures 3.21d and 3.21i, in accord with Conjecture 3.2.1.

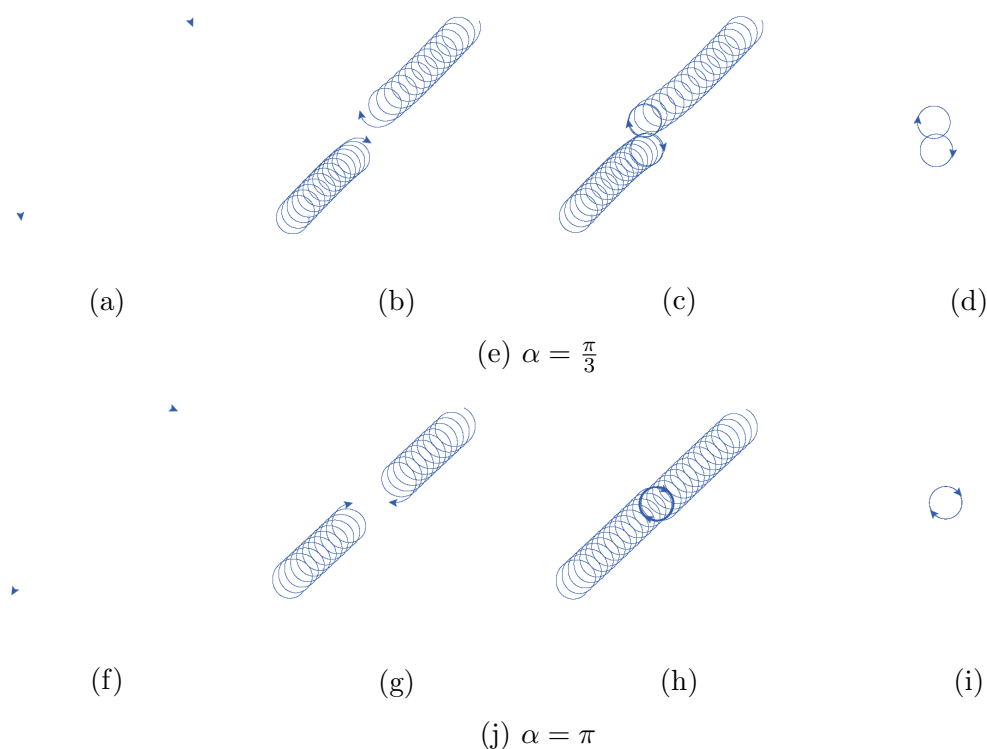


Figure 3.21: Two NetLogo simulations of a 2-agent system with $R = 6$ and $r = 4$.

3.3 Balanced States of the Swarm

In previous sections we analyzed the mechanics involved in converging from any initial conditions to a confined space in systems of two agents and agent-beacon systems. In this section, we consider a system with N agents. Two theorems regarding the steady states of an N -agent system are presented, and conjectures regarding reaching these states are provided as well. For the duration of this section, $R_v = \infty$.

Theorem 3.3.1. *If $N = nm$ such that $n, m \in \mathbb{N}$, and if $S \leq m$ and each agent's field of view α is set such that $\alpha = \frac{2\pi}{n}$, then if at some point in time, the agents are set in m clusters of n agents such that, without loss of generality due to arbitrarily naming the agents and setting the origin's location and orientation:*

$$\begin{bmatrix} x_{i,k} \\ y_{i,k} \\ \theta_{i,k} \end{bmatrix}_{t=t_0} = \begin{bmatrix} R \sin \theta_{i,k} \\ -R \cos \theta_{i,k} \\ \frac{2\pi}{n}i + \varphi_k \end{bmatrix}, \quad (3.9)$$

where $i \in \{0, \dots, n-1\}$, $k \in \{0, \dots, m-1\}$ and φ_k is some arbitrary phase common to all agents within a n -cluster, then for every moment t such that

$t \geq t_0$:

$$\begin{bmatrix} x_{i,k} \\ y_{i,k} \\ \theta_{i,k} \end{bmatrix} = \begin{bmatrix} R \sin \theta_{i,k} \\ -R \cos \theta_{i,k} \\ \frac{2\pi}{n}i + \varphi_k + \frac{v}{R}(t - t_0) \end{bmatrix}.$$

Proof. Given a state where Equation 3.9 holds, all agents perceive exactly m other agents, and therefore all agents rotate simultaneously around the same center of rotation, $c = c_0 = c_1 = c_{N-1}$. Every consecutive agents' locations, along with c , create an isosceles triangle with side length R and base angle $\frac{\pi - \alpha}{2}$, maintaining the equilibrium for all time. \square

Theorem 3.3.2. *If $N = nm$ such that $n, m \in \mathbb{N}$, and if $S > m$ and each agent's field of view α is set such that $\alpha = \frac{2\pi}{n}$, then if at some point in time, the agents are set in m clusters of n agents such that, without loss of generality due to arbitrarily naming the agents and setting the origin's location and orientation:*

$$\begin{bmatrix} x_{i,k} \\ y_{i,k} \\ \theta_{i,k} \end{bmatrix}_{t=t_0} = \begin{bmatrix} r \sin \theta_{i,k} \\ -r \cos \theta_{i,k} \\ \frac{2\pi}{n}i + \varphi_k \end{bmatrix}, \quad (3.10)$$

where $i \in \{0, \dots, n-1\}$, $k \in \{0, \dots, m-1\}$ and φ_k is some arbitrary phase common to all agents within a n -cluster, then for every moment t such that $t \geq t_0$:

$$\begin{bmatrix} x_{i,k} \\ y_{i,k} \\ \theta_{i,k} \end{bmatrix} = \begin{bmatrix} r \sin \theta_{i,k} \\ -r \cos \theta_{i,k} \\ \frac{2\pi}{n}i + \varphi_k + \frac{v}{r}(t - t_0) \end{bmatrix}$$

Proof. Given a state where Equation 3.10 holds, all agents perceive exactly m other agents, therefore all agents rotate simultaneously around the same center of rotation, $c = c_0 = c_1 = c_{N-1}$ with radius r . Every consecutive agents' locations, along with c , create an isosceles triangle with side length r and base angle $\frac{\pi - \alpha}{2}$, maintaining the equilibrium for all time. \square

Figure 3.22 shows the course of a NetLogo simulation experiment conducted in order to verify Theorem 3.3.2 over a 10-agent system. Due to limitations of the simulation, discussed briefly in the beginning of Chapter 5, Theorem 3.3.1 cannot be reliably simulated, but the verification of Theorem 3.3.2 by simulation may serve to verify Theorem 3.3.1 as well, since the two theorems are closely related. From the difficulties to simulate the balanced states in Theorem 3.3.1 we may learn that the balanced states there are unstable in the sense that they are sensitive to error in measurements, while the balanced states in Theorem 3.3.2 are more stable in that sense.

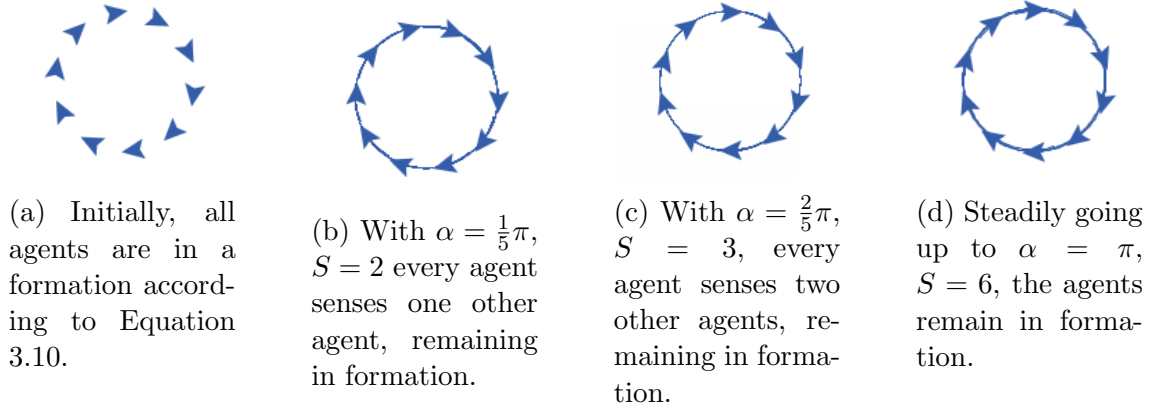


Figure 3.22: A simulation with 10 agents. By changing S along with α , the swarm formation is kept the same.

By observing numerous simulations of the model presented in Chapter 2, the following conjectures, based on the gathering behaviors observed, are made:

Conjecture 3.3.1. *A system of $N \geq 2$ agents controlled by (2.2) with $0 < \alpha < \pi$, such that $0 < S \leq N - 1$, converges in finite time to a cohesive behavior in which the every agent's trajectory intersects another agent's trajectory at least once every $\frac{2\pi R}{v}$ time period.*

Though according to Conjecture 3.3.1, the swarm ultimately converges, it doesn't always do so to balanced states as presented in Theorems 3.3.1 and 3.3.2. Figure 3.23 shows a set of simulations where six agents with ratio $\frac{r}{R} = \frac{1}{2}$ initialized at random x_i, y_i, θ_i ultimately converge such that every agent's trajectory intersects another at least once in a completion of a θ cycle. The exception is Figure 3.23f, where $S > N - 1$ and the agents do not converge at all.

Conjecture 3.3.2. *A system of $N = nm$ agents controlled by (2.2), such that $n, m \in \mathbb{N}$, $\alpha = \frac{2\pi}{n}$ and $S = m$ converges in finite time to a periodic orbit consisting of m rotating n -regular polygons.*

Figure 3.24 shows one example of convergence to a periodic orbit, while Figure 3.25 shows six agents with radius ratio $\frac{r}{R} = \frac{1}{2}$, initialized at random x_i, y_i, θ_i and the end behavior they display.

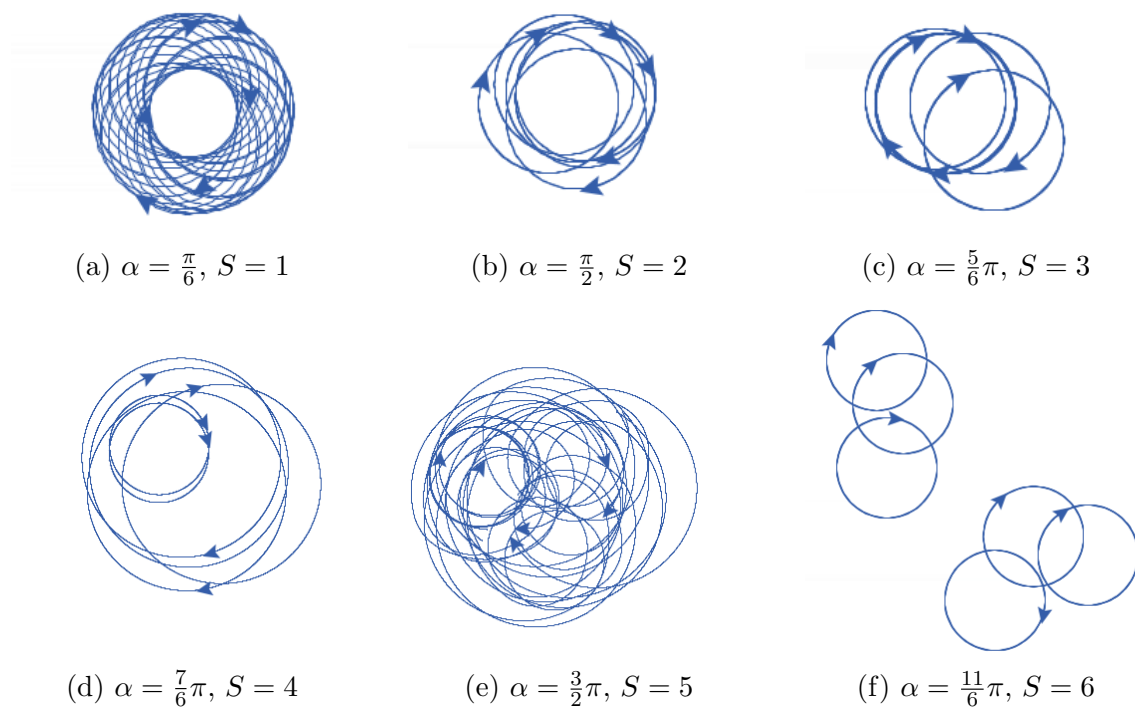


Figure 3.23: A simulation with 6 agents with different S values.

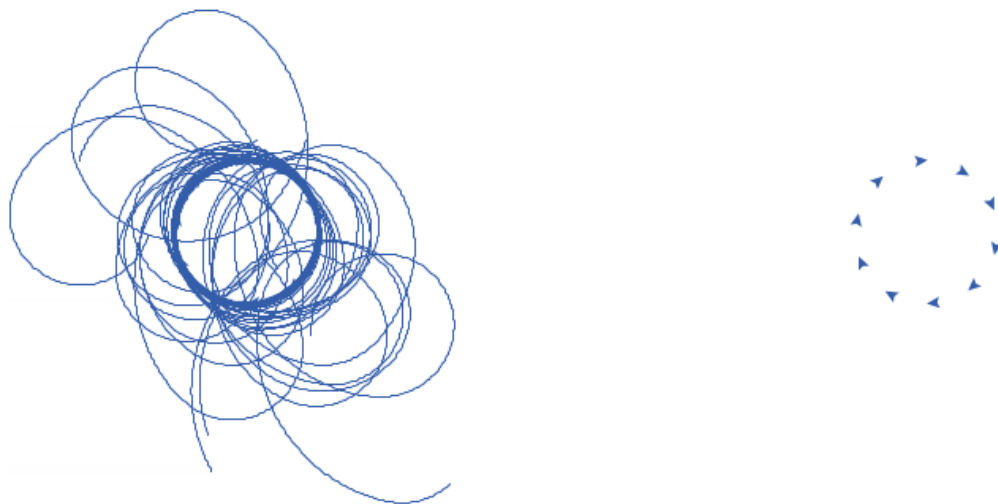
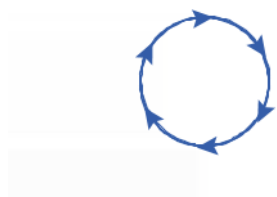


Figure 3.24: A simulation of a swarm of 10 agents converging from random initial conditions to a balanced state (left). On the right, a snapshot of the resulting balanced state.



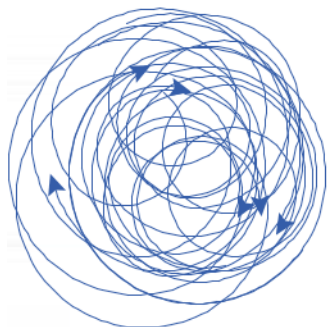
(a) $\alpha = \frac{\pi}{3}$, $S = 1$, resulting in a regular hexagon periodic orbit.



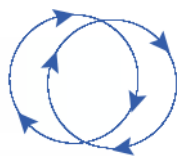
(b) $\alpha = \frac{2}{3}\pi$, $S = 2$, resulting in two equilateral triangles, in this case one on top of the other.



(c) $\alpha = \pi$, $S = 3$, resulting in three pairs of agents facing opposite directions.



(d) $\alpha = \frac{4}{3}\pi$, $S = 4$. 4 is not a divisor of 6, and the swarm converges to some cohesive behavior as opposed to a periodic orbit.



(e) $\alpha = \frac{2}{3}\pi$, $S = 2$, resulting in two equilateral triangles, clearly defined in this case.



(f) $\alpha = \pi$, $S = 3$, resulting in three pairs of agents facing opposite directions.

Figure 3.25: A simulation with 6 agents with different S values.

Chapter 4

Controlling the location of the Swarm

Control over the location of the swarm may be achieved in a number of ways, briefly discussed in this chapter. The fact that we have not used the velocity control input in gathering the swarm, leaves this input free for use in controlling the swarm, as described in Subsections 4.2 and 4.3. In addition, the swarm's gathering nature may also be utilized in order to control the swarm, as described below.

4.1 Control by Leader Agents

The swarm can be manipulated by either introducing "shepherd" agents as demonstrated in Figure 2.1, or by hijacking agents that are already part of the swarm, as demonstrated in simulation in Figure 4.1. The scalability of the swarm allows for the addition and removal of agents without compromising the self-stabilizing behavior of the swarm. Adding shepherd agents, i.e. agents that are controlled by some operator, or hijacking one or more agents by overriding their interaction protocol with an operator command, introduces leader agents into the swarm. The existence of leader agents in the swarm causes the swarm's agents, unaware that the leader agents' protocol is any different than their own, to try and incorporate these agents into the swarm's formation. Since the leader agents do not adhere to the swarming protocol, the swarm implicitly adapts by following the leaders.

4.2 Control by Predefined or Broadcast Potential Field

Another way of controlling a swarm rotating in a circular formation is by letting the single agent's speed be dictated by a global scalar potential field induced in the environment. Figure 4.2 shows a simulation of such a swarm. In the example presented, each agent is equipped with a location sensor, e.g. a GPS receiver, and a radio receiver. An operator is assumed to broadcast a potential function $\varphi(x, y, t)$, and every agent that detects the broadcast

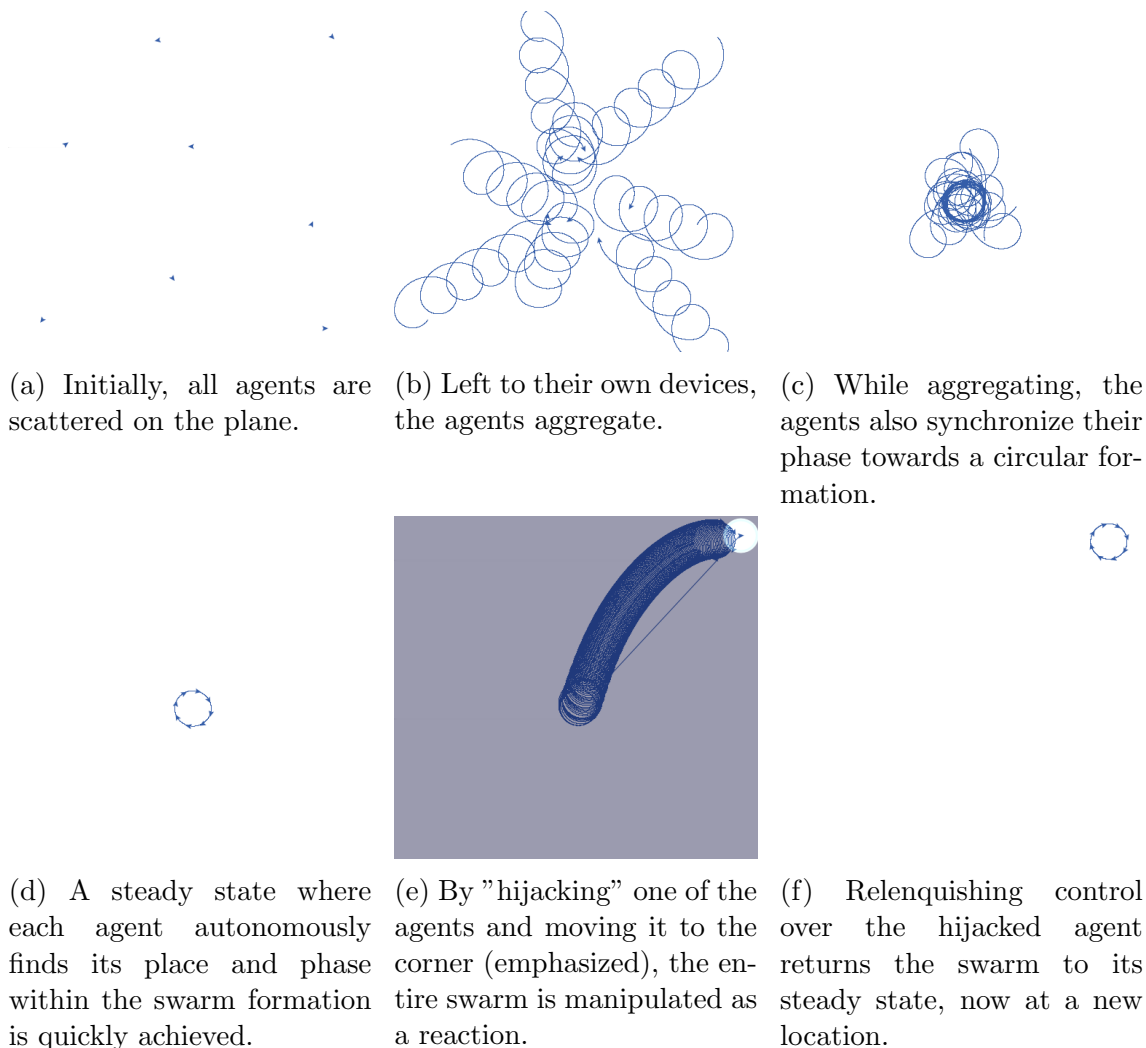


Figure 4.1: A simulation with 8 agents. Notice the agent's trajectories in each phase of the experiment.

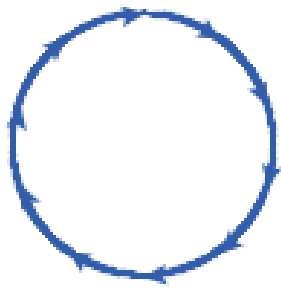
updates its speed, v , according to

$$v = \varphi(x, y, t)$$

where (x, y) is the agent's location. As a result, a difference in speed between agents is introduced on top of the swarm's protocol, causing the slower agents to pull at the swarm, and the swarm moves in a direction perpendicular to the potential field's gradient. Instead of broadcasting the potential function, the function can be preloaded into the agent's controlling protocol. Since the swarm moves in the direction of the left perpendicular to the potential field's gradient, the swarm can readily be made to patrol the potential field along a certain contour line.

4.3 Control by Local Sensing

Instead of being explicitly known to the agents, the potential field could be sampled by the agent's sensors at the agent's location, as described in [11].



(a) Steady state, no potential field present.



(b) A potential field with a horizontal gradient causes the swarm to move vertically.



(c) A potential field with a vertical gradient causes the swarm to move horizontally.

Figure 4.2: A swarm in circular formation rotating under the influence of a potential field.

Electromagnetic signal strength, a specific chemical particle count, sound frequency and intensity, are examples of quantities that can be measured on the fly by an agent's sensors. Since changes in these quantities over time and space describe a potential field function, a swarm of agents equipped with sensors that can measure these quantities can readily function without a GPS or radio receiver.

Chapter 5

Simulation Results

In this chapter simulation verifications of the theoretical results introduced in Chapter 3 are presented. Simulations were conducted using `NetLogo`¹ and `python`². In both environments, the numeric value assigned for π is 3.141592653589793, which is smaller than the actual π [1]. The numeric nature of the simulations lead to inaccuracies in the simulated agent's behavior, as can be seen in Figures 3.17 and 3.21, causing the agents with $\alpha = \pi$ to continue to converge to an r radius around the center of rotation when in a perfect simulation they would have found some radius r_f such that $r \leq r_f \leq R$, as dictated by Corollary 3.1.6. Due to this inherent imperfection, this chapter loosely uses the term π as the numeric value and not the exact one. This imperfection of the numeric world actually has implications to the real world implementation of the model suggested here. Any robot implemented using a digital processor would have the same issue. However, the only consequence is that the agents continue to converge to a smaller radius than prescribed by theory, practically rendering the resulting steady states in Corollaries 3.1.3 and 3.1.6 highly improbable, being replaced in real world scenarios by the steady states described in Lemma 3.1.9 and Corollary 3.1.5. On the other hand, robots in the real world have dimension, as opposed to the simulated agents in this chapter, introducing the opposite problem to that of simulated π being inaccurate, since this problem causes the agents to over-detect other agents instead of under-detecting them as they do in the simulations presented here. Fortunately, as seen in experiments conducted on real robots such as the one shown in Figure 2.1, the control protocol in (2.2) is able to bring the robot agents to the desired formation despite the inherent differences between theory and practice.

5.1 A Single Agent and A Beacon

This section serves to validate the theoretical results obtained in Section 3.1 by simulation. Three simulation experiments were conducted and are described here. In Section 5.1.1, an illustrative simulation is shown to validate the existence of the different states described in the proof for Lemma 3.1.9. In Section 5.1.2, the upper bound on convergence time obtained in Theorem

¹<https://ccl.northwestern.edu/netlogo/>

²<https://www.python.org/>

3.1.1 is validated. In Section 5.1.3, the relationship between initial conditions and the time it takes for the system to converge to a periodic orbit is verified by multiple simulations with preset constant system parameters, a set of distances between the agent’s initial center of rotation and the beacon, and otherwise random initial conditions.

5.1.1 Evolution of Distance to Beacon

An example python simulation for a system comprised of an agent and a beacon is presented here. The beacon was set at $(0, 0)$ and an agent with parameters $R = 6[m]$, $r = 4[m]$, $\alpha = \frac{\pi}{3}$, $v = 1 \frac{[m]}{[Sec]}$ and random initial θ_a had its center of rotation planted at $(100, 0)$. Figure 5.1 shows the evolution of both $\|p_a(t)\|$ and $\|c_a(t)\|$ through simulation time. The different colors of the plot represent the different states the agent is in, according to Lemma 3.1.9. The simulated agent starts at state E , goes through states D , A , C , until reaching state B and converging to $\|c_a(t)\| = 3.46 \pm 0.01$. The agent’s state transitions, as well as the convergence of $\|c_a(t)\|$ are in agreement with Lemma 3.1.9, where we have

$$\|c_a(t \rightarrow \infty)\| \leq r \cos\left(\frac{\alpha}{2}\right).$$

By plugging in the simulation parameters we get

$$r \cos\left(\frac{\alpha}{2}\right) = 4 \cos\left(\frac{\pi}{6}\right) \approx 3.464.$$

In addition, two periodic behaviors can be clearly seen in this simulation. One corresponds with state E in Lemma 3.1.9, described in Lemma 3.1.5, where the cycle period was obtained as

$$T = \frac{2\pi r + \alpha(R - r)}{v}.$$

Assigning the simulation parameters we get $T_t = \frac{26}{3}\pi \approx 27.227$, in compliance with the value measured in the simulation $T_s = 27.23 \pm 0.01$. The other periodic behavior corresponds with the steady "sink" state in Lemma 3.1.9, described in Lemma 3.1.1, Section 3.1, where $T_t = \frac{2\pi r}{v}$. In the simulation, the time period for the steady state is measured at $T_s = 25.13 \pm 0.01$, and is in accord with the theoretic result using the simulation parameters, $T_t \approx 25.133$.

5.1.2 Convergence Time is Linearly Bounded as a function of the Beacon’s Initial Distance to Agent’s Center of Rotation

In order to verify the validity of the convergence time upper bound in Theorem 3.1.1, over a thousand simulations were conducted with initial conditions and parameters randomly selected over a uniform distribution such that for each simulation: $R \in [2, 10)$, $r \in [1, R)$, $\alpha \in [0.1, \pi - 0.1)$, $c_a(t_{initial}) \in [R, 100)$. Figure 5.2 shows a plot of the results, where each data point has coordinates (x, y) , with x being the calculated theoretical upper bound for the simulation’s initial conditions and parameters and y being the actual time it took the

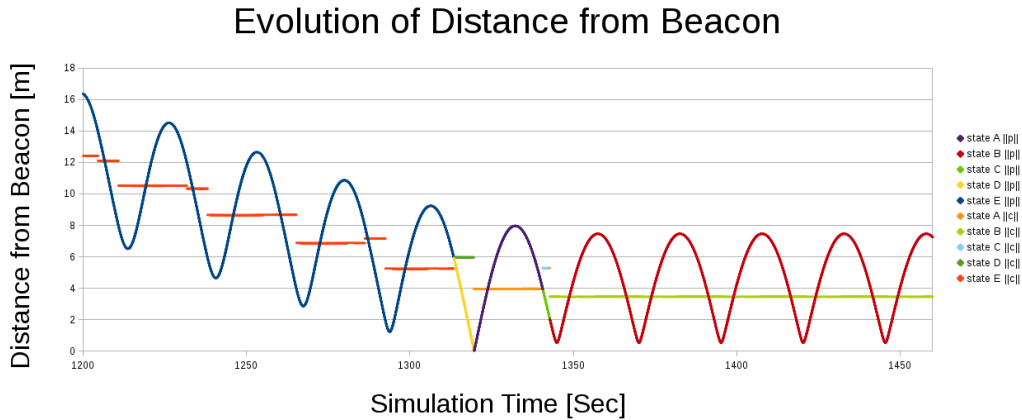


Figure 5.1: A simulation for a beacon and an agent with parameters $R = 6[m]$, $r = 4[m]$, $\alpha = \frac{\pi}{3}$ and $v = 1 \frac{[m]}{[Sec]}$. Evolution of both $\|p_a(t)\|$ and $\|c_a(t)\|$ is shown, the different colors represent the different states the agent is in.

simulation to reach the point where $c_a(t) \leq r \cos \frac{\alpha}{2}$. For convenience, the line $y = x$ is also plotted on the same graph to show that all data points fall under it, indicating that the theoretical upper bound is never broken in all the simulations conducted.

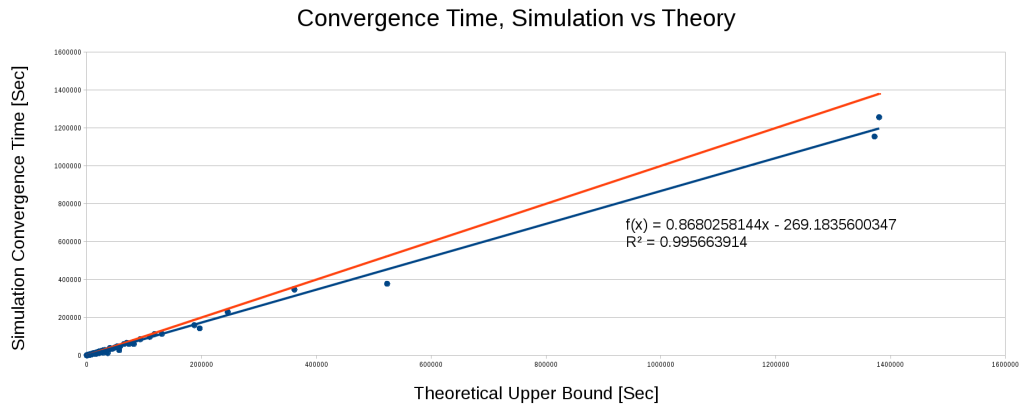


Figure 5.2: Each data point on the graph is one simulation result out of over one thousand. The data point coordinates are the theoretical upper bound on convergence time as X and the convergence time reached by the simulation as Y. Two trend lines are also shown, the upper one is $y = x$, showing that the theoretical upper bound is verified in these simulation results.

5.1.3 Convergence Time is Affine over Beacon Initial Distance to Agent's Center of Rotation

For each initial center of rotation in the range $[10, 20, \dots, 100]$ meters, 100 python simulations were initialized with preset parameters $R = 6[m]$, $r = 4[m]$, $\alpha = \frac{\pi}{3}$, $v = 1 \frac{[m]}{[Sec]}$ and random initial θ_a . For this set of parameters, the

$c_a(t_0)[m]$	10	20	30
mean convergence time [Sec]	118.553	259.0467	395.0646
standard deviation [Sec]	7.3607479994	7.5403591607	7.7186442809
max convergence time [Sec]	130.1	272.2	408.78
min convergence time [Sec]	104.5	246.94	383.42
theoretical bound [Sec]	376.051423867	512.187105522	648.322787178
$c_a(t_0)[m]$	40	50	60
mean convergence time [Sec]	530.6733	668.8577	804.6137
standard deviation [Sec]	7.1806059021	7.2219569601	6.9680382375
max convergence time [Sec]	544.75	681.57	817.53
min convergence time [Sec]	519.67	655.62	792.13
theoretical bound [Sec]	784.458468833	920.594150489	1056.72983214
$c_a(t_0)[m]$	70	80	90
mean convergence time [Sec]	938.7692	1076.6386	1213.0104
standard deviation [Sec]	7.1392699284	7.4628384423	6.7324358718
max convergence time [Sec]	953.03	1089.65	1225.33
min convergence time [Sec]	928.29	1064.02	1200.21
theoretical bound [Sec]	1192.8655138	1329.00119546	1465.13687711
$c_a(t_0)[m]$	100		
mean convergence time [Sec]	1348.0998		
standard deviation [Sec]	7.632927471		
max convergence time [Sec]	1361.62		
min convergence time [Sec]	1336.35		
theoretical bound [Sec]	1601.27255877		

Table 5.1

upper bound on convergence time becomes

$$\begin{aligned}
 T_{total} &= \frac{2\pi r + \alpha(R-r)}{2v(R-r)\sin\left(\frac{\alpha}{2}\right)} \|c_a(t_{initial})\| + \frac{R-r}{v} \tan\left(\frac{\alpha}{2}\right) \\
 &+ \frac{3\alpha R + (6\pi + \alpha)r}{v} + \frac{(2\pi + \alpha)r^2}{v(R-r)} + \frac{\alpha R + 2\pi r}{2v\sin\left(\frac{\alpha}{2}\right)} + \frac{\pi r^2}{v(R-r)\sin\left(\frac{\alpha}{2}\right)} \\
 &= \frac{13\pi}{3} \|c_a(t_{initial})\| + 76\pi + \frac{2}{\sqrt{3}} \approx 13.614 \|c_a(t_{initial})\| + 239.916.
 \end{aligned}$$

Table 5.1 shows the simulation results obtained, plotted in Figure 5.3.

The results indicate that the actual convergence time as a function of the initial distance between the beacon and the agent's center of rotation is indeed linear, with a slope corresponding to the theoretical analysis.

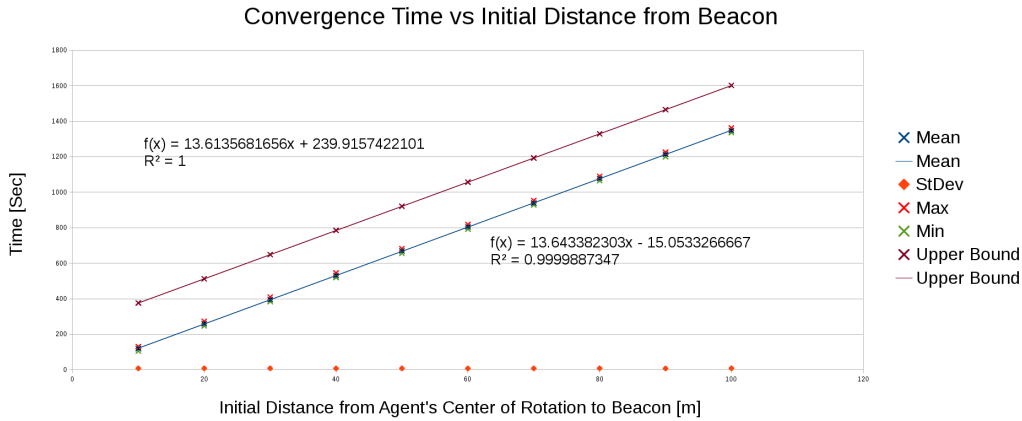


Figure 5.3: Simulation results for a system composed of an Agent and a Beacon. Theoretical upper bound on convergence time juxtaposed the mean, maximal and minimal convergence times for 100 simulations for each initial distance of the agent’s center of rotation from the beacon.

5.2 Two Agents

This section serves to validate the theoretical results obtained in Section 3.2 by simulation. Four simulation experiments were conducted and are described here. In Section 5.2.1, an illustrative simulation is presented in order to show the parallelism between the evolution of distances between the agents in a 2-agent system and the different states of the beacon-agent system described in the proof for Lemma 3.1.9. In Section 5.2.2, the evolution of the agents’ orientation is measured through simulation and some observations supporting Conjecture 3.2.1 are made. In Section 5.2.3, the relationship between initial conditions and the time it takes for the system to converge to a periodic orbit is explored by multiple simulations with preset constant system parameters, a set of distances between the agent’s initial center of rotation and the beacon, and otherwise random initial conditions. The results obtained support both Theorem 3.2.1 and Conjecture 3.2.1. The results obtained in Section 5.2.3 are further investigated in Section 5.2.4, further fortifying Conjecture 3.2.1.

5.2.1 Evolution of Distance between the Agents

An example python simulation for a 2-agent system is presented here. Both agents were initialized with parameters $R = 6[m]$, $r = 4[m]$, $\alpha = \frac{\pi}{3}$, $v = 1 \frac{[m]}{[Sec]}$ and random initial θ_a . One agent had its center of rotation set at $(0, 0)$ and the other agent had its center of rotation set at $(100, 0)$. Figure 5.4 shows the evolution of both $\|p_2(t) - p_1(t)\|$ and $\|c_2(t) - c_1(t)\|$ through simulation time. The different colors of the plot represent the different states the agent would have been in, according to Lemma 3.1.9, had there been a ”moving beacon” present at $\frac{p_1(t) + p_2(t)}{2}$. The states, though not applicable here, are presented in order to show the resemblance to the results shown in Figure 5.1. A convergence to a steady state is clearly seen from about $t = 670$ onward, where $\|c_2(t) - c_1(t)\| = 6.92 \pm 0.02$. This is well within the bounds of Theorem

3.2.1, where stated:

$$\|c_j - c_i\| (t \rightarrow \infty) < \sqrt{\left(\frac{R(1 + 2 \cos(\frac{\alpha}{2})) - r(1 - 2 \cos^2(\frac{\alpha}{2}))}{2 \sin(\frac{\alpha}{2})}\right)^2 + \left(R + r \cos(\frac{\alpha}{2})\right)^2}$$

$$\approx 20.684,$$

and even within the bounds of Theorem 3.2.2, where stated:

$$\|c_j - c_i\| (t > t_0 + T_{total}) \leq 2r \cos\left(\frac{\alpha}{2}\right) \approx 6.93,$$

and

$$T_{total} \approx 920.594.$$

This result is surprising, since the initial conditions for this simulation were not such that $\cos(\theta_2 - \theta_1) = -1$, as required by Theorem 3.2.2. Since it seems that the results obtained in this simulation adhere to the bounds presented in Theorem 3.2.2 without meeting the requirements of the theorem, further investigation seems necessary, and is presented at Section 5.2.2.

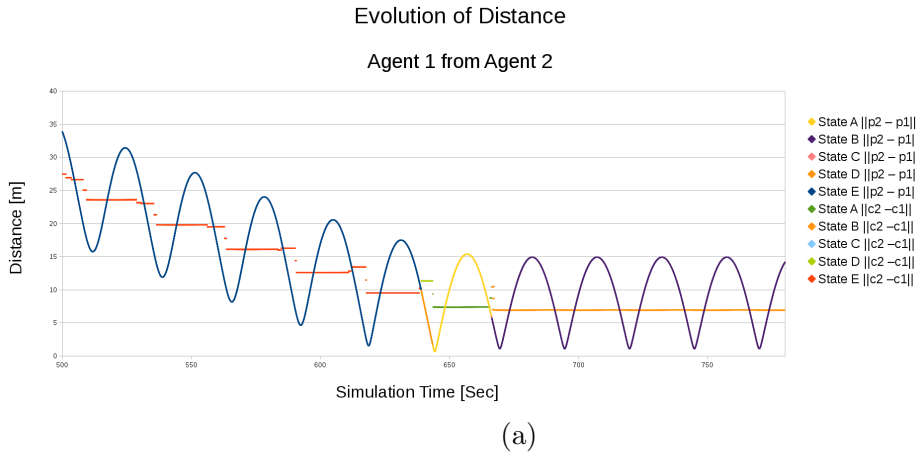


Figure 5.4: A simulation for a 2-agent system with parameters $R = 6[m]$, $r = 4[m]$, $\alpha = \frac{\pi}{3}$ and $v = 1 \frac{[m]}{[Sec]}$. Evolution of both $\|p_2(t) - p_1(t)\|$ and $\|c_2(t) - c_1(t)\|$ is shown, the different colors represent the different states the agent is in with regards to a point half way towards the other agent.

5.2.2 Evolution of Orientation

Analyzing the results obtained from the experiment held in Section 5.2.1, we notice that the difference in the agents' orientations approach π as the simulation approaches its converged state. Figure 5.5 shows the evolution of both agents' orientation, along with the difference in orientation, through time.

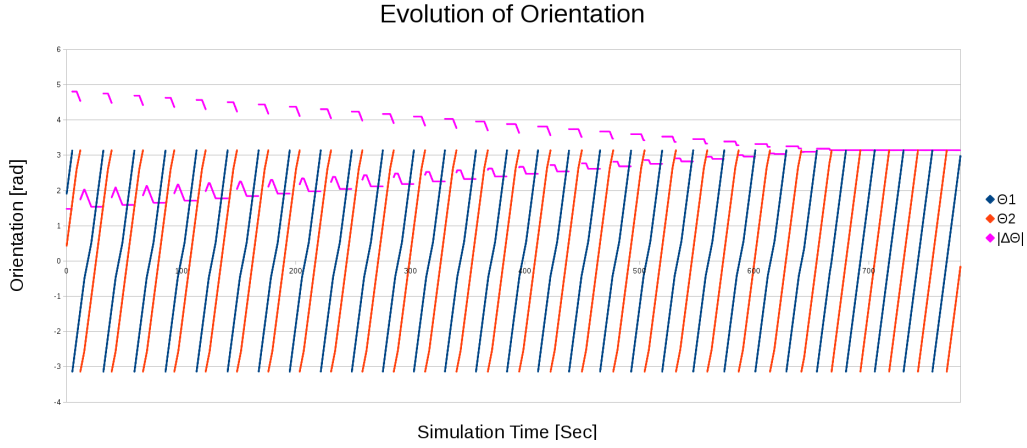


Figure 5.5: A simulation for a 2-agent system with parameters $R = 6[m]$, $r = 4[m]$, $\alpha = \frac{\pi}{3}$ and $v = 1 \frac{[m]}{[Sec]}$. Evolution of θ_1 , θ_2 and $|\theta_2 - \theta_1|$ is shown.

5.2.3 Upper Bound on Convergence Time

Given the results in Sections 5.2.1 and 5.2.2, a series of tests were conducted in order to verify Theorem 3.2.1, as well as Conjecture 3.2.1. As no upper bound for time is provided in these statements, and having observed the evolution of orientation in Section 5.2.2, we set the simulations to terminate either when a time period of $T = \frac{2\pi R}{v}$ lapsed without any switching and with no change to $\Delta\theta$, implying an orbit, or when the upper bound on time in Theorem 3.2.2 elapsed. For each initial distance between centers of rotation in the range $[10, 20, \dots, 100]$ meters, 100 python simulations were initialized with preset parameters $R = 6[m]$, $r = 4[m]$, $\alpha = \frac{\pi}{3}$, $v = 1 \frac{[m]}{[Sec]}$ and random initial θ_a . For this set of parameters, the upper bound on convergence time becomes

$$\begin{aligned}
 T_{total} &= \\
 &\left(\frac{2\pi r + \alpha(R - r)}{2v(R - r) \sin\left(\frac{\alpha}{2}\right)} \right) \frac{\|c_2(t_0) - c_1(t_0)\|}{2} + \frac{R - r}{v} \tan\left(\frac{\alpha}{2}\right) \\
 &+ \frac{3\alpha R + (6\pi + \alpha)r}{v} + \frac{(2\pi + \alpha)r^2}{v(R - r)} + \frac{\alpha R + 2\pi r}{2v \sin\left(\frac{\alpha}{2}\right)} + \frac{\pi r^2}{v(R - r) \sin\left(\frac{\alpha}{2}\right)} \\
 &= \frac{13}{6}\pi \|c_2(t_0) - c_1(t_0)\| + 76\pi + 2 \tan\left(\frac{\pi}{6}\right) \approx 6.807 \|c_2(t_0) - c_1(t_0)\| + 239.916.
 \end{aligned}$$

Table 5.2 shows the simulation results obtained, plotted in Figure 5.6. Notice that no convergence time exceeds or even comes close to the upper bound, meaning that a steady state was achieved in each of the simulations before reaching the time upper bound. This result, along with that in Sections 5.2.2 and 5.2.4 support reasonable grounds for Conjecture 3.2.1.

$\ c_1(t_0) - c_2(t_0)\ [m]$	10	20	30
mean convergence time [Sec]	96.3233	166.4391	231.9716
standard deviation [Sec]	16.830511798	14.2570158589	12.2491573588
max convergence time [Sec]	158.76	186.24	263.82
min convergence time [Sec]	96.3233	166.4391	216.32
theoretical bound [Sec]	307.983583039	376.051423867	444.119264695
$\ c_1(t_0) - c_2(t_0)\ [m]$	40	50	60
mean convergence time [Sec]	304.5203	369.5082	442.1633
standard deviation [Sec]	12.804248305	13.2689676229	9.4976772338
max convergence time [Sec]	320.04	397.69	470.22
min convergence time [Sec]	270.98	352.67	412.25
theoretical bound [Sec]	512.187105522	580.25494635	648.322787178
$\ c_1(t_0) - c_2(t_0)\ [m]$	70	80	90
mean convergence time [Sec]	508.4133	577.9575	642.7951
standard deviation [Sec]	15.3977590561	9.1886678534	13.8263284561
max convergence time [Sec]	535.98	591.87	672.04
min convergence time [Sec]	488.71	546.68	624.33
theoretical bound [Sec]	716.390628006	784.458468833	852.526309661
$\ c_1(t_0) - c_2(t_0)\ [m]$	100		
mean convergence time [Sec]	714.9467		
standard deviation [Sec]	10.0881046113		
max convergence time [Sec]	728.9		
min convergence time [Sec]	683.2		
theoretical bound [Sec]	920.594150489		

Table 5.2

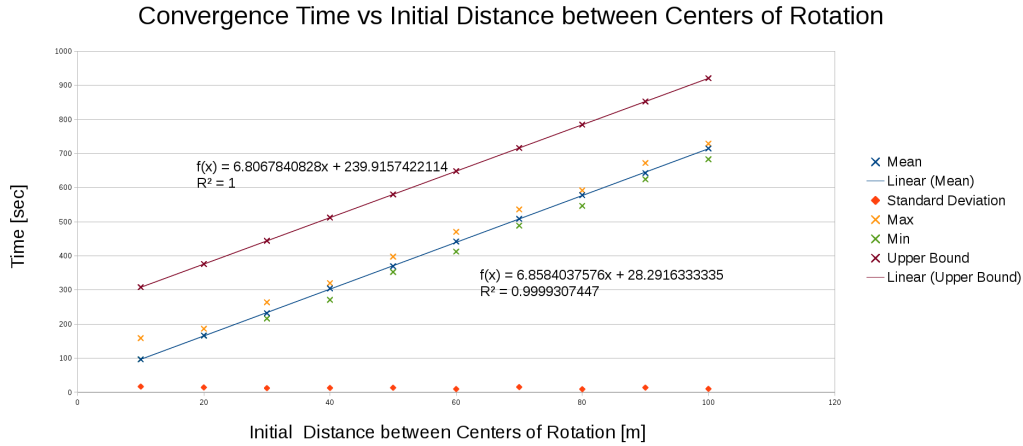
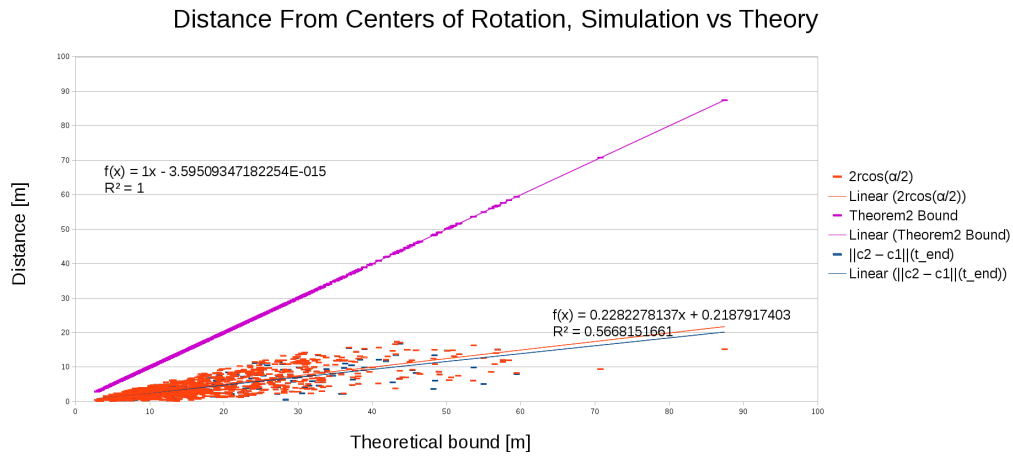


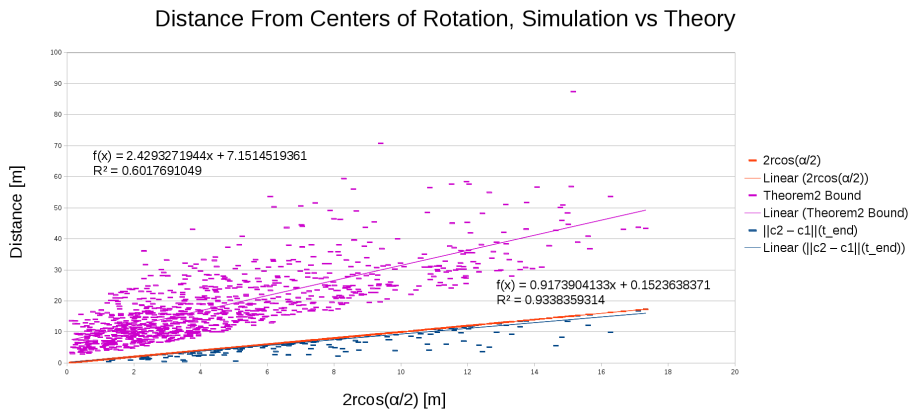
Figure 5.6: Simulation results for a 2-agent system. A suggested linear upper bound on convergence time based on Theorem 3.2.2 juxtaposed the mean, maximal and minimal convergence times for 100 simulations for each initial distance between the agents' centers of rotation.

5.2.4 Upper Bound on Distances

To further investigate the results obtained in Section 5.2.3, as well as the configurations reached by the end of time elapsed, over a thousand simulations were conducted with initial conditions and parameters randomly selected over a uniform distribution such that for each simulation: $R \in [2, 10)$, $r \in [1, R)$, $\alpha \in [0.1, \pi - 0.1)$, $\|c_2 - c_1\| (t_{initial}) \in [R, 100)$. The simulations terminate either by reaching a steady state where no switching occurred and $|\theta_1 - \theta_2|$ remained constant for more than $\frac{2\pi R}{v}$ time, or by reaching the time bound as prescribed by Theorem 3.2.2. At the end of each simulation the distance between the centers of rotation was recorded. Figure 5.7 shows the results of this experiment. Three data series are presented at each plot - the theoretical bound from Theorem 3.2.1, $d_{critical}$, and $2r \cos(\frac{\alpha}{2})$ corresponding the random parameters set for the simulation, along with the distance between centers of rotation at the end of the simulation. In Figure 5.7a, the data series are plotted against the theoretical bound from Theorem 3.2.1, and in Figure 5.7b the data series are plotted against $2r \cos(\frac{\alpha}{2})$. These results verify Theorem 3.2.1, as no result ever reached the theoretical distance upper bound by the end of simulation time. These results also strongly suggest $2r \cos(\frac{\alpha}{2})$ as an upper bound, implying a synchronization of orientations as seen in Section 5.2.2, leading to the conditions required for Theorem 3.2.2 to manifest, ultimately fortifying Conjecture 3.2.1.



(a) The data series vs $d_{critical}$



(b) The data series vs $2r \cos\left(\frac{\alpha}{2}\right)$

Figure 5.7: The distances between centers of rotation at the end of over a thousand simulations are presented here as the $\|c_2(t_{end}) - c_1(t_{end})\|$ data series, along with $2r \cos\left(\frac{\alpha}{2}\right)$ and $d_{critical}$ from Theorem 3.2.1.

Chapter 6

Discussion

The model presented is a decentralized, scalable, self organizing swarm of anonymous unicycle type agents which solves a formation problem by evolving to either a regular polygon formation or to a set of regular polygons in some particular cases described here. The model requires the agents to have only limited sensing abilities which enable the agents to make a crude judgment on how many other agents are in a sector in front of them utilizing limited computation power and with no knowledge of the global frame. The simplicity of the agents allow for a cost effective implementation of the model, since the use of sophisticated equipment is rendered unnecessary. This work contains a full analysis of a beacon-agent system, as well as convergence theorems for a 2-agent system and equilibrium analysis for a N -agent system. Gathering in the N -agent case and orientation synchronization in the 2-agent case were demonstrated in simulation. Methods of controlling the location of the swarm were presented and demonstrated in simulation as well.

Current research efforts are aimed at fully understanding the orientation synchronizing mechanism which was observed in the 2-agent and N -agent cases. The understanding of this mechanism is key to a full analytic solution to the formation of regular polygons in the N -agent case, and may prove useful in the analysis of future models based on the model presented here. Obstacle avoidance hasn't been covered in this work, yet the "Turtle Bale" project has incorporated obstacle avoidance by adding range sensors, without hindering the gathering nature of the swarm.

Acknowledgement

We thank Prof. Daniel Zelazo and Dr. Gavriel Davidov for their careful reading of this manuscript and their useful suggestions.

Bibliography

- [1] Jörg Arndt and Christoph Haenel. *Pi-unleashed*. Springer Science & Business Media, 2001.
- [2] L. B. Arranz, A. Seuret, and C. Canudas de Wit. Translation control of a fleet circular formation of auvs under finite communication range. In *Decision and Control, 2009 held jointly with the 2009 28th Chinese Control Conference. CDC/CCC 2009. Proceedings of the 48th IEEE Conference on*, pages 8345–8350, Dec 2009.
- [3] Ariel Barel, Rotem Manor, and Alfred M Bruckstein. Come together: Multi-agent geometric consensus. 2016.
- [4] Alfred M. Bruckstein. Why the ant trails look so straight and nice. *The Mathematical Intelligencer*, 15(2):59–62, 1993.
- [5] J. Cortes. Discontinuous dynamical systems. *IEEE Control Systems*, 28(3):36–73, June 2008.
- [6] J. L. Deneubourg, S. Aron, S. Goss, and J. M. Pasteels. The self-organizing exploratory pattern of the argentine ant. *Journal of Insect Behavior*, 3(2):159–168, 1990.
- [7] Dimos V Dimarogonas and Kostas J Kyriakopoulos. On the rendezvous problem for multiple nonholonomic agents. *Automatic Control, IEEE Transactions on*, 52(5):916–922, 2007.
- [8] M. Dorigo, M. Birattari, and T. Stutzle. Ant colony optimization. *IEEE Computational Intelligence Magazine*, 1(4):28–39, Nov 2006.
- [9] Magnus B Egerstedt and Xiaoming Hu. Formation constrained multi-agent control. 2001.
- [10] Yotam Elor and Alfred M Bruckstein. A thermodynamic approach to multi-robot cooperative localization. *Theoretical Computer Science*, 457:59–75, 2012.
- [11] Yotam Elor and Alfred M. Bruckstein. Robot cloud gradient climbing with point measurements. *Theoretical Computer Science*, 547:90 – 103, 2014.
- [12] Melvin Gauci, Jianing Chen, Wei Li, Tony J. Dodd, and Roderich Groß. Self-organized aggregation without computation. *The International Journal of Robotics Research*, 33(8):1145–1161, 2014.
- [13] Aviram Gelblum, Itai Pinkoviezky, Ehud Fonio, Abhijit Ghosh, Nir Gov, and Ofer Feinerman. Ant groups optimally amplify the effect of transiently informed individuals. *Nature Communications*, 6:7729 EP –, Jul 2015. Article.

- [14] Noam Gordon, Israel A Wagner, and Alfred M Bruckstein. A randomized gathering algorithm for multiple robots with limited sensing capabilities. *Proc. of MARS 2005 workshop at ICINCO*.
- [15] J. Halloy, G. Sempo, G. Caprari, C. Rivault, M. Asadpour, F. Tâche, I. Saïd, V. Durier, S. Canonge, J. M. Amé, C. Detrain, N. Correll, A. Martinoli, F. Mondada, R. Siegwart, and J. L. Deneubourg. Social integration of robots into groups of cockroaches to control self-organized choices. *Science*, 318(5853):1155–1158, 2007.
- [16] Anoop Jain and Debasish Ghose. Synchronization of multi-agent systems with heterogeneous controllers. *CoRR*, abs/1512.07362, 2015.
- [17] Anoop Jain and Debasish Ghose. Phase balancing of two and three-agent heterogeneous gain systems with extensions to multiple agents. *CoRR*, abs/1605.08958, 2016.
- [18] Malvin H Kalos and Paula A Whitlock. *Monte carlo methods*. John Wiley & Sons, 2008.
- [19] J. A. Marshall, M. E. Broucke, and B. A. Francis. Formations of vehicles in cyclic pursuit. *IEEE Transactions on Automatic Control*, 49(11):1963–1974, Nov 2004.
- [20] B. J. Moore and C. Canudas de Wit. Source seeking via collaborative measurements by a circular formation of agents. In *Proceedings of the 2010 American Control Conference*, pages 6417–6422, June 2010.
- [21] Iñaki Navarro and Fernando Matía. An introduction to swarm robotics. *ISRN Robotics*, 2013, 2012.
- [22] Iñaki Navarro and Fernando Matía. A survey of collective movement of mobile robots. *International Journal of Advanced Robotic Systems*, 10(73), 2013.
- [23] Kwang-Kyo Oh, Myoung-Chul Park, and Hyo-Sung Ahn. A survey of multi-agent formation control. *Automatica*, 53:424 – 440, 2015.
- [24] L.C.A. Pimenta, G.A.S. Pereira, N. Michael, R.C. Mesquita, M.M. Bosque, L. Chaimowicz, and V. Kumar. Swarm coordination based on smoothed particle hydrodynamics technique. *Robotics, IEEE Transactions on*, 29(2):383–399, 2013.
- [25] Mark Read, Christoph Möslinger, Tobias Dipper, Daniela Kengyel, James Hilder, Ronald Thenius, Andy Tyrrell, Jon Timmis, and Thomas Schmickl. *Profiling Underwater Swarm Robotic Shoaling Performance Using Simulation*, pages 404–416. Springer Berlin Heidelberg, Berlin, Heidelberg, 2014.
- [26] Craig W. Reynolds. Flocks, herds and schools: A distributed behavioral model. *SIGGRAPH Comput. Graph.*, 21(4):25–34, August 1987.
- [27] Gal Ribak, David Rand, Daniel Weihs, and Amir Ayali. Role of wing pronation in evasive steering of locusts. *Journal of Comparative Physiology A*, 198(7):541–555, 2012.
- [28] E. Schoof, A. Chapman, and M. Mesbahi. Bearing-compass formation control: A human-swarm interaction perspective. In *2014 American Control Conference*, pages 3881–3886, June 2014.

- [29] Ilana Segall and Alfred Bruckstein. *On Stochastic Broadcast Control of Swarms*, pages 257–264. Springer International Publishing, Cham, 2016.
- [30] R. Sepulchre, D. A. Paley, and N. E. Leonard. Stabilization of planar collective motion: All-to-all communication. *IEEE Transactions on Automatic Control*, 52(5):811–824, May 2007.
- [31] R. Sepulchre, D. A. Paley, and N. E. Leonard. Stabilization of planar collective motion with limited communication. *IEEE Transactions on Automatic Control*, 53(3):706–719, April 2008.
- [32] Nicholi Shiell and Andrew Vardy. *A Bearing-Only Pattern Formation Algorithm for Swarm Robotics*, pages 3–14. Springer International Publishing, Cham, 2016.
- [33] Israel A Wagner, Michael Lindenbaum, and Alfred M Bruckstein. Smell as a computational resource—a lesson we can learn from the ant. In *ISTCS*, volume 96, pages 219–230, 1996.
- [34] D. Weihs. Hydromechanics of fish schooling. *Nature*, 241(5387):290–291, Jan 1973.
- [35] X. Yu and L. Liu. Cooperative control for moving-target circular formation of nonholonomic vehicles. *IEEE Transactions on Automatic Control*, PP(99):1–1, 2016.
- [36] S. Zhao and D. Zelazo. Bearing-based formation maneuvering. In *2015 IEEE International Symposium on Intelligent Control (ISIC)*, pages 658–663, Sept 2015.
- [37] Ronghao Zheng, Zhiyun Lin, and Ming Cao. Rendezvous of unicycles with continuous and time-invariant local feedback. *Proceedings of the 18th World Congress of the International Federation of Automatic Control*, 18:10044–10049, 2011.
- [38] Ronghao Zheng, Zhiyun Lin, Minyue Fu, and Dong Sun. Distributed control for uniform circumnavigation of ring-coupled unicycles. *Automatica*, 53(0):23 – 29, 2015.
- [39] Ronghao Zheng, Zhiyun Lin, and Gangfeng Yan. Ring-coupled unicycles: Boundedness, convergence, and control. *Automatica*, 45(11):2699–2706, 2009.
- [40] Ronghao Zheng, Yunhui Liu, and Dong Sun. Enclosing a target by non-holonomic mobile robots with bearing-only measurements. *Automatica*, 53:400 – 407, 2015.
- [41] Ronghao Zheng and Dong Sun. Rendezvous of unicycles: A bearings-only and perimeter shortening approach. *Systems & Control Letters*, 62(5):401–407, 2013.
- [42] Ronghao Zheng and Dong Sun. Multirobot rendezvous with bearing-only or range-only measurements. *Robotics and Biomimetics*, 1(1):1–13, 2014.